Parallel Connected Voltage Source Converters using Coupled Inductors

by

Marius Takongmo

A thesis submitted in partial fulfillment of the requirements for the degree of

Doctor of Philosophy

in

Energy Systems

Department of Electrical and Computer Engineering
University of Alberta

Abstract

Multi-level coupled inductor voltage source converter topologies using two level inverters and advanced pulse width modulation (PWM) schemes are presented to reduce the footprint of high-power non isolated converters by lowering the size/weight of the magnetics.

Interleaved PWM switching of two-level inverter legs connected to coupled inductors (CIs) having cross-coupled windings is a topic examined for low voltage high power converters. The winding arrangement significantly reduces the series output inductance as seen at the output of each phase of the voltage source converter. Balanced ac currents flowing through the inductor low series output inductance produce a small fundamental voltage drop across the coupled inductor windings and insignificant lowers the fundamental flux in the inductor magnetic core. In consequence, the peak flux and hence, the size/weight of the interface inductors required to average the outputs of the parallel connected two-level inverter legs can be reduced. The low series output inductance equally favors rapid transient response and makes it feasible to generate high-frequency fundamental multi-level PWM output voltages in the kilohertz range.

A common mode (CM) dc-choke and a differential mode (DM) ac coupled inductor are investigated to separately filter the common mode and differential mode PWM voltages experienced between two parallel connected voltage source converters using to the same dc-link. The dc choke presents a high inductance to common mode PWM, and the ac inductor presents a high inductance to differential mode PWM voltages. The size and weight of the two coupled inductor types is smaller than using three conventional coupled

inductors, which can cope with both common mode and differential mode PWM voltages across their windings. The system described is useful to reduce common mode to ground noise in uninterrupted power supplies and motor drives, reduce cable interactions, and increase the power density of interleaved PWM switching converters by reducing the size/weight of the converter's magnetics.

Neutral point clamped (NPC) coupled inductor topologies having inner high-frequency PWM modules are presented for high voltage high current applications such as ultra fast electric vehicle chargers and electric drives. The neutral point clamped converters reduce the voltage stress across all the switching devices to $V_{dc}/2$ and lowers switching losses. The first NPC converter examined, unidirectional converter, has a reduced switch count and produce more voltage levels at the coupled inductor outputs when compared with VSCs having the same number of switching devices. Such multi-level PWM output voltages can easily be filtered with a small ac inductance, thereby reducing the size/weight of the overall converter. The second neutral point clamped converter, bidirectional converter, has two high-frequency modules at the output stage of each phase and connected together using a 3-limb interface coupled inductor. This inductor is smaller than using three conventional C-shaped coupled inductors. A PWM scheme that produces no common mode voltage across the 3-limb inductor windings is used to control the bidirectional NPC converter.

A discontinuous PWM, DPWM, control for neutral point clamped converters having inner high-frequency PWM modules is presented to reduce the peak flux, size, and weight of the magnetics in high voltage high current voltage source converters. The

iii

DPWM control ensures that the flux patterns remain centered at zero with no jumps; thereby reducing the peak flux and the required size/weight of interface coupled inductors.

Preface

This thesis is an original work done by Marius Takongmo partly in the electrical and computer engineering department of the University of Alberta and partly at eleapPower in Toronto, under the supervision of Dr. John Salmon. Some parts of this thesis have been published as a journal and conference publication and have been reorganized for clearer presentation. Chenhui Zhang assisted in preparing the laboratory prototypes; Saeed Wdaan, Wael Telmesani, and Dohitha Yapa helped to get more experimental results for two journal papers which were under revision while I was away on internship.

Chapter 2 has been published as a journal paper and two conference papers.

Journal:

[1]   M. Takongmo, C. Zhang and J. Salmon, "Coupled Inductors for High-Frequency Drives With Parallel-Connected Inverter Legs," in *IEEE Transactions on Power Electronics*, vol. 37, no. 6, pp. 7055-7066, June 2022.

Conference papers:

[2]   M. Takongmo and J. Salmon, "Design of Three Limb Coupled Inductor using Cross-Coupled Windings to Produce Multi-Level Output Voltages and Reduced Magnetics," 2021 IEEE Applied Power Electronics Conference and Exposition (APEC), 2021, pp. 226-232, doi: 10.1109/APEC42165.2021.9487260.

[3]   M. Takongmo, C. Zhang and J. Salmon, "Multi-level Voltage Source Converters using Coupled Inductors and Parallel Connected Inverter Legs," 2022 IEEE Applied Power Electronics Conference and Exposition (APEC), 2022, pp. 524-530, doi: 10.1109/APEC43599.2022.9773376.

.

Chapter 3 has been published as a journal paper and a conference paper.

Journal:

[4]   M. Takongmo, C. Zhang, S. Wdaan, W. A. M. Telmesani, D. Yapa and J. Salmon, "Parallel-Connected Voltage Source Converters with a DC Common Mode and an AC Differential Mode PWM Filter," in *IEEE Transactions on Power Electronics*, vol. 38, no. 3, pp. 3664-3675, March 2023.

Conference Paper:

[5]   M. Takongmo, C. Zhang and J. Salmon, "Parallel Inverters using a DC Common Mode PWM Filter with an AC Differential Mode PWM Filter," 2021 IEEE Applied Power Electronics Conference and Exposition (APEC), 2021, pp. 1189-1196, doi: 10.1109/APEC42165.2021.9487453.

Chapters 4 has not yet been published.

Chapter 5 is an improvement of a PWM scheme which has been published as a conference paper. The published PWM control technique has been improved and modified for neutral point clamped converters having inner interleaved inverter modules:

[11]   C. Zhang, M. Takongmo, V. Perera and J. Salmon, "Flux Minimization in Interphase Coupled Inductors of Parallel-Connected Voltage Source Converters," 2022 IEEE Applied Power Electronics Conference and Exposition (APEC), 2022, pp. 843-847, doi: 10.1109/APEC43599.2022.9773424.

To my parents Claire & Pascal Dongmo and my

sweetheart Stelie Navela…

Acknowledgment

I thank the Almighty God for His guidance and protection throughout the past four years. Thanks to God, I was in good health and had the strength to successfully complete a PhD program at the prestigious University of Alberta. I would equally like to express my gratitude toward a few people who helped on this journey.

First and foremost, I would like to thank Dr. John Salmon for giving me the opportunity to pursue a PhD degree at the University of Alberta under His supervision, for His constant feedback, trust, care, and love. Thank you for the numerous opportunities you provided over the years like letting me build hardware prototypes for experimental testing, and a one-year industrial experience at eleapPower in Toronto. Thank you, Dr.

Secondly, I would like to thank my parents Mr. and Miss. Dongmo, for giving me the permission to travel to Canada for further studies, for the constant support, and care. I would forever be indebted to my parents for the seed of hard work and resilience they planted in me at a very early age, greatly helped me to stand on my feet with confidence. I thank my brother Ing. Herman Jiope for his friendship and advice.

A special thanks to Dr. Chatumal Perera, Mr. Albert Terheide, and Sukhjt Singh who greatly helped me to speed up on the learning curve to familiarize myself with the lab equipment at the University of Alberta. Another special thanks to Chenhui Zhang with whom I investigated and developed numerous advanced PWM schemes, to Saeed Wdaan, Wael Telmesani, and Dohitha Yapa for their friendship and for helping get more experimental results for two journals which were under revision while I was away on internship at eleapPower. Thanks also to Stephen Aleje, Vishwa Perera, Juan Zuniga, Pasan Gunawarden, Sheron Bolonne, Anjana Wijesekera, and Ronald for your friendship. I would not forget Fr. Philip, Fr. Ben, Fr. David, Mr. and Miss. Ngoko, and Mr. and Miss. Yonga for the constant spiritual and moral support. May God reward you a thousand time.

Finally, I would like to thank the University of Alberta Future Energy System Fund, the Natural Science and Research Council of Canada, and eleapPower for funding my PhD research.

~ Marius Takongmo, August 2023.

Contents

List of Tables

List of Figures

xvi

xvii

Abbreviations

APOD-PWM	Alternate Phase Opposition Disposition
A_{CS}	Core cross-sectional area
A_w	Core window area
A_P	Core product area
B_{ave}	Average flux density
B_{HF}	High frequency flux density
B_{dc}	dc flux density
B_1	fundamental frequency flux density
B_{max}	Maximum flux density
B_{sat}	Saturation flux density
CI	Coupled Inductor
CM	Common mode
CB-PWM	Carrier-Based Pulse Width Modulation
DSP	Digital Signal Processor
DM	Differential mode
DPWM	Discontinuous Pulse Width Modulation
D_w	Diameter of a winding
FPGA	Field-programmable Gate Array
$f_1 = f_f$	Fundamental frequency
f_s	Supply frequency
f_c	Carrier frequency
ILPP	Inverter Leg Per Phase
$i_a = i_{phA}$	Phase current
$i_{cir} = i_{a1,c}$	Circulating current

I_{dc_offset}	Parasitic dc offset current
J	Current density
K_1	Intra-limb coupling coefficient
K_2	Inter-limb coupling coefficient
K_w	Window utilization factor
LS-PWM	Level-Shifted PWM
L_w	Coupled inductor winding inductance
L_e	Coupled inductor leakage inductance
L_m	Coupled inductor magnetizing inductance
L_L	Coupled inductor effective series inductance
L_{CM}	Inductance on the part of common mode circulating currents
L_{DM}	Inductance on the part of differential mode circulating currents
ma	Amplitude modulation index
M_DPWM	Modified Discontinuous Pulse Width Modulation
M_SPWM	Modified Sinusoidal Pulse Width Modulation
M	Mutual inductance
MLT	Inductor mean length turn
NPC	Neutral Point Clamped
N_T	Inductor number of turns
PWM	Pulse Width Modulation
PD-PWM	Phase Disposition pulse width modulation
POD-PWM	Phase Opposition Disposition pulse width modulation
PLECS	Piecewise linear electrical circuit simulation
PS-PWM	Phase shift pulse width modulation
P_{out}	Output power

P_{core}	Inductor core losses
P_{cu}	Inductor copper losses
ϕ	flux
SHE	Selective Harmonic Elimination
SVC	Space Vector Control
SVM	Space Vector Modulation
SPWM	Sinusoidal Pulse Width Modulation
v_{pha}	PWM phase voltage
V_{line}	PWM line voltage
v_{ab}	Voltage difference between two phases
VSC	Voltage source converter
V_{CM}	Common mode voltage
V_{DM}	Differential mode voltage
v_P	Fundamental voltage drop across an inductor winding
ΔT	Temperature rise
μ	Permeability of free space

Chapter 1

Introduction

As the world moves toward green energy generation and consumption, the significance of power electronics converters grows greater day by day. The conventional six switch voltage source converter (VSC) has been the workhorse of many industrial applications for decades. However, as the power and voltage level of application increases, and as the restrictions on the qualities of the converters become stricter, the conventional six switch VSC becomes less preferred [6]-[18]. Also, there is a growing need for VSCs with power ratings ranging from 10 kW to 3MW capable of supplying high quality high frequency fundamental output voltages in the kilohertz range for high/ultra-high-speed machines [19]-[23].

The rated power of an energy conversion unit can be increased by increasing the system voltage or current. The former can be achieved using multi-level voltage source converters, a few include active neutral point clamped converters (ANPC), cascaded H-bridges. This is because they can deal with higher voltages that are shared among a high number of semiconductor switches [24]-[36]. The main drawbacks of these multi-level converters are their use of many capacitors which require a complex control mechanism to regulate their voltages and the need for numerous isolated dc sources [37].

Two level voltage source converters or inverter legs can be connected in parallel to increase the current rating of a power converter [38]-[47]. This approach has numerous attractive features such as sharing the load current between the converters and the production of multi-level pulse width modulated (PWM) outputs with voltage steps lower than the dc-link voltage. These PWM outputs generate less audible noise, less electromagnetic emissions (EMI), and very low rate of change of voltage ($dv/_{dt}$) because of the smaller voltage steps. In addition, the frequency of the converter PWM outputs is much higher than the converter switching frequency. In consequence, interleaved PWM switching converters can operate with smaller switching frequencies while enhancing the converter output qualities. Most importantly, modular designs can be used that allow, the

implementation of fault-tolerant techniques to guarantee high reliability. However, the voltage difference between the output terminals can create circulating currents between parallel modules. These circulating currents can lead to unbalance current stress, uneven distribution of the load currents between the parallel-connected converters, and low converter efficiency. Isolating transformers and inductors can be used to suppress the flow of circulating currents between the converters, but they can be bulky and increase the overall size/weight of the power converter.

Paralleling several switching devices in a six-switch VSC is another way of increasing the output current of a power converter. Nevertheless, semiconductor mismatches which is inevitable may lead to additional switching and conduction losses [48]-[50].

1.1. Technology related to parallel connected VSCs

Magnetic configurations, advanced PWM schemes and control algorithms have been topics of research over the years to control the flow of circulating current between interleaved PWM switching converters while reducing the size and weight of passive devices like transformers, filter inductors, and capacitors.

1.1.1. Magnetic configurations

The circulating current between parallel inverter legs can be suppressed by introducing an impedance in the circulating current path. This can be done using ac filter inductors, see Fig. 1.1 (a). However, a high value of inductance is required to achieve a reasonable suppression of the circulating currents which then leads to slow transient response. In addition, ac filter inductors experience a significant fundamental voltage drop across their windings which is not desirable. Most importantly, their size/weight are directly proportional to the peak of the fundamental frequency ac currents which in turns produces fundamental flux in the inductor magnetic core [51]-[53].

Wye-delta transformers can be used to electrically isolate parallel-connected converters and to prevent the flow of circulating currents between them, Fig. 1.1 (b), [54]. However, such low frequency transformers can be massive, bulky, and expensive. A common mode (CM) choke can be placed on the dc side of each converter to suppress the flow of circulating currents, Fig. 1.1 (c). Nevertheless, this approach increases the number of magnetics structures in the systems [55].

(a)   (b)   (c)
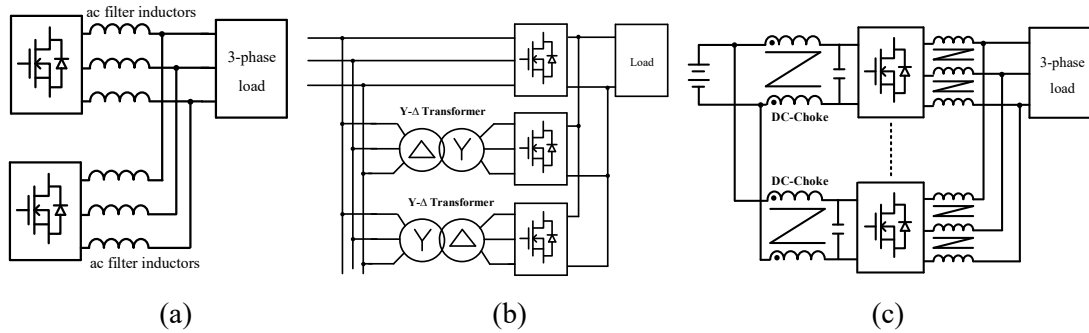
Fig. 1.1 Magnetics in high power converters (a) ac filter inductors, (b) Y-Δ transformers, (c) dc-chokes.

Inter-cell transformers and multi-limb coupled inductors can be used to reduce the size of the magnetics required to average the outputs of interleaved PWM switching converters, Fig. 1.2 (a). These magnetic structures present a low series output inductance, related to the leakage inductance of the coupled windings, to the flow of balanced ac currents. However, they present a very high inductance, related to the magnetizing inductance of the coupled windings, to the flow of unbalanced currents or circulating currents between the converters. Most importantly, fundamental flux produced by the flow of ac currents cancels in the magnetic core of coupled inductors [46], [56]-[66]. Consequently, the size, weight, and cost of coupled inductor cores can be reduced as a result of their size being directly related to the high-frequency switch mode voltages imposed across the inductor windings which produce high frequency flux in the core. The windings of widely used conventional coupled inductors are loosely coupled and have large a leakage flux especially when wound on a large magnetic core [46], [56]-[65]. This is the result of having windings located on different limbs of the magnetic core. The higher leakage flux produces electromagnetic emissions (EMI) which are not environmentally

friendly. In addition, the inductance associated with this leakage flux, hence leakage inductance, determines the series output inductance of the coupled inductors. Fundamental currents flowing through large leakage inductances can produce a significant fundamental voltage drop across the coupled inductor windings. The voltage drop increases as the magnitude, the phase-shift angle, and the frequency of the fundamental current increases, leading to an increase in the peak flux and the required size/weight of the core.

Magnetic structures that integrate coupled inductor and ac filter inductors, integrated inductors, can be used to significantly reduce the size and weight of the magnetics in parallel-connected VSCs, see Fig. 1.2 (b) & (c), [66]–[68]. However, the proposed inductors use nonstandard magnetic cores and often have coupled windings located on separate limbs.

(a)   (b)

(c)
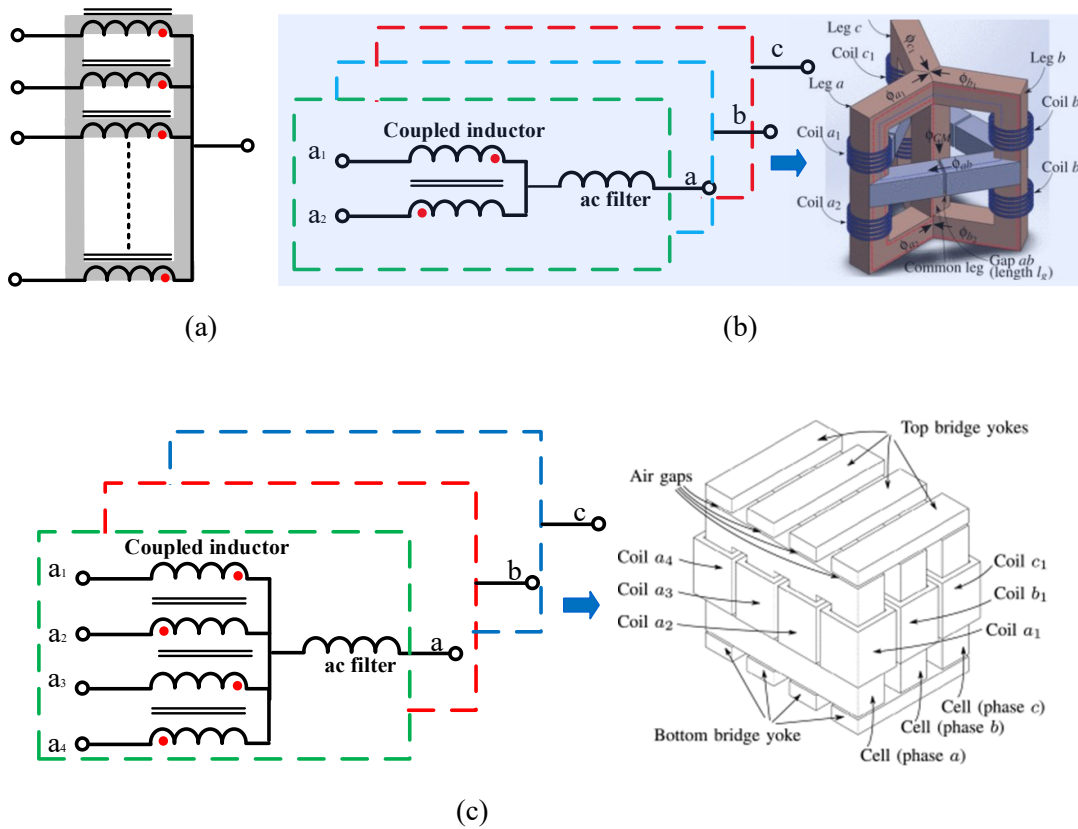
Fig. 1.2 Multi-limb inductors (a) multi-limb coupled inductor, (b) integrated inductors for dual converters (c) integrated inductors for four parallel connected converters [66]–[68].

4

A C-core can be attached to a three-limb core to provide a path for common mode (CM) flux, Fig. 1.3. The combined inductor structure faces the challenge of achieving symmetry in the magnetic paths [69].
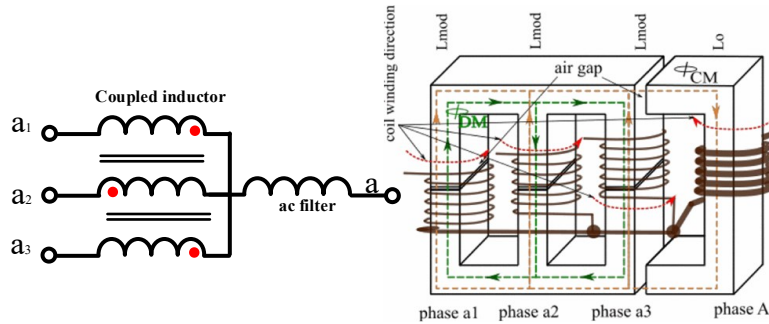
Fig. 1.3 Combined inductor.

A 3-limb coupled inductor (CI) and an ac common mode choke with six coupled windings were introduced to separately suppress the flow of differential mode (DM) and common mode (CM) circulating currents between two interleaved PWM switching converters [70]-[71]. The combined mass of the two magnetic structures described (CM & DM filters) is smaller than that of three separate coupled inductors (CIs) which can suppress both common mode and differential mode circulating currents. The ac choke has coupled windings located on different limbs of a C-shaped core or toroid, inter-limb coupled windings with large leakage inductances. The coupled inductor can experience a significant fundamental voltage drop especially when used to generate high frequency fundamental outputs. Two three-limb coupled inductors were used to suppress the flow of positive and negative sequence harmonic currents in three voltage source converters connected to separate dc links. The system was designed for electrically isolated inverters and not intended to filter common mode PWM voltages between the converters [72].

A very interesting filter building block was introduced for an arbitrary number of parallel-connected voltage source converters [73] – [75]. The filter block is composed of series-connected common mode and differential mode inductors having coupled windings located on different limbs of the magnetic core. The filter block has a relatively high series output inductance related to high inter-limb leakage inductance of the series connected coupled inductors. Consequently, they would equally experience a significant fundamental

voltage drop across their windings when generating high frequency fundamental outputs in the kilohertz range. The filter block is suitable for converters, which produce low-frequency fundamental output voltages like grid connected converters.

1.1.2. Modulation techniques

An overview of the several modulation techniques for parallel connected voltage source converters is presented. The on/off state of semiconductors in a power converter is determined by the modulation technique. Many PWM techniques have been investigated over the years and can be grouped into fundamental and high frequency modulation techniques. The former includes selective harmonic elimination (SHE), and space vector control [76]-[79]. SHE eliminates certain harmonics from the converter outputs which are difficult to filter. The latter includes space vector pulse width modulation (SV-PWM) and the carrier-based pulse width modulation (CB-PWM) [80]-[84]. The carrier-based pulse width modulation scheme can further be classified into level-shifted pulse width modulation (LS-PWM) [85]-[92] and phase-shifted pulse width modulation (PS-PWM) [93]-[96]. The level-shifted pulse width modulation includes phase-disposition PWM (PD-PWM), phase-opposition disposition PWM (POD-PWM) and alternative phase-opposition disposition PWM (APOD-PWM). When sinusoidal references are used the carrier-based pulse width modulation (CB-PWM) is referred to as sinusoidal PWM (SPWM) [97]. When the reference signals are discontinuous, the CB-PWM is referred to as discontinuous PWM (DPWM) [98],[100]. A commonly used DPWM scheme is the 60^0 clamped DPWM scheme.

Space vector PWM (SVPWM) based techniques produce high quality waveforms by using the nearest three vector approach. The subsector in which the reference space vector resides at a given time must be identified, which is not a trivial task especially for voltage source converters with numerous interleaved PWM switching inverter legs. Additionally, during the implementation of a space vector PWM scheme on hardware such as a DSP, the dwell times calculated from the space vector PWM must almost always be converted into reference signal values. These need to be compared against a carrier signal to determine the switching instances.

Carrier-based pulse width modulation (CB-PWM) are less complex when compared with space vector PWM and can easily be developed for voltage source converters with any arbitrary number of parallel-connected inverter legs. Level-shifted pulse width modulation (LS-PWM) produces high-quality outputs like the space vector PWM but cannot be applied directly to converters with interleaved PWM switching inverter legs. This is because it would drive huge dc and ac circulating currents at the fundamental frequency between them [101]. Phase-disposition PWM (PD-PWM) with double commutations at the zero crossover of the reference signals was proposed to mitigate the injection of direct-current voltages in coupled inductors during band transitions, thereby suppressing circulating currents [86]. An alternative phase disposition PWM injects a square wave into the reference signals and uses state machine postprocessing to correct the switching patterns of each inverter leg [87]. Similarly, a single carrier can be used to control the switching of each inverter leg in each phase of a voltage source converter for flux-balancing control. The reference signals are modified during band transitions to balance the flux in the coupled inductors and produce a smooth transition as the reference signals move between the modulation bands [88]. Sinusoidal PWM (SPWM) uses phase-shifted carriers to produce evenly spaced inverter leg switching patterns, but the highest quality multilevel three-phase line voltages are not achieved due to poor alignment of the line voltage PWM switching patterns. This can be improved using a modified SPWM (M-SPWM) that controls the switching of each inverter leg by swapping between two sets of phase-shifted carrier signals, carrier swapping, in relation to the magnitude of the modulating signals in each phase [5], [101]. An alternative approach manipulates the modulating reference signals based on phase shifted PWM [9], [102]. Both approaches use relatively straightforward digital techniques but cause the circulating current and the flux in interface coupled inductors to experience jumps and dc offsets, thereby increasing the required size/weight of the converter magnetics. Reference modification techniques were implemented to generate high quality PWM outputs using the space vector PWM scheme without causing the circulating current or the flux in the interface inductor to experience a jump. However, the techniques proposed cannot be applied to converters with an arbitrary number of inverter legs [2], [6], [7]. Carrier transition techniques were developed to generate high quality multi-level PWM output

7

voltages. The carrier transition techniques can effectively be implemented with VSCs having an arbitrary number of parallel-connected inverter legs [8]. Discontinuous PWM schemes were investigated to reduce switching losses in VSCs. Modified discontinuous PWM schemes referred to as DPWM1, DPWM2 and DPWM3 were investigated to eliminate the common mode voltage between two interleaved PWM switching converters, making it feasible to use only a differential mode coupled inductor (3-limb coupled inductor) to average their outputs [103] – [108]. However, these discontinuous PWM schemes equally cause the circulating current between the VSCs to jump. The different PWM schemes developed for parallel-connected converters have been summarized in Fig. 1.4.
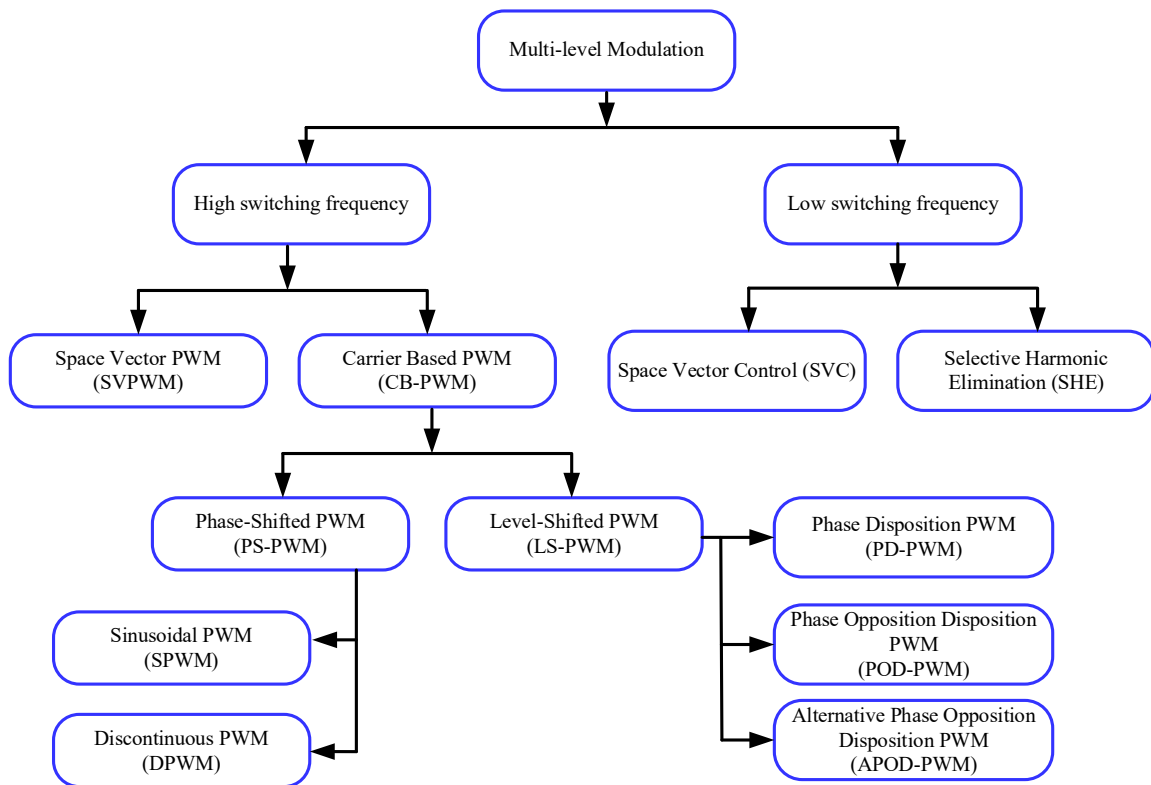
Fig. 1.4 Classification of modulation technique for parallel-connected VSCs.

1.1.3. Current control algorithm

It is important to make sure that the load current is evenly shared between the parallel-connected converters or inverter legs. This is mostly achieved using proportional-integral controllers [109]-[112]. A control scheme which involves changing the carrier frequency at any carrier cycle was investigated to achieve a rapid response of the current balancing controller which avoids long transitory over-currents on one converter or inverter leg [113]. Circulating currents between interleaved PWM switching voltage source converters can equally lead to uneven current sharing. A control algorithm was proposed to control the circulating current between interleaved PWM switching converters [114]-[118]. Coupled inductor winding arrangements are presented to guarantee an even distribution of the output currents between the parallel-connected inverter legs without the need for a current controller.

1.2. Research objectives and contribution

A central theme of the work presented is to develop high power highly reliable non isolated voltage source converters (VSCs) with a reduced footprint by reducing the size/weight of the magnetics. Novel coupled inductor (CI) winding configurations, coupled inductor arrangements, and advanced PWM techniques are thoroughly investigated to reduce the peak flux, size, and weight of the magnetics in high power converters which often constitute more than 50% of the system's size and weight.

1.2.1. Cross-coupled inductors

Interleaved PWM switching of two-level inverter legs connected to coupled inductors having crossed-coupled windings is investigated to significantly reduce the series inductance as seen at the output of each phase of the converter. Balanced ac currents flowing through the inductor windings produce an insignificant fundamental voltage drop. This results in an insignificant fundamental flux in the inductor magnetic core which reduces the peak flux and the size/weight of the inductors. The low series output inductance

produced by the cross coupled windings equally favors rapid transient response and makes it feasible to generate high-frequency fundamental multi-level PWM output voltages in the kilohertz range with a very small fundamental voltage drop across the coupled inductors.

1.2.2. DC common mode choke and ac differential mode inductor

A common mode dc-choke and a differential mode coupled inductor, 3-limb CI, are examined to separately filter the common mode and differential mode components of the switched mode voltages experienced between two 180^0 interleaved PWM switching converters connected to the same dc-link. The peak flux produced by the separate common mode and differential mode components of the switched mode voltage between the two converters is smaller than the peak flux with the common mode and differential mode combined. Consequently, the size and weight of the two coupled inductor type (dc-choke, 3-limb CI) is smaller when compared with using three conventional coupled inductors, designed to absorb both common mode and differential mode PWM voltages together. The coupled inductor arrangement considered is useful to increase the power density of interleaved PWM switching voltage source converters by reducing the size/ weight of the converter's magnetics, reduce common mode to ground noise in uninterrupted power supplies and motor drives, reduce cable interactions, and generate multi-level PWM outputs voltages with voltage step much smaller than the dc-link voltage.

1.2.3. Neutral point clamped CI converters

Neutral point clamped (NPC) coupled inductor converters with inner high-frequency modules are examined for high voltage high current applications such as ultra fast electric vehicle chargers and electric drives. The NPC converters reduce the voltage stress across of all the converter switching devices to $V_{dc}/2$ which lowers switching losses and reduces the voltage stress across the windings of the coupled inductors. The low inductor voltage stress lowers the peak flux and the size/weight of interface coupled

inductors (CIs) when compared with that of other converters designed to operated with the same dc-link voltage. The first NPC converter examined, unidirectional converter, has a reduced switch count and produces more voltage levels at the CI outputs terminals when compared to other converters having the same number of semiconductor switching devices. Such multi-level PWM output voltages can easily be filtered with a much smaller ac inductance thereby reducing the size/weight of the overall converter. A second NPC converter examined, bidirectional converter, has two inner connected interleaved PWM switching modules connected to a 3-limb interface coupled inductor. A 3-limb core can be smaller than using three conventional C-shaped cores. A PWM scheme that produces no common mode voltage between the inner inverter modules is used to operate the bidirectional converter.

1.2.4. DPWM control for NPC CI converters

A discontinuous PWM, DPWM, control is investigated to reduce the peak flux and the size/weight of the magnetics in a 3-phase coupled inductor neutral point clamped converter having inner switching modules. The discontinuous PWM control ensures that the flux/circulating current patterns remain centered on zero with no jumps; thereby reducing the peak flux and the required size/weight of interface coupled inductors in high voltage, high current voltage source converters.

Chapter 2

Two Level VSCs using cross coupled inductor windings

The electrical model of inductors having cross coupled windings (cross coupled inductors) and their performance are examined and compared with that of conventional coupled inductors (CIs) used to average the outputs of voltage source converters (VSCs) having parallel-connected 2-level inverter legs in each phase. The flux and circulating current ripple in the two inductor types are examined. Cross coupled inductors have very low series output inductances when compared with conventional coupled inductors. Consequently, they can be used to significantly lower the fundamental voltage drop at the phase output terminals. This is closely related to lowering the peak flux in the magnetic core of interface inductors and reduces the size/weight of the magnetic core required to prevent saturation.

2.1. Interleaved PWM for 2-level inverter legs

Two level inverter legs can use interleaved PWM switching in each phase of a three-phase system using coupled inductors (CIs) to produce multi-level PWM output voltage waveforms. This has numerous attractive features such as modularity, high reliability and semiconductor devices having lower current ratings. When n-inverter legs are connected in parallel in each phase, n-evenly phase-shifted carriers are used
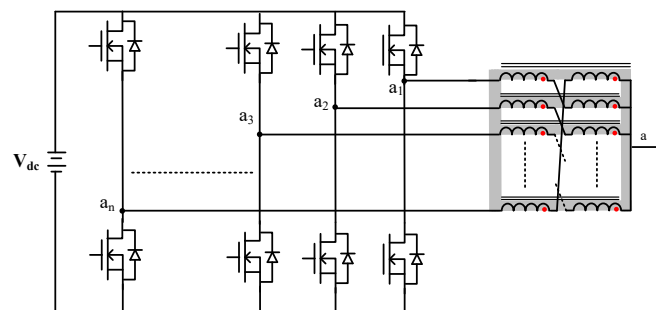
Fig. 2.1 n^{th} interleaved inverter legs with coupled inductors in each phase of a VSC.

to generate n+1 level phase (v_{pha}) and 2n+1 PWM line voltages (v_{line}). In addition, the frequency of the PWM line voltage is 2n times greater than the inverter switching frequency (f_s). The phase-shift angle of the carriers used for an arbitrary number of interleaved inverter legs are presented in Table 2.1. Where n refers to the number of parallel-connected inverter legs per phase (ILPP). Multi-level outputs have a reduced harmonic content and can easily be filtered using small ac inductances. The number of output levels is equally related to the amplitude modulation index (ma), see Fig. 2.2 and Fig. 2.3. These multi-level outputs have PWM voltage steps much smaller than the dc-link voltage. The quality of a converter output can be appreciated using the harmonic volt-second of the PWM line voltage and the converter current total harmonic distortion (THD).

Table 2.1: Phase-Shifted Carriers for Interleaved VSCs

Number of ILPP	Phase-shifted carrier
2	0^0, 180^0
3	0^0, 120^0, 240^0
4	0^0, 90^0, 180^0, 270^0
n	$360 \times [0, \frac{1}{n}, \frac{2}{n} \dots, \frac{n-1}{n}]$
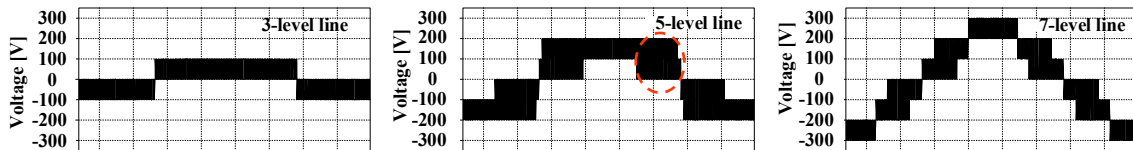
Fig. 2.2 Output waveforms of a VSC having three parallel-connected inverter legs in each phase, V_{dc} = 300 V, f_s = 20 kHz, (a) ma = 0.2, (b) ma = 0.5, (c) ma = 1.1.
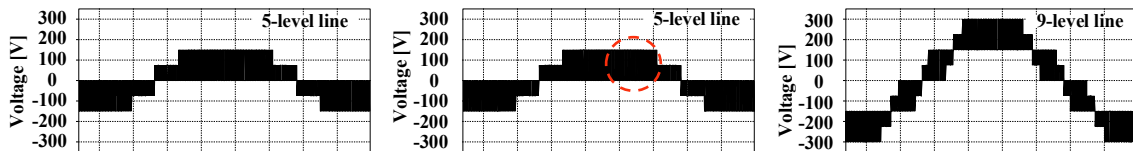
Fig. 2.3 Output waveforms of a VSC having four parallel-connected inverter legs in each phase, V_{dc} = 300 V, f_s = 20 kHz, (a) ma = 0.2, (b) ma = 0.5, (c) ma = 1.1.

13

The quality of multi-level voltages increases as the number of parallel-connected inverter legs/levels increases. However, the small improvement of the quality of the PWM line voltage does not justify the use of more than four inverter legs in each phase of a three-phase system, see Fig. 2.4. When the amplitude modulation index (ma) is between 0.65 and 1, the harmonic volt-second of the converter PWM line voltage having four inverter leg per phase (ILPP) is greater than that of a converter having three parallel-connected inverter legs per phase. This is because a significant portion of PWM line voltage of the converter having three interleaved PWM switching inverters legs has a voltage step of $2V_{dc}/3$ and the frequency of the PWM line voltage is three times greater than the carrier/ switching frequency. However, the voltage step of the converter having four interleaved PWM switching inverters legs is smaller ($V_{dc}/2$) and the frequency of the PWM line voltage is four times greater than the carrier switching frequency, Fig. 2.2 and Fig. 2.3.
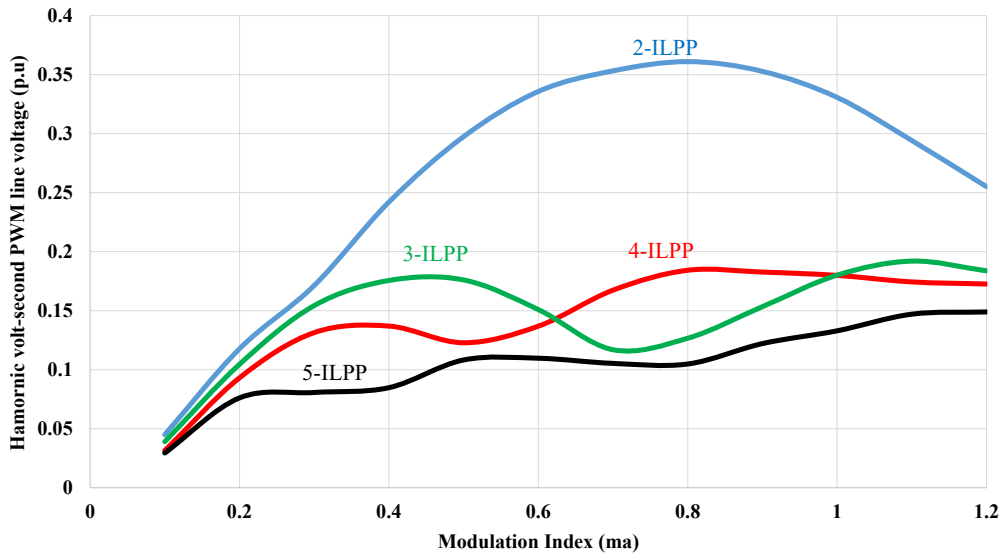
Fig. 2.4 Harmonic volt-second of the PWM line voltage (p.u), $V_{dc} = 300$ V, $f_s = 20$ kHz.

Fundamental flux produced by the flow of ac currents cancels in the magnetic core of coupled inductors, so the size and weight of coupled inductors can be greatly reduced as a result of their size being directly related to the high frequency switch mode voltages across their windings which produce high frequency flux in their magnetic core. However, conventional coupled inductors with their loosely coupled windings (windings located on different limbs of the core) can still experience a significant

14

fundamental voltage drop (v_d) across their windings as a result of ac currents (i_{ac}) flowing through the large leakage inductances (L_e). The fundament voltage drop (v_d) across the coupled inductor windings, expressed as (2.1), increases as the magnitude, frequency (f_f) and the phase-shift (α) between the fundamental ac currents and voltage increases. The fundamental voltage drop could increase the peak flux (ϕ) and the required size of the inductor magnetic core. In addition, conventional coupled inductors generate a lot of electromagnetic emissions which is related to the large leakage flux and are not environmentally friendly.

$$v_d = 2\pi \times f_f \times L_e \times |i_{ac}| \sin(\theta - \alpha) \qquad (2.1)$$

Inductors with cross coupled windings are investigated to mitigate the drawbacks of conventional coupled inductors. When using a 3-limb inductor, the winding arrangement is very similar to that of zig-zag transformers which are often used as ground transformers in power systems with the significant difference that cross coupled inductors are used in separate phase of the voltage source converter [119], [120]. Zig-zag transformers have equally been used in numerous industrial applications to improve the power factor of a high-power AC-DC converter [121]. These transformers can be used to mitigate voltage disturbance caused by single-phasing in a 3-phase system [122]-[124]. Zig-zag connected transformers have been used in an isolated multi-level inverter composed of four voltage source converters to reduce the number of transformers as well as the current and voltage stress across their windings [125]. A high-frequency zig-zag transformer was proposed to average the outputs of interleaved DC-DC converters (Boost, Buck) [126].

2.2. Coupled inductors with cross coupled windings

Cross coupled inductors can be used separately in phase of a voltage source converter to generate multi-level output voltages while reducing the fundamental voltage drop at the phase output terminal. These inductors have two windings on the same limb of the core which are tightly coupled to significantly reduce leakage flux and the associated leakage inductance (L_e). The inductor winding arrangement can be

implemented using either multi-limb core or modular and commercially available off-the-shell magnetic cores. Fundamental flux cancelation in cross coupled inductors can be explained using Fig. 2.5. Note that the flow of fundamental ac currents (i_1, i_2) produces no flux in the magnetic core, if they have the same magnitude and are in phase, see the dot notation in Fig. 2.4. The low leakage inductance reduces the series output inductance of the coupled inductor, making it feasible to generate high frequency fundamental multi-level PWM output voltages with a very small fundamental voltage drop across the inductor windings. The inductance experience between the inverter leg terminals (a_1, a_2) is related to the relatively large magnetizing inductance of the coupled windings and can be used to suppress the flow of unbalanced or circulating currents. Also, since the coupled inductor magnetizing inductance is significantly larger than the series output inductance, the load current can evenly be shared between the two parallel paths without the need for a current controller.

Coupled inductors with cross-coupled windings on a C-shaped magnetic core were used to average the outputs of a converter having two interleaved PWM switching inverter legs per phase, see Fig. 2.6 [6], [11]. The system produced 3-level phase (v_{pha}) and 5-level PWM line voltages (v_{line}). Cross-coupled windings on a standard 3-limb core were used in each phase of a 3-phase system to produce 4-level phase and 7-level PWM line voltages, Fig. 2.7 [1], [3], [7], [8]. Cross-coupled windings on modular C-shape cores connecting the output of four interleaved PWM switching inverter legs in each phase of a 3-phase voltage source converter were investigated to generate 5-level phase and 9-level PWM line voltages, see Fig. 2.8 [5].
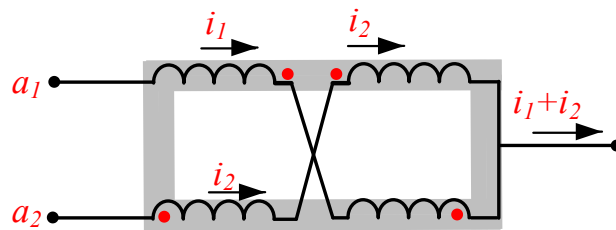
Fig. 2.5 Fundamental flux cancelation in CIs with cross coupled windings.

Cross-coupled windings on modular C-shape cores are more convenient when designing converters with more than three interleaved PWM switching inverter legs. The coupled inductors (CIs) average the outputs of the inverter legs in each phase to produce multi-level phase output voltages. The muti-level voltage at the output of each inductor and the output current can be expressed as (2.2) and (2.3) respectively. The characteristics of cross coupled inductors can be examined using their electrical model. Where v_{ax} and i_{ax} are respectively the output voltage and output current of each inverter leg.
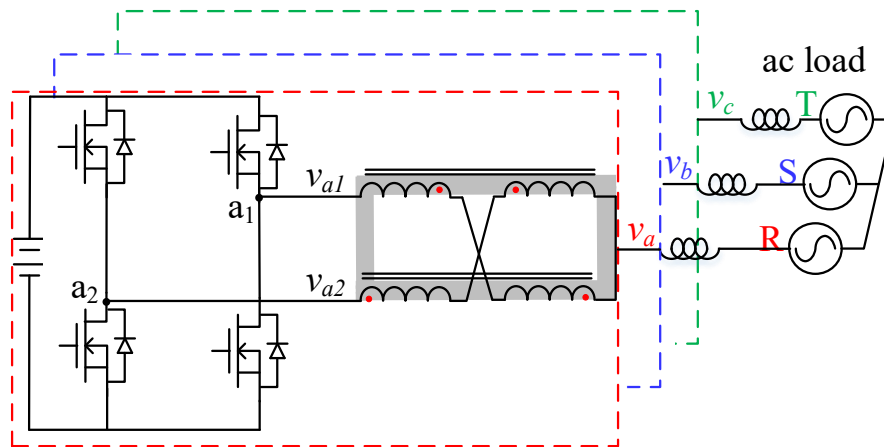
(a)
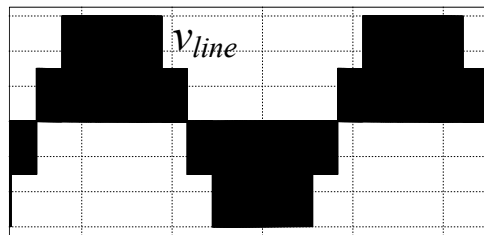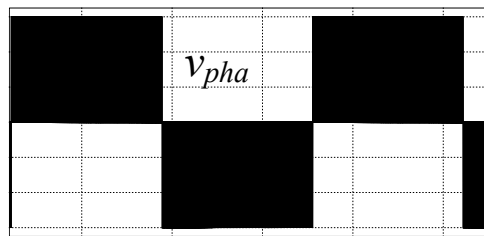
(b)

Fig. 2.6 Coupled inductor VSC with two interleaved inverter legs per phase (a) circuit diagram (b) output voltage waveforms.

17
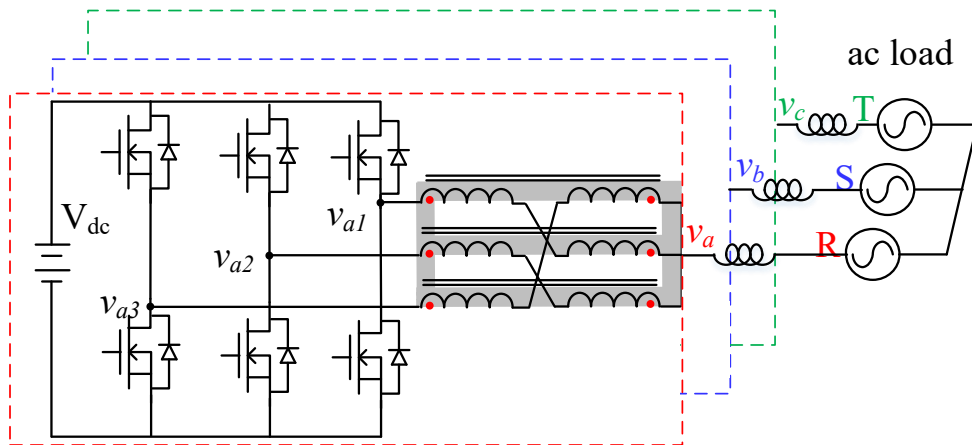
(a)
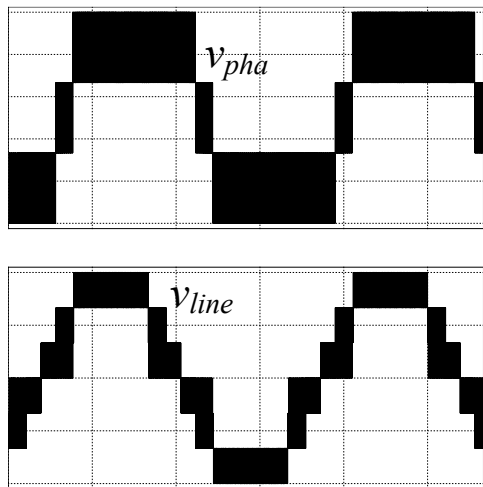
(b)

Fig. 2.7 Coupled inductor VSC with three interleaved inverter legs per phase (a) circuit diagram (b) output voltage waveforms.

18
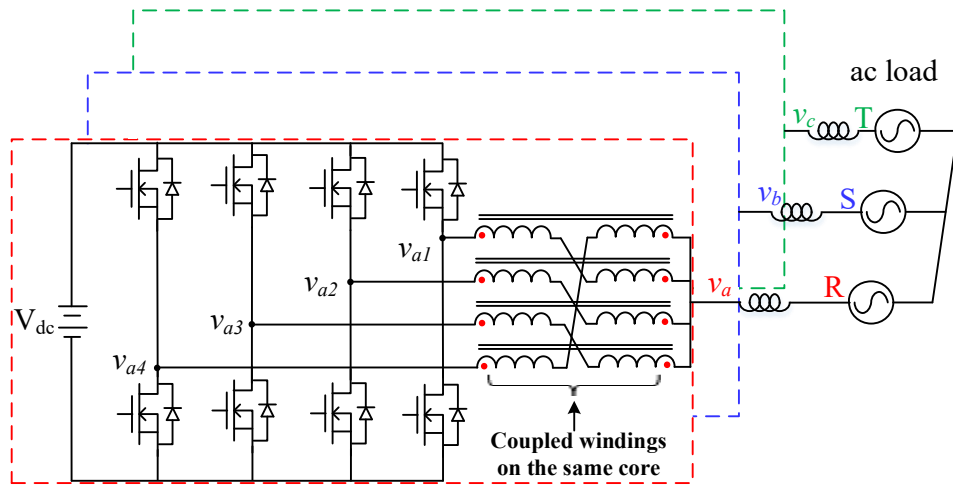
(a)
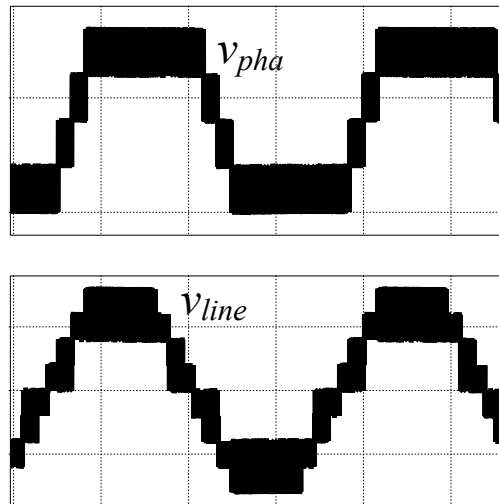
(b)

Fig. 2.8 Coupled inductor VSC with four interleaved inverter legs per phase (using modular C-shaped cores) (a) circuit diagram (b) output voltage waveforms.

$$v_{pha} = \frac{1}{n} \sum_{x=1}^{n} v_{ax} \qquad (2.2)$$

$$i_a = \frac{1}{n} \sum_{x=1}^{n} i_{ax} \qquad (2.3)$$

2.3. Electrical model of coupled inductors for VSCs having parallel-connected inverter legs in each phase

The fundamental characteristics of coupled inductors is to present a high inductance between the output terminals of parallel-connected inverter legs in each phase of a 3-phase system and a low series inductance at the phase output terminal. The large inductance between the inverter legs reduces the peak-to-peak circulating current ripple and losses. The electrical model compares the series output inductance (L_L), the effective inductance between inverter legs (L_{cir}), and the peak circulating current ripple in conventional coupled inductors and cross coupled inductors.

2.3.1. Two inverter legs

Conventional coupled inductors (CIs) for connecting two inverter legs have two coupled windings located on separate limbs of a C-shaped magnetic core. Cross coupled inductors would have four windings wound such that two windings are connected in series but located on separate limbs of a C-shaped magnetic core. The analysis assumes that the four windings have the same number of turns (N), Fig. 2.9 (a), and the base inductance (L_w) is the inductance of one winding when only that winding is excited, while the remaining windings are open circuited. We equally assume the conventional coupled inductors have windings with the same number of turns (2N), see Fig. 2.9 (b).

(a) (b)
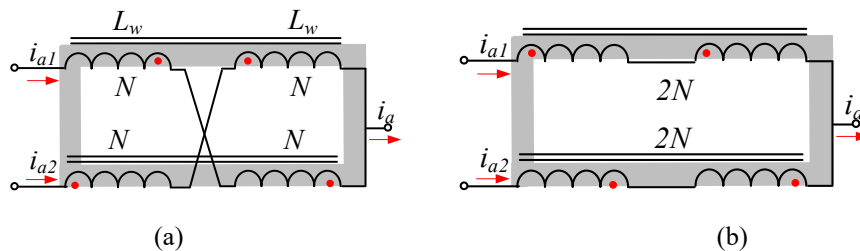
Fig. 2.9 Coupled inductors for VSCs having two parallel-connected inverter legs in each phase (a) cross coupled inductors (b) conventional coupled inductors.

Fundamental ac currents (i_{a1}, i_{a2}) flowing through both inductor types would produce a balanced ampere-turn (Ni) in the magnetic core and would not produce flux in the magnetic core, see Fig. 2.10. These currents would flow through the leakage inductance of the coupled inductors. The series output inductance (L_L) of both inductor types, expressed as (2.4), is related to the leakage inductance of the coupled windings. Conventional coupled inductors with windings located on separate limbs of the core (inter-limb coupled windings) have relative larger leakage inductances (L_{e_C}) when compared with cross coupled inductors (intra-limb coupled windings) ($L_{e_{cs}}$).

Unbalanced current or circulating currents (i_{cir1}, i_{cir2}) would flow between the inverter legs and would produce flux in the magnetic core of both inductor types. Since these currents do not flow to the load, their algebraic sum equals to zero. The inductance of one winding (L_w) in both inductor types when only that winding is exited while the others are not can be expressed as (2.5); where R_{leg} is the reluctance of each limb of the magnetic core, see Fig. 2.11 (a). The circulating currents flow through the four coupled windings connected in series, Fig. 2.11 (b). The flux linkage and the inductance (L_{cir}) associated with circulating currents flow can be expressed as (2.6) derived from Faraday's law. Hence, the effective inductance of both inductor types between the inverters relative to the inductance of one winding can be determined as (2.7). The two coupled inductor types can equally be modeled in a simulation software using (2.8), where k1 and k2 are respectively the inductor intra-limb and interlimb coupling coefficients.

(a)   (b)
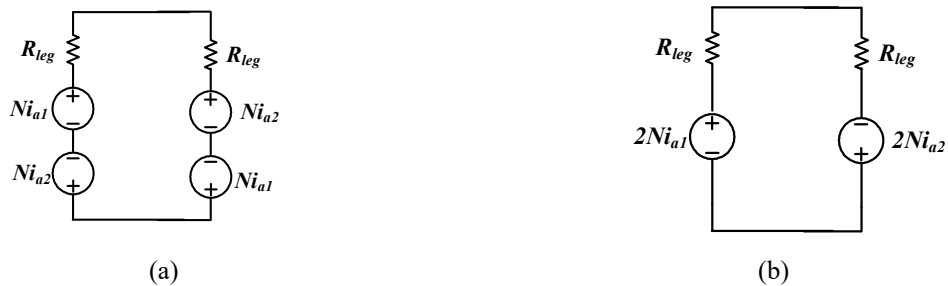
Fig. 2.10 Coupled inductors for connecting two inverter legs (a) cross coupled inductors (b) conventional coupled inductors.

$$L_L = \begin{cases} L_{e_C}, & conventional\ inductors \\ L_{e_{cs}}, & cross\ coupled\ inductors \end{cases} \qquad (2.4)$$
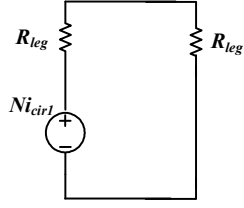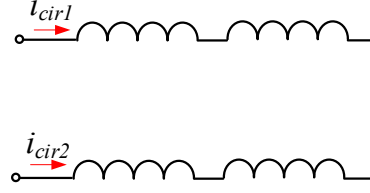
(a)   (b)

Fig. 2.11 Coupled inductors equivalent circuit (a) magnetic circuit showing one exited winding (b) path for unbalanced or circulating currents.

$$L_w = \frac{N^2}{2R_{leg}} \tag{2.5}$$

$$L_{cir}(i_{cir1} - i_{cir2}) = 4N\left(\frac{4Ni_{cir1}}{2R_{leg}} - \frac{4Ni_{cir2}}{2R_{leg}}\right)$$

$$= \frac{8N^2}{R_{leg}}(i_{cir1} - i_{cir2}) \tag{2.6}$$

But $\quad R_{leg} = \frac{N^2}{2L_w};$

Hence, $\quad\quad L_{cir} = 16L_w \tag{2.7}$

$$\boldsymbol{L} = L_w \times \begin{bmatrix} 1 & k_1 & k_2 & k_2 \\ k_1 & 1 & k_2 & k_2 \\ k_2 & k_2 & 1 & k_1 \\ k_2 & k_2 & k_1 & 1 \end{bmatrix} \tag{2.8}$$

For the worst-case scenario both coupled inductor types would experience a voltage step of V_{dc} for half the switching cycle across their terminals (a_1, a_2). Consequently, the peak-to-peak circulating current ripple ($i_{cir_{pk}}$) between the parallel-connected inverter legs can be expressed as (2.9); where fc is the converter carrier frequency. The inductor model reveals that both inductor types for a converter having two parallel-connected inverter legs per phase would provide approximately the same inductance between the inverters. However, cross coupled inductors would have a much small series output inductance related to the intra-limb leakage flux as opposed to the much larger interlimb leakage inductance associated with the conventionally wound coupled inductor.

$$i_{cir_{pk}} = \frac{V_{dc}}{32 \times L_w \times f_c} \qquad (2.9)$$

2.3.2. Three inverter legs

Conventional coupled inductors connecting three inverter legs in each phase of a 3-phase system has one winding located on each limb of a 3-limb core. Cross-coupled inductors would have two windings on each limb; two connected in series but located on separate limbs of a 3-limb core, Fig. 2.12 (a). The analysis assumes that all the six coupled windings of the cross coupled inductor have the same number of turns (N), have an insignificant winding resistance, and the base inductance (L_w) is the inductance when only one winding is exited and the other windings are open circuited. We equally assume that the windings of the conventional inductor have the same number of turns, one winding per limb with 2N turns, see Fig. 2.12 (b).

Balanced ac currents (i_{a1}, i_{a2}, i_{a3}) flowing through both inductor types would produce equal and opposite ampere-turns (*Ni*) in each limb, Fig. 2.13 (c) and (d). These currents could flow through the inductor leakage inductances and would not produce flux in the magnetic core. The series output inductance (L_L) of both inductor types expressed as (2.10) is related to their leakage inductances. Conventional coupled inductors have large a leakage inductance (L_{e_C}) associated with their low inter-limb coupling coefficients when compared with that of cross coupled inductor having intra-limb coupled windings ($L_{e_{CS}}$).

$$L_L = \begin{cases} \frac{L_{e_C}}{3}, & conventional\ inductors \\ \frac{L_{e_{CS}}}{3}, & cross\ coupled\ inductors \end{cases} \qquad (2.10)$$

(a)   (b)   (c)   (d)
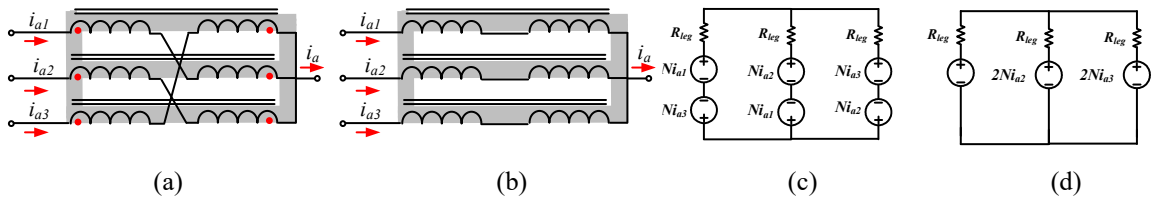
Fig. 2.12 Three limb coupled inductors (a) cross coupled inductors, (b) conventional inductor, (c) magnetic circuit of cross coupled inductors, (d) magnetic circuit of conventional coupled inductors.

Unbalanced or circulating currents would flow exclusively between the parallel-connected inverter legs and would produce flux in the inductor magnetic core. The circulating currents (i_{cir1}, i_{cir2}, i_{cir3}) flowing from the inverter output terminals (a_1, a_2, a_3) of phase "a", see Fig. 2.14 (a) and (b) adds up to zero since they do not flow to the load, see (2.11). If only one winding on both inductor types is excited while the other windings are open circuited, the flux (ϕ_z) produced by that winding can be expressed as (2.12), see Fig. 2.12 (c). The resultant winding inductance (L_w) can be determined as (2.13). The flux produced by the flow of two different currents in each limb of the cross coupled inductor (ϕ_1, ϕ_2, ϕ_3) can be expressed as (2.14). The effective inductance associated with the flux in each limb (L_{13}, L_{21}, L_{32}) can be determined with (2.15). These inductances can be three times bigger than the winding inductance of one winding.

(a)   (b)   (c)
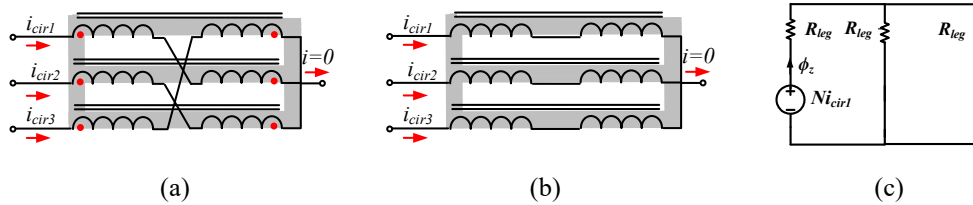
Fig. 2.13 Circulating current path in a 3-limb coupled inductor (a) cross coupled inductors, (b) conventional inductor, (c) magnetic circuit when only one winding is exited.

$$i_{cir1} + i_{cir2} + i_{cir3} = 0 \qquad (2.11)$$

$$\phi_z = \frac{N \times i_{cir1}}{1.5 \times R_{leg}} \qquad (2.12)$$

$$L_w = \frac{N^2}{1.5 \times R_{leg}} \qquad (2.13)$$

$$\left.\begin{array}{l} \phi_1 = \frac{N(i_{cir1} - i_{cir3})}{R_{leg}} \\[2mm] \phi_2 = \frac{N(i_{cir2} - i_{cir1})}{R_{leg}} \\[2mm] \phi_3 = \frac{N(i_{cir3} - i_{cir2})}{R_{leg}} \end{array}\right\} \qquad (2.14)$$

$$\left.\begin{array}{l} L_{13} = \frac{2N^2}{R_{leg}} \\[2mm] L_{21} = \frac{2N^2}{R_{leg}} \\[2mm] L_{32} = \frac{2N^2}{R_{leg}} \end{array}\right\}; \quad \text{But } L_w = \frac{N^2}{1.5 \times R_{leg}}$$

$$\text{Hence, } L_{13} = L_{21} = L_{32} = 3L_w \qquad (2.15)$$

The effective flux linkage ($L_{11}i_{cir1}$) associated with the flow of circulating current (i_{cir1}) through two series connected windings on different limbs can be expressed as (2.16), see Fig. 2.14 (a). The inductance associated with that flux linkage can be determined as (2.17). Consider the flow of circulating currents from one terminal (a_1) to the other terminals (a_2, a_3), see Fig. 2.14 (b); for the worst-case scenario, the two series connected windings through which i_{cir1} flows would experience a maximum voltage step of $2V_{dc}/3$ while the other windings sharing the circulating currents would experience a voltage step of $V_{dc}/3$ within one third a switching cycle, Fig. 2.14 (c). The effective inductance of cross coupled inductors between three parallel-connected inverter legs (L_{cir}) can be expressed as (2.18).
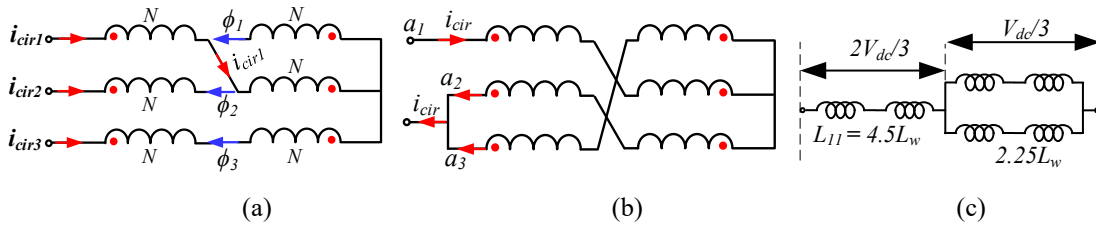
Fig. 2.14 3-limb inductor with cross coupled windings (a) flux in each limb of the core, (b) circulating current path, (c) equivalent circuit of the inductor between the inverter legs.

$$L_{11}i_{cir1} = N(\phi_1 - \phi_2) = N\left(\frac{N(i_{cir1} - i_{cir3})}{R_{leg}} - \frac{N(i_{cir2} - i_{cir1})}{R_{leg}}\right)$$

$$= \frac{N^2}{R_{leg}} (i_{cir1} - i_{cir3} - i_{cir2} + i_{cir1}) \qquad (2.16)$$

But, $i_{cir1} = -(i_{cir2} + i_{cir3})$ and $L_w = \frac{N^2}{1.5 \times R_{leg}}$

Hence, $L_{11} = 4.5 L_w$ $\qquad (2.17)$

$$L_{Cir} = 6.75 L_w \qquad (2.18)$$

The effective flux linkage ($L_{11}i_{cir1}$) associated with the flow of circulating current (i_{cir1}) through two series connected windings on the same limb, conventional coupled inductors, can be expressed as (2.19), see Fig. 2.15 (a). The inductance associated with that flux linkage can be determined as (2.20). When current flows from one terminal (a_1) of the 3-limb core to the other terminals (a_2, a_3), see Fig. 2.15 (b), the windings through which the circulating current (i_{cir1}) flows experience a maximum voltage step of $2V_{dc}/3$ while the other windings sharing the circulating currents experience a voltage step of $V_{dc}/3$ within one third a switching cycle, Fig. 2.15 (c). Consequently, the effective inductance of a conventional 3-limb coupled inductor between parallel-connected inverter legs (L_{cir}) can be expressed as (2.21). The effective inductances of both inductor types can equally be modelled in a simulation software using (2.22).
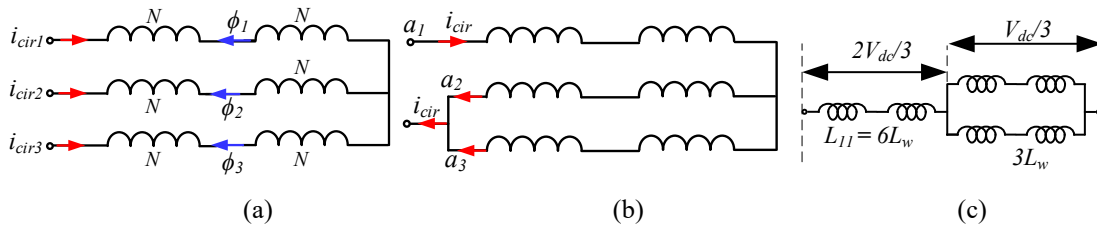
Fig. 2.15 Conventional coupled inductors (a) flux in each limb of the core, (b) circulating current path, (c) equivalent circuit of the inductor between the inverter legs.

$$L_{11}i_{cir1} = 2N\phi_1 = 2N\frac{2Ni_{cir1}}{R_{leg}} = 4N\frac{i_{cir1}}{R_{leg}} \qquad (2.19)$$

But, $L_w = \frac{N^2}{1.5 \times R_{leg}}$

Hence, $L_{11} = 6L_w$ $\qquad (2.20)$

26

$$L_{Cir} = 9L_w \tag{2.21}$$

$$\boldsymbol{L} = L_w \times \begin{bmatrix} 1 & k_1 & -k_2 & -k_2 & -k_2 & -k_2 \\ k_1 & 1 & -k_2 & -k_2 & -k_2 & -k_2 \\ -k_2 & -k_2 & 1 & k_1 & -k_2 & -k_2 \\ -k_2 & -k_2 & k_1 & 1 & -k_2 & -k_2 \\ -k_2 & -k_2 & -k_2 & -k_2 & -k_2 & k_1 \\ -k_2 & -k_2 & -k_2 & -k_2 & k_1 & 1 \end{bmatrix} \tag{2.22}$$

For the worst-case scenario, the voltage between three PWM switching inverter legs would experience a voltage step of V_{dc} for one-third the switching cycle, see Fig. 2.14 (c) and Fig. 2.15 (c). In consequence, the peak-to-peak circulating current ripple ($i_{cir_{pk}}$) between them can be expressed as (2.23).

The effective inductance of a 3-limb cross coupled inductor between the three parallel-connected inverter legs can be 25% smaller than that of a 3-limb conventional coupled inductor. However, the 3-limb cross coupled inductor would have a have a very small series output inductance (can be 3% that of a conventional inductor winding depending on the size of the core) which would significantly reduce the fundamental voltage drop across the inductor, lower the fundamental flux produced in the core, and increase dynamic response.

$$i_{cir_{pk}} = \begin{cases} \dfrac{V_{dc}}{40.5 \times L_w \times f_c} ; cross\ coupled\ inductors \\ \dfrac{V_{dc}}{54 \times L_w \times f_c} ; conventional\ inductors \end{cases} \tag{2.23}$$

2.3.3. More than three inverter legs

Modular inductors using C-shaped cores can be used with more than three inverter legs in each phase, Fig. 2.16 (a). Balanced ac currents flowing through the windings of the modular coupled inductors would produce equal and opposite magnetic ampere-turns (*Ni*) in each modular core and would not produce fundamental flux in the magnetic cores, Fig. 2.16 (b). The phase output inductance is related to the leakage inductance of the two coupled windings on each limb while the inductance between inverter legs is related to magnetizing inductance. The effective inductance of the cross coupled

27

windings can be determined using the mathematical model of each core expressed as (2.24). Where L_w is the winding inductance and k_1 is the coupling coefficient.

(a)   (b)
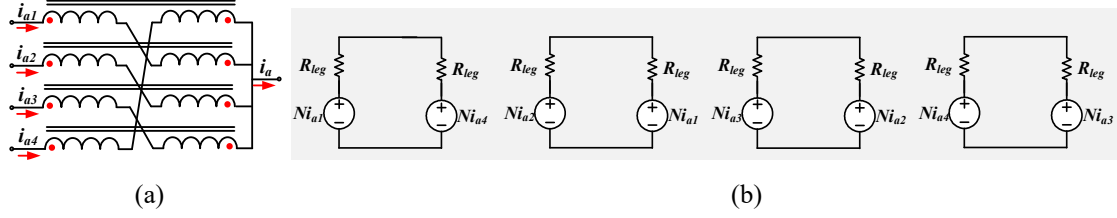
Fig. 2.16 Modular cross coupled inductors (a) balanced ac current path, (b) magnetic circuit.

$$L = L_w \times \begin{bmatrix} 1 & k_1 \\ k_1 & 1 \end{bmatrix} \tag{2.24}$$

2.4. Flux in coupled inductors

Fundamental flux produced by the flow of ac currents cancel in cross-coupled inductors. So mainly high-frequency flux produced by the switched mode voltages across the coupled windings exist in the core. When using two inverter legs, Fig. 2.9, each winding experiences a PWM voltage step of $V_{dc}/4$ for a switching cycle of $f_s/2$. In consequence, the peak high frequency flux (ϕ_{HF,pk_2}) induced in the core can be expressed as (2.25). Where, N_T is the number of turns of each winding and f_s is the switching frequency. Likewise, each coupled winding on a 3-limb core, Fig. 2.13, experiences a PWM voltage step of $V_{dc}/3$ for a switching cycle of $f_s/3$. This switched mode voltage would induced high frequency flux in the core (ϕ_{HF,pk_3}), expressed as (2.26). When using four interleaved inverter legs, Fig. 2.16 (a), a PWM voltage step of $V_{dc}/2$ for a switching cycle of $f_s/4$ is experienced. Consequently, the peak high frequency flux induced in the magnetic core can be determined with (2.27). The peak flux induced in the magnetic cores (ϕ_{HF,pk_4}) of coupled inductors for a converter having four inverter legs is higher than the peak flux induced in 3-limb cores. This implies that a large magnetic core would be required to prevent core saturation, assuming the same number of turns are used in both scenarios. This drawback discourages the use of more than three inverter legs in each phase of a multi-level coupled inductor converter.

$$\Phi_{HF,pk\_2} = \frac{V_{dc}}{8 \times N_T \times f_s} \tag{2.25}$$

$$\Phi_{HF,pk\_3} = \frac{V_{dc}}{18 \times N_T \times f_s} \tag{2.26}$$

$$\Phi_{HF,pk\_4} = \frac{V_{dc}}{16 \times N_T \times f_s} \tag{2.27}$$

Although the flow of balanced ac currents does not produce fundamental flux in conventional coupled inductors (CIs), a significant fundamental flux in their core can be present; related to the fundamental voltage drop across their windings. Their loosely coupled windings have a large series output inductance which is related to the larger leakage flux. The flow of fundamental ac currents (i_{ac}) through the leakage inductance (L_e) results in a significant fundamental voltage drop (v_d). This increases as the magnitude, frequency (f_f) and the phase-shift angle (α) of the fundamental ac currents is increased. The fundamental voltage drop induces fundamental flux in the magnetic core which increases the peak flux (ϕ).

2.5. Coupled inductor design

The size and weight of coupled inductors is determined mainly by the high frequency flux produced by the switched mode voltage across their windings. The design process based on peak flux is divided into four major groups: electrical design, physical design, mechanical design, and thermal design. The electrical design determines the flux, the number of turns and the inductance value.

2.5.1. Electrical design

The voltage difference between interleaved PWM switching inverter legs produces flux in the inductors including the fundamental voltage drop. The magnitude of the flux produced determines the size and weight of the magnetic core required to avoid saturation. The high frequency flux density (B_{HF}) can be determined with (2.28); where N_T and A_{CS}

are the number of turns and the core cross sectional area. Parasitic dc offset currents (I_{dc_offset}) caused by the improper switching of the converter semi-conductors can produce dc flux (B_{dc}) expressed as (2.29). Where l_g is the length of the inductor air gap. However, the dc-offset currents are much smaller than the inductor winding currents (less than 1% of the peak of the load current). Fundamental voltage drop (v_p) across the windings is associated with the inductor leakage inductance. This voltage drops produce a fundamental flux (B_1), expressed as (2.30). The peak flux in the coupled inductors (B_{max}) expressed as (2.31) should be smaller than the core saturation flux density (B_{sat}), ($B_{max}<$ $0.8B_{sat}$). Magnetic cores with a high saturation flux density (1.2 Tesla @ 200°C) and low high frequency losses, such as metglas, are preferred in high-power applications. The coupled inductor winding inductance (L_w) which is related to the effective inductance between the parallel-connected inverter legs and can be determined as (2.32). From the converter specifications (V_{dc}, P_{out}, v_{line}, i_{pha}, and B_{max}) and equations (2.28) to (2.32), the cross-sectional areas of the inductors, their number of turns, and the winding inductance can be calculated. Note that the core cross-sectional areas are inversely proportional to their number of turns. These two parameters are carefully chosen to balance core losses (P_{core}) and copper losses (P_{cu}) in each core.

$$B_{HF} = \begin{cases} \dfrac{V_{dc}}{8 \times N_T \times f_c \times A_{CS}} & ; VSC \ with \ 2 \ ILPP \\[2mm] \dfrac{V_{dc}}{18 \times N_T \times f_c \times A_{CS}} & ; VSC \ with \ 3 \ ILPP \\[2mm] \dfrac{V_{dc}}{16 \times N_T \times f_c \times A_{CS}} & ; VSC \ with \ 4 \ ILPP \end{cases} \tag{2.28}$$

$$B_{dc} = \frac{\mu \times N_T \times I_{dc\_offset}}{l_g} \tag{2.29}$$

$$B_1 = \frac{v_p}{4 \times N_T \times A_{CS} \times f_1} \tag{2.30}$$

$$B_{max} = B_{HF} + B_{dc} + B_1 \tag{2.31}$$

$$L = \frac{\mu \times N_T^2 \times A_{CS}}{l_g} \tag{2.32}$$

2.5.2. Physical design

The size of a coupled inductor magnetic core can be expressed as the core cross-sectional area (A_{cs}) and the window area (A_w). The core cross-section (A_{cs}) is designed to limit the peak high-frequency flux density to avoid core saturation. The core window area (A_w) is designed to host the inductor windings. The dimensions of a family of standard metglas cores, Fig. 2.17, were plotted (a v_s b, a v_s c, & a v_s d) to determine the relationship between the core dimensions as their sizes changed. The resultant relationships grouped into (2.33) approximates the dimensional relationships of standard metglas cores with their size. These design guidelines were used together with the core window and cross-sectional areas to determine the dimensions of the inductor magnetic cores. The window area (A_W) using an appropriate fill factor should be large enough to host the coupled windings and can be determined with (2.34). The core cross-sectional area (A_{CS}) is expressed as (2.35). Where D_W is the diameter of the windings, i_{al} is the winding currents, J is the current density, and K_w is the window utilization factor. The parameters a, b, c and d are the dimensions of the core window and cross-sectional areas.

(a)   (b)
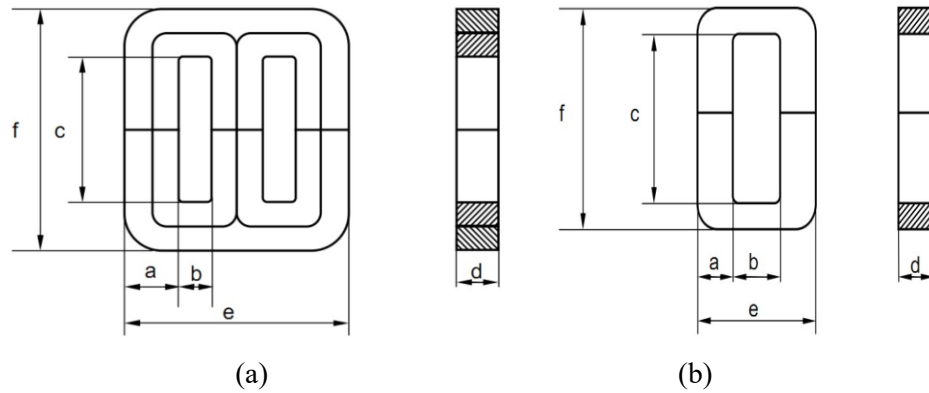
Fig. 2.17 Physical dimensions of the CI cores: (a) 3-Limb core, (b) C-cores.

$$
\left.
\begin{array}{ll}
c = 3.2a + 14 \ \geq N_T \times D_W & mm \\
b = \frac{c-24}{1.9} \ \geq 4 \times D_W & mm \\
d = 2.26a - 6.667 & mm \\
e = 3a + 2b \quad (E - core) & mm \\
e = 2a + b \quad (C - core) & mm \\
f = 2a + c & mm
\end{array}
\right\}
\qquad (2.33)
$$

$$A_{W_x} = c_x \times b_x \geq \frac{N_x \times I_x}{K_w \times J} \tag{2.34}$$

$$A_{CS_x} = a_x \times d_x \geq \frac{v_x}{4 \times N_x \times B_{HF_x} \times f_c} \tag{2.35}$$

2.5.3. Mechanical design (winding arrangement)

The effective output inductance of the coupled inductors under consideration is directly related to the leakage flux. This leakage flux can significantly be reduced by putting the inductor windings close together, on the same limb. Cross coupled inductors have two windings on the same limb which can be wound one over the other to significantly reduce leakage flux, Fig. 2.18. The inductance associated with the low leakage flux allow for: (a) a rapid transient response and power reversal, (b) operation at very high fundamental frequencies with a very small fundamental voltage drop across the inductor windings. A thin tape is used to thermally isolate the different winding layers and to increase the voltage breakdown of the winding insulation.
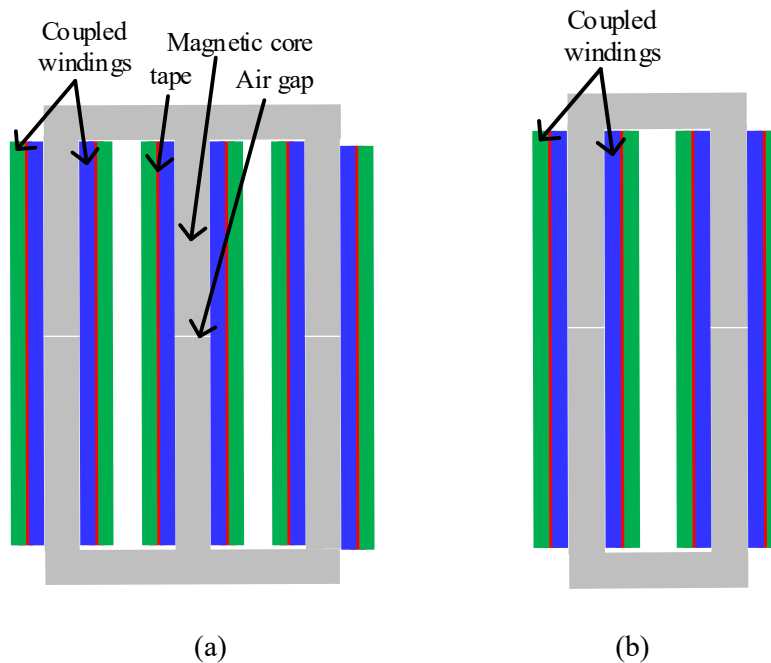
Fig. 2.18 Cross-sectional view of cross coupled inductors: (a) 3-limb CI, (b) 2-limb CI.

2.5.4. Thermal design

Design estimations for the copper and core losses relative to the core size are necessary in a thermal design to prevent the coupled inductors cores from heating up to the curie temperature (T_{curie}) and to prevent the degradation/breakdown of the winding insulation. Inductor losses can be a balance between copper and iron losses as the core cross-section is a trade off with the window available for the inductor windings. Loss minimization can be a result of designing so that the copper and core losses are equal. The core losses of the coupled inductors (P_{core}) can be expressed as (2.36) using the average flux density (B_{av}) and mass (M) of the coupled inductors: simulated core losses obtained the core losses per switching cycle and averaged these losses over a fundamental cycle. The coupled inductor copper losses (P_{CU}) are expressed as (2.37). Where *MLT,* is the average mean length turn of inductors and ρ_{cu} is the resistivity of copper. If the core and copper losses of the coupled inductors differ by a significant factor (> 30%), the core cross-sectional area and the number of turns of the inductor windings are recalculated in the electrical design sub-section to balance the losses. The temperature rise of the inductors (ΔT) designed to be air-cooled can be predicted with equation (2.38). Active cooling techniques with the help of a fan or liquid cooling could be used to further reduce the temperature of the coupled inductors. Metglas cores were used in the inductor designs, they have a curie temperature of 450 ℃ and have low core losses for PWM frequencies in the range of 10 ~ 20 kHz. The coupled inductors used in this thesis were designed to have a temperature rise (ΔT) of 60 ℃. The coupled inductor design flowchart is presented in Fig. 2.19.

$$P_{core} = 6.5 \times M \times f_c^{1.51} \times B_{av}^{1.74} \qquad (2.36)$$

$$P_{CU} = i_a^2 \times \rho_{Cu} \times N_T \times MLT \times \frac{4}{\pi \times D_W^2} \qquad (2.37)$$

$$\Delta T = 450 \left(\frac{P_{core} + P_{cu}}{CI\ surface\ area} \right)^{0.826} \qquad (2.38)$$

- System Specifications : P_{out}, v_{out}, i_{out}, J
- Select the core material and determine (B_{max}): $B_{max} \leq 0.8 B_{sat}$
- Calculate the winding cross sectional area and diameter: D_W
- Calculate the core cross-sectional area : A_{CS}
- Calculate the number of turns: N_T
- Calculate the CI winding inductance : L_s *Electrical Design*

- Determine the core dimensions
$$
\left.
\begin{aligned}
c &= 3.2a + 14 & mm \\
b &= \frac{c-24}{1.9} & mm \\
d &= 2.26a - 6.667 & mm \\
e &= 3a + 2b \ (\text{E} - \text{core}) & mm \\
e &= 2a + b \ (\text{C} - \text{core}) & mm \\
f &= 2a + c & mm
\end{aligned}
\right\}
$$
Physical Design

- Double check the dimensions of the core window area is big enough to host the coupled windings.
- The windings on each limb are placed one over the other to minimize the leakage inductance

$$
c \geq N_T \times D_W \\
\&\& \\
b \geq 4 \times D_W
$$
NO

Mechanical Design

Yes

- Calculate core losses (P_{core})
- Calculate Cu losses (P_{Cu})

Yes

$$
P_{core} \approx P_{cu} \\
\&\& \\
\Delta T \leq 60
$$
NO

Thermal Design

Yes

Coupled Inductor Core

Re-calculate the core dimensions

Re calculate N_T && A_{CS}

Fig. 2.19 Coupled inductor design flowchart.

34

2.6. Simulations

A dc-link of 300V and a switching frequency of 20 kHz was used to simulate and compare the performance of a 3-limb inductor using cross coupled windings vs conventional windings in a high-frequency electric drive having three parallel-connected inverter legs in each phase. Unlike the conventional coupled inductor, the 3-limb cross-coupled inductors experienced a very low fundamental voltage drop across its windings even when used to generate high-frequency fundamental PWM outputs in the kilohertz range. The fundamental voltage drop in the conventional coupled inductor distorts the converter output voltages. The output voltage waveforms (v_{pha}, v_{line}) of the electric drive using both inductor types are compared when it operates at different amplitude modulation index (ma), see Fig. 2.20.

(a)

(b)
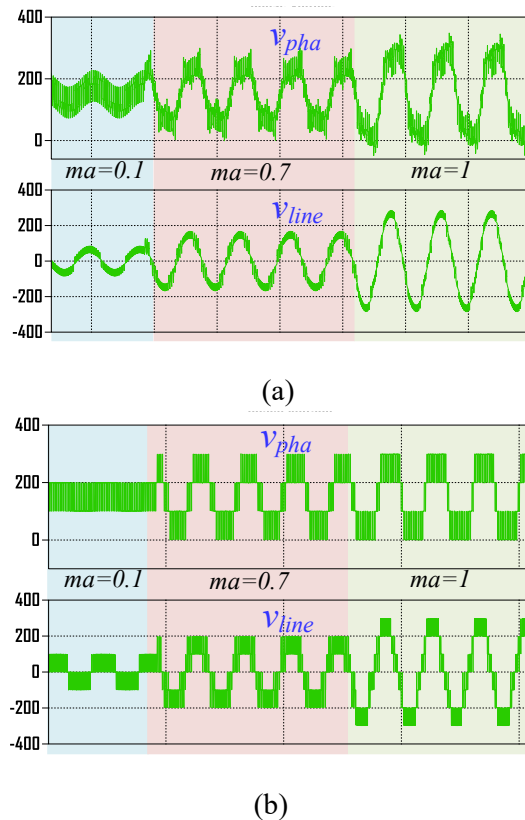
Fig. 2.20 Output waveforms of a VSC operating with a fundamental frequency of 2.5 kHz using (a) conventional 3-limb CIs, (b) 3-limb cross coupled inductors: V_{dc}= 300 Vdc, L_w = 0.8mH, L_f= 30 uH, f_f=23kH.

The fundamental voltage drop across the conventional coupled inductors significantly increases as the frequency of the fundamental currents increases and reduces the voltage across the load. The dc-link voltage can be increased to compensate for this fundamental voltage drop. The drawback of this approach is that it increases switching losses and reduces the overall system efficiency. When using cross coupled windings, the fundamental voltage drop is very small even when generating fundamental frequencies in the kilohertz range, see Fig. 2.21. The flux in coupled inductors with cross-coupled windings is mainly the high frequency flux induced by the high-frequency switched mode voltage across their windings, Fig. 2.22. The peak flux in conventional coupled inductors increases as the magnitude of the winding currents increases, Fig. 2.23 (a), and can even double when the drive operates with a low power factor (PF $\ll$1), see Fig. 2.22 (b) and Fig. 2.24. However, the relatively large leakage inductance can be used to lower unwanted harmonics from the load currents.
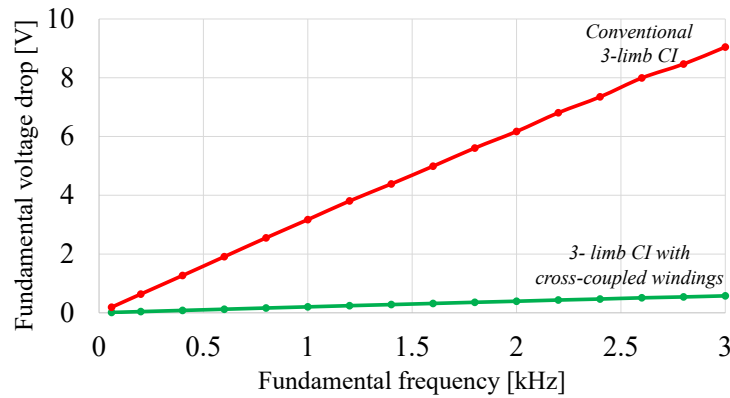
Fig. 2.21 Fundamental voltage drop across interface 3-limb coupled inductors, i_a = 30 A.
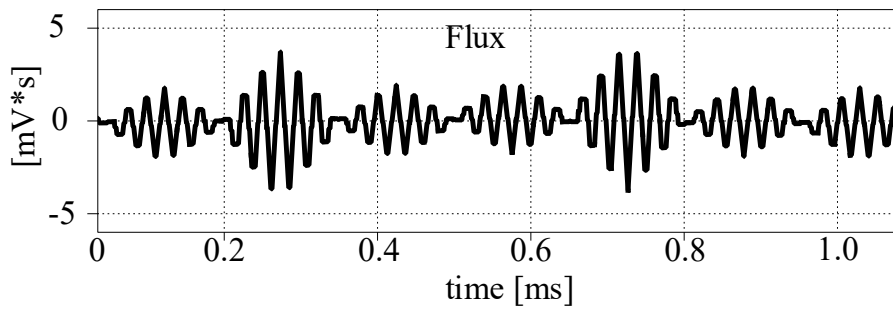
Fig. 2.22 Flux in 3-limb CIs with cross coupled windings, f_f= 1.1 kHz.

The current total harmonic distortion (THD$_f$) of an electric drive using a 3-limb inductor for both winding types was compared. The electric drive using conventional inductors produced lower current THD$_f$ because it's larger leakage inductance adds to the ac filter inductance to filter unwanted harmonics from the load currents, see Fig. 2.25.
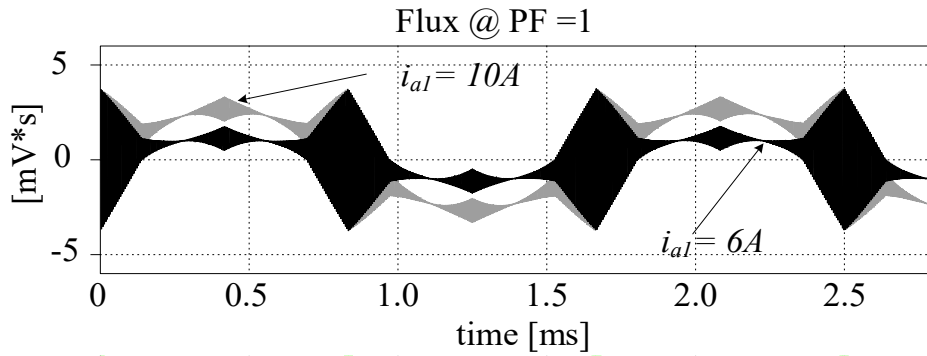
(a)
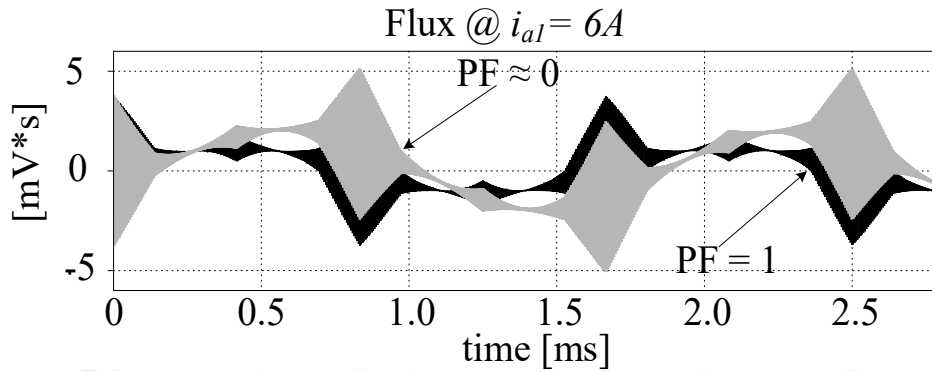
(b)

Fig. 2.23 Flux in conventional 3-limb CIs (a) VSC operating with a unity power factor at different current magnitudes (b) VSC operating with the same current magnitude at different power factors, f_f= 60 Hz.
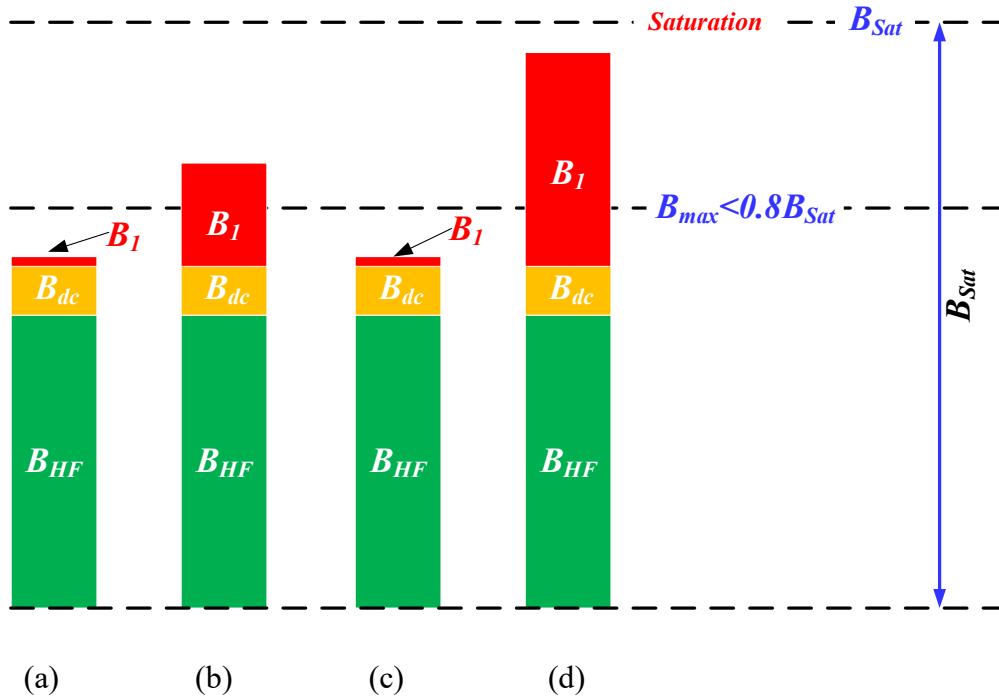
Fig. 2.24 Flux in the magnetic core of interface coupled inductors, V_{dc}=300 V, f_f= 60 Hz, i_{a1} = 10A (a) 3-limb cross coupled inductors operating at unity power factor, (b) conventional 3-limb CI operating a unity power factor, (c) 3-limb cross coupled inductors operating with a low power factor, (d) conventional 3-limb CI operating with a low power factor.
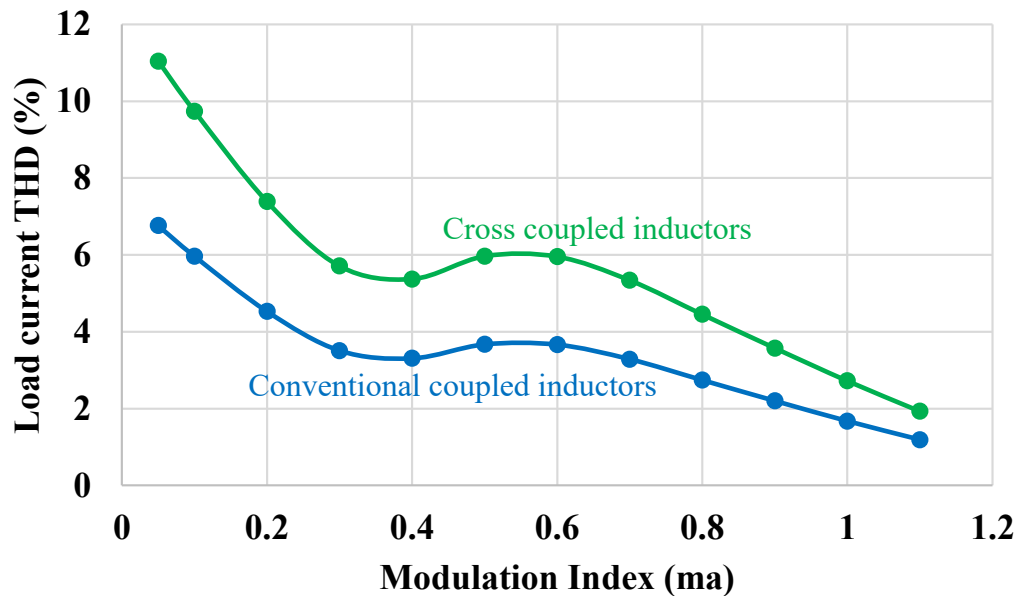
Fig. 2.25 Current THD_f of the high frequency electric drive.

2.7. Experimental verification

Inductors with cross-coupled windings were designed based on peak flux rather than temperature rise using metglas amorphous cores and tested using high-frequency outputs. An 11 kW (300Vdc, 208Vac/30A) laboratory prototype having two, three and four inverter legs in each phase were tested using and an R-L load over a wide range of fundamental frequencies.

2.7.1. Two inverter legs

The parameters of the crossed coupled winding inductor used for a voltage source converter having two parallel-connected inverter legs per phase, is presented in Table 2.2. A DSP controller was used to perform experimental test over a wide range of fundamental frequencies (60 Hz ~ 1.1 kHz). The experimental setup is presented in Fig. 2.26. The system produced 3-level phase (v_{pha}) and 5-level PWM line voltages (v_{line}). Note that the converter produces waveforms with flat voltage levels even when generating high-frequency fundamental outputs in the kilohertz range, Fig. 2.27 (a). The flat distinct voltage waveforms reveal that an insignificant fundamental voltage is dropped across the inductor winding.

Table 2.2: Parameters of the Coupled inductors for a converter with two inverter legs per phase

Parameters	values
Core type	AMCC 4
Wire gauge	22*2
N_T	21 turns
L_w	0.2 mH
L_L	2.1 uH
L_{cir}	3.1 mH
R-L load	3.5 Ω, 70 μH
f_c	20 kHz
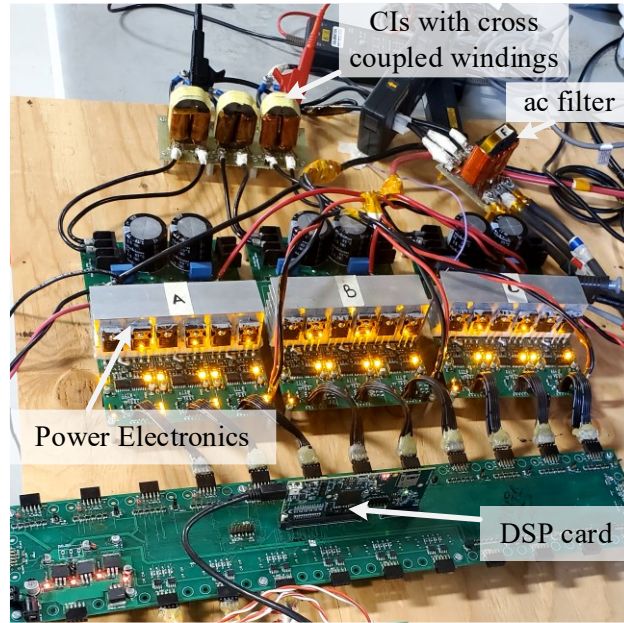
Fig. 2.26 Experimental setup of a converter with two parallel-connected inverter legs per phase, Vdc = 300V, fc= 20kHz, Pw= 11 kW (208V/ 30A).

Since the core flux could not be measured experimentally, the difference the two currents ($i_{cir} = i_{a1} - i_{a2}$) was used to represent the flux in the core. The measured circulating current, hence the core flux, have had no fundamental components, Fig. 2.27 (b). The experimental results implies that the coupled inductors with cross coupled winding inductor can be designed based upon the high-frequency flux in the magnetic core, thereby reducing the size/ weight of the magnetic core.
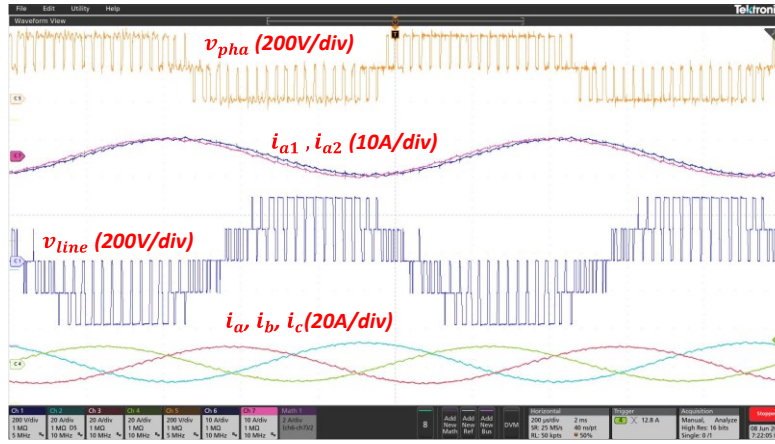
(a)
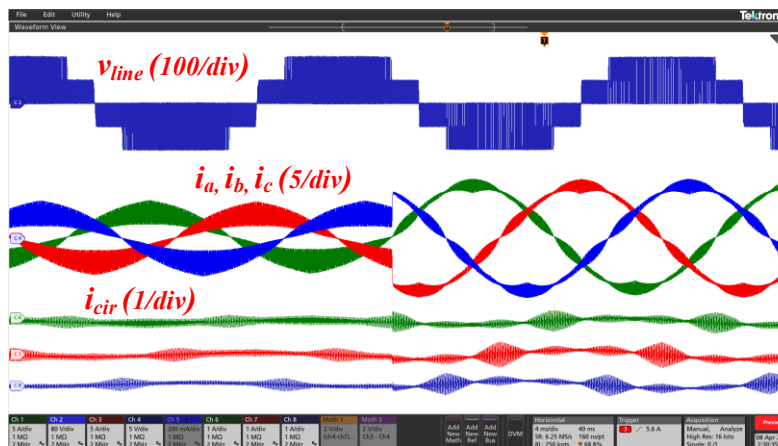
(b)

Fig. 2.27 Experimental waveforms of a VSC with two interleaved inverter legs operating with (a) 1.1 kHz fundamental output voltage, (b) 60 Hz fundamental output voltage, Vdc = 300V, fc= 20kHz, Pw= 11 kW (208V/ 30A).

2.7.2. Three inverter legs

Three 3-limb coupled inductors using six windings, two winding per limb, having the same number of turns (N_T) were designed based on peak flux for a voltage source converter using three inverter legs per phase. The windings of the coupled inductors were first cross coupled (CI$_{CS}$), see Fig. 2.28 (a) and later rearranged such that the two windings on the same limb were connected in series, conventional connection using a winding with 2N turns (CI$_{NCS}$), see Fig. 2.28 (b).

41
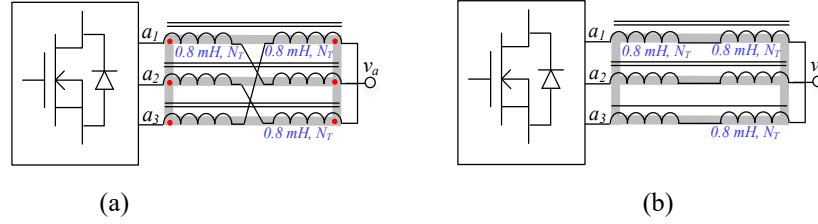
Fig. 2.28 Coupled inductor winding arrangements (a) 3-limb CI with cross coupled windings, (b) conventional 3-limb CI.

The parameters of the designed 3-limb coupled inductors are shown in Table 2.3. Note that the series output inductance (L_L) of the cross coupled winding arrangement (CI$_{CS}$) is significantly smaller, 3% of the inductance of conventional inductors (CI$_{NCS}$). The inductance in the circulating current path for the cross coupled arrangement 25% smaller then when using conventional windings. Consequently, conventional coupled windings are better than cross coupled windings at filtering the flow of circulating currents, see Fig. 2.29. However, conventional windings at the phase output terminal experience a significant fundamental voltage drop which would reduce the voltage across the load, induces fundamental flux in the magnetic core and increases the core peak flux, Fig. 2.30. Experimental tests were done over a wide range of fundamental frequencies (60 Hz ~ 5.0 kHz) using an R-L load (3.5 Ω, 30 μH), a switching frequency of 23 kHz and the PLECS RT-Box as a digital controller.

Table 2.3: Parameters of the Coupled inductors for a converter with three inverter legs per phase

Parameters	CI$_{CS}$	CI$_{NCS}$
Core type & dimensions	Metglas (B_{sat} =1.2T @ 200 ºC) (A_{cs}=0.75 cm^2, A_w=2.71 cm^2, mass=91g)	
Wire gage	18 AWG (0.262mm^2/20.94 mΩ/m)	
N_T	38 (N) turns	76 (2N) turns
Winding length	1.9 m	3.8 m
wire mass	26.76 g	26.76 g
L_w	0.8 mH	3.2 mH
L_L	1.7 uH	60 uH
L_{cir}	5.1 mH	6.9 mH
Mass of CIs	3*117.8 g	3*117.8 g
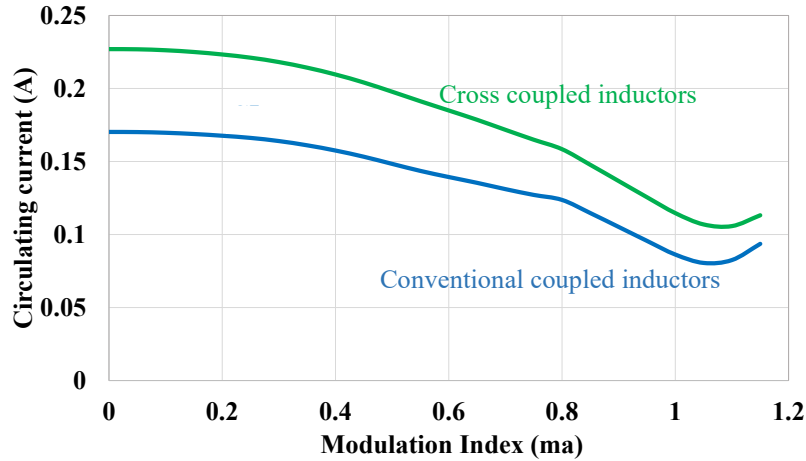
Fig. 2.29 Circulating current between the parallel-connected inverter legs, V_{dc}=300V, f_f=2.5 kHz, f_s= 23kHz, i_a = 30A.
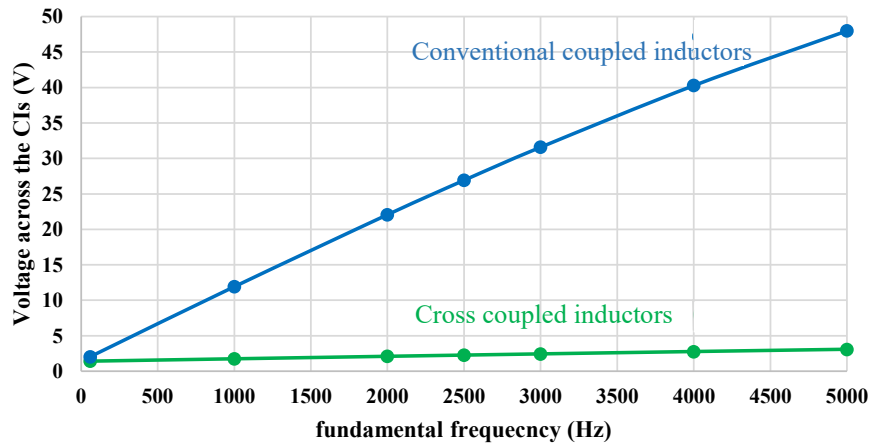
Fig. 2.30 Fundamental voltage drop across the interface coupled inductors, V_{dc}=300V, f_f=2.5 kHz, f_s= 23kHz, P_{out} = 11kW.

The designed coupled inductors and the experimental setup are presented in Fig. 2.31 and Fig. 32 respectively. The system generates 4-level phase (v_{pha}) and 7-level PWM line voltages (v_{line}). The output voltage waveforms using conventional winding (CI$_{NCS}$) were distorted; because of the leakage inductance voltage drop, Fig. 2.33. However, when using cross coupled windings, the PWM voltage level were flat, Fig. 2.34. The measured waveforms clearly indicate that cross coupled windings experience an insignificant drop in the output voltage even when producing high-frequency fundamental outputs in the kilohertz range. Since the flux in the core cannot be measured experimentally, the

43

circulating current difference ($i_{cir} = i_{a1} - i_{a3}$) which has the same waveform as the flux in the magnetic core was measured. When cross coupled inductors were used, the circulating current difference (i_{cir}) between the inverter legs had no fundamental component, see Fig. 2.35 (a). However, when using conventional winding inductors, the circulating current difference (i_{cir}) between the inverter legs had a significant fundamental component, Fig. 2.35 (b).
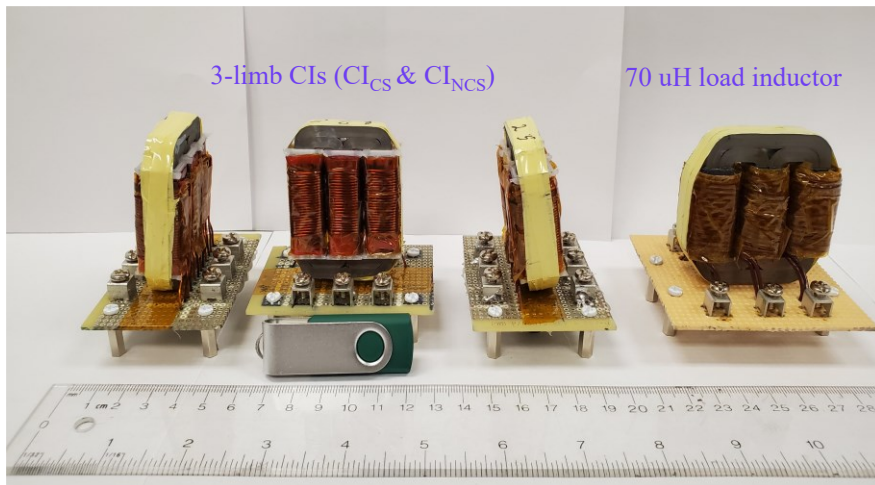
Fig. 2.31 Designed 3-limb coupled inductors.
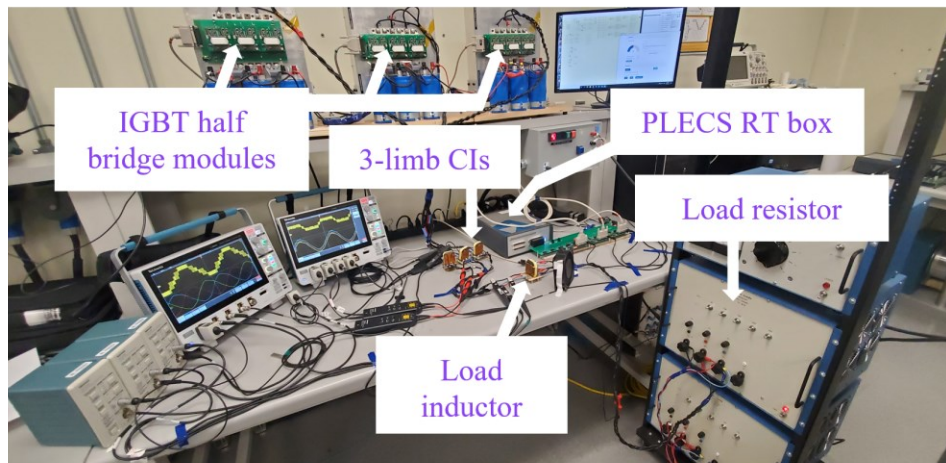
Fig. 2.32 Experimental setup of a converter with three parallel-connected inverter legs per phase.

These measurements confirm that the flux in the conventional coupled inductor can have a significant fundamental component which could double the peak flux and the size of the core required to avoid saturation, especially when the voltage source converter is operated with a low power factor.

(a)

(b)

(b)

(d)
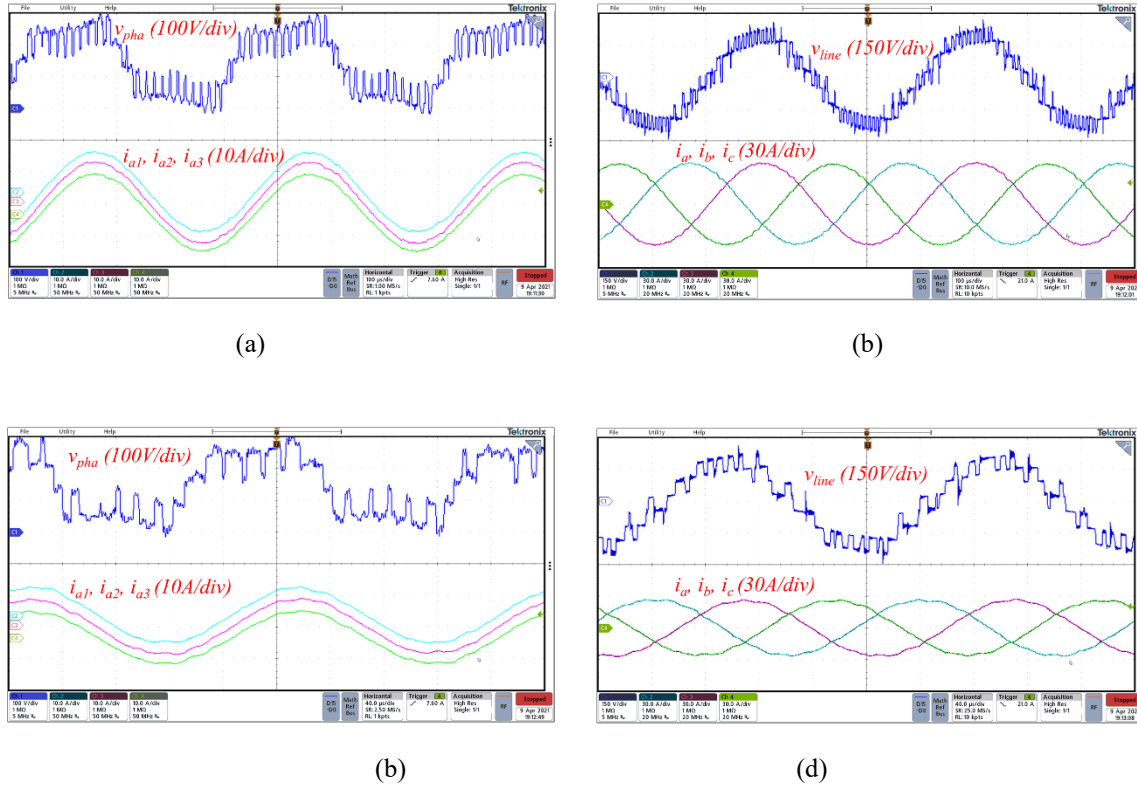
Fig. 2.33 Experimental waveforms of the converter using 3 ILPP and conventional 3-limb inductors, (a) PWM phase voltages and inductor winding currents, f_f =2.5 kHz, (b) PWM line voltage and converter load currents, f_f=2.5 kHz, (c) PWM phase voltages and inductor winding currents, f_f= 5 kHz, (d) PWM line voltage and converter load currents, f_f=2.5 kHz, V_{dc} =300V, f_s= 23kHz, P_{out} = 11kW.
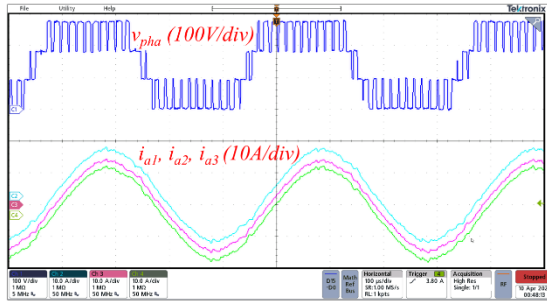
(a)
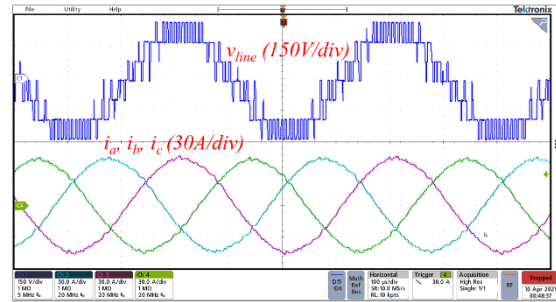
(b)
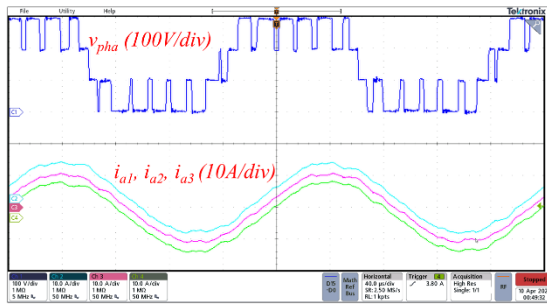
(c)
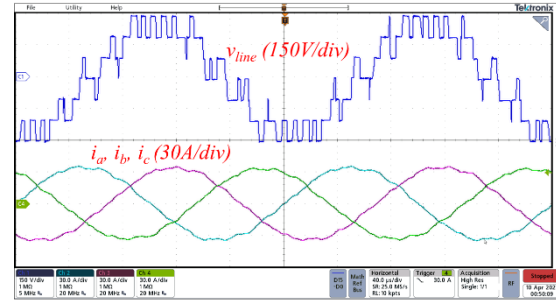
(d)

Fig. 2.34 Experimental waveforms of the converter using 3 ILPP and 3-limb inductors with cross coupled windings, (a) PWM phase voltages and inductor winding currents, f_f=2.5 kHz, (b) PWM line voltage and converter load currents, f_f=2.5 kHz, (c) PWM phase voltages and inductor winding currents, f_f= 5 kHz, (d) PWM line voltage and converter load currents, f_f=2.5 kHz, V_{dc}=300V, f_s= 23kHz, P_{out} = 11kW.
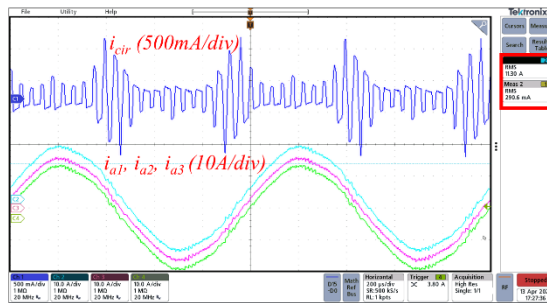
(a)
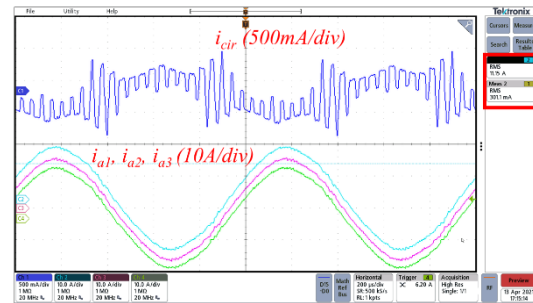
(b)

Fig. 2.35 Experimental waveforms of the circulating currents between the interleaved inverter legs, (f_f=2.5 kHz) (a) 3-limb CIs with cross coupled windings, (b) conventional 3-limb CIs.

2.7.3. Four inverter legs

Modular coupled inductors using C-shaped cores and cross-coupled windings were designed and built to demonstrate their feasibility in a voltage source converter having four inverter legs in each phase. Experimental tests were done using an R-L load (3.5 Ω, 30 μH), a switching frequency of 20 kHz and the PLECS RT-Box as a digital controller. The inductor parameters and the experimental setup of laboratory prototype are presented in Table 2.4 and Fig. 2.36 respectively. Measurements reveals that the modular inductors present a high inductance (L_{cir}) between the parallel-connected inverter legs to supress the flow of circulating current and a very low series output inductance (L_{cir}). These characteristics result in the even distribution of the load currents between the inverter legs without the need for a current controller. In addition, the low series output inductance can have rapid dynamic response with negligible drop in the phase output voltage. The system generates 5-level phase (v_{pha}) and 9-level PWM line voltages (v_{line}) with a very low harmonic content, see Fig. 2.37. Note that the converter output voltage waveforms have flat voltage levels which indicates an insignificant fundamental voltage drop across their windings. A circulating current difference (i_{cir}) was measured to represent the flux in the core. This current had no fundamental component, Fig. 2.37 (a). In consequence, modular coupled inductors using cross coupled windings can be designed for high frequency flux patterns.

Table 2.4: Parameters of the Coupled inductors for a VSC with four inverter legs per phase

Parameters	values
Core size (A_{CS}/A_W)	0.47 cm^2/ 1.79 cm^2
Wire gauge	22*2
L_w	1 mH
L_L	1.6 uH
L_{cir}	3 mH
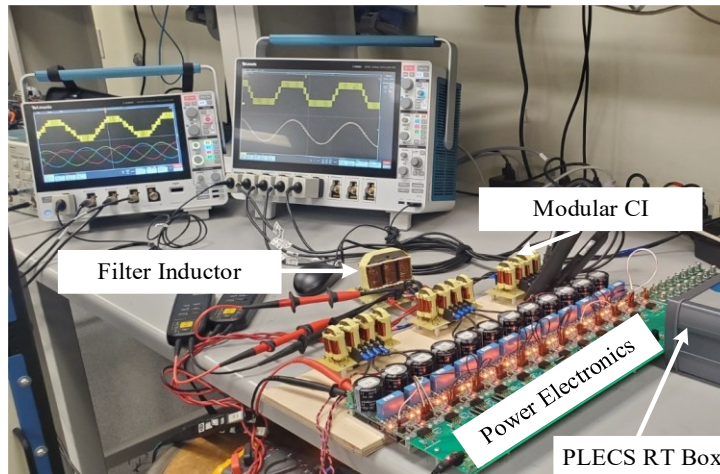
Fig. 2.36 Experimental setup of a converter with four parallel-connected inverter legs per phase.

|(a)|(b)|
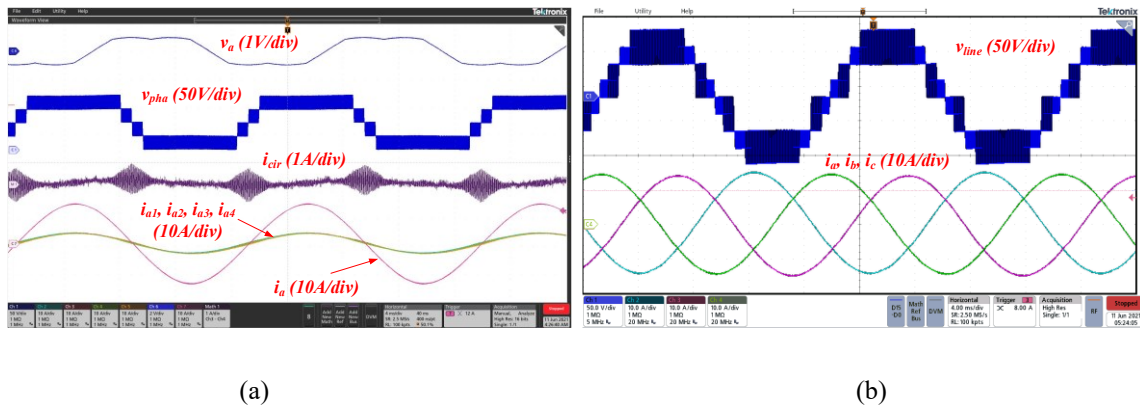
Fig. 2.37 Experimental waveforms of a converter having four interleaved inverter legs in each phase (a) reference signal, PWM phase voltage, circulating current, winding and load currents (b) PWM line voltage and load currents, f_f=60 kHz, V_{dc}=300V, f_s= 20kHz, i_a = 10 A.

2.8. Conclusion.

The performance of inductors with cross coupled windings is presented for connecting parallel inverter legs. Two windings are connected in series with each inverter leg output and each winding located on separate magnetic cores or separate limbs of the same core. These inductors can be implemented with converters having an arbitrary number of parallel-connected inverter legs per phase. Windings located on the same limb

are more coupled than when located on separate limbs and have a low leakage flux that reduces electromagnetic emissions (EMI).

For three inverter legs connected in parallel using 3-limb cores and crosss coupled windings have an inductance, $6.75Lw$, in the circulating current path that is 25% smaller than using conventional current coupled inductor windings, $9Lw$. Consequently, conventional coupled inductors in the 3-limb case are slightly better at filtering high frequency circulating currents than cross coupled windings. However, the series phase output inductance with cross-coupled windings can be 3% that of conventional coupled windings. This low series output inductance favors rapid transient responses and the production of high-frequency fundamental multi-level PWM outputs in the kilohertz. Conventional coupled windings can experience a significant fundamental voltage drop across at their phase output terminals which reduces the voltage across the load. The dc-link voltage can be increased to compensate this fundamental voltage drop, but this also increases switching losses.

For conventional coupled windings, the droop with the increasing load current in the phase fundamental output voltage increases as the magnitude phase-shift and as the frequency of the converter currents increases. This voltage induces fundamental flux in the magnetic core which can significantly increase the peak flux and the size/weight of the core required to avoid saturation. Output voltage drop is very small when using cross coupled windings. In consequence, these inductors can be designed more precisely, and their size/weight can be smaller, solely related to the peak high-frequency flux in the core. Inductors using cross coupled windings are useful to reduce the size/weight of the magnetics in high-power voltage source converter. Target applications include uninterrupted power supplies, flywheel energy storage systems, and high-frequency electric drives in mobile applications where lightweight magnetics are required.

Chapter 3

Parallel VSCs using DC and an AC Filters.

The converter and coupled inductors presented separate the filtering of the common mode (CM) and differential mode (DM) PWM voltages experienced between two 3-phase parallel converters. A 3-limb coupled inductor (CI), between the 3-phase output terminals of the two converters to filter differential mode circulating currents. A DC common mode choke is located between the two converter dc input terminals to filter common mode circulating current, see Fig. 3.1 (a). The combined weight of the two coupled inductors can be 13% smaller with 16% lower losses when compared with using three C-shaped cores to connect the converter output terminals in each phase, representing a conventional arrangement, see Fig. 3.1 (b).

Two 3-phase converters (six switch) can be connected in parallel using a range of coupled inductor types. These coupled inductors (CIs) can be designed to have a high inductance for control circulating currents, combined with a low per-phase output inductance. Conventional CIs use 3 C-shaped cores, one in each phase of the parallel-connected converters, Fig. 3.3. The 3-phase PWM voltage between the two converters (e.g v_{a1}-v_{a2}) consists of two PWM components, common mode, and differential components, expressed as (3.1) and (3.2), see Fig. 3.2. Two separate cores can be used to separately filter the common and differential PWM voltage components in the circulating current path. The two inductor types presented places a 3-limb ac inductor between the output terminals of the two converters and a dc inductor or dc choke between the two converter dc input terminals, see Fig. 3.1 (a).
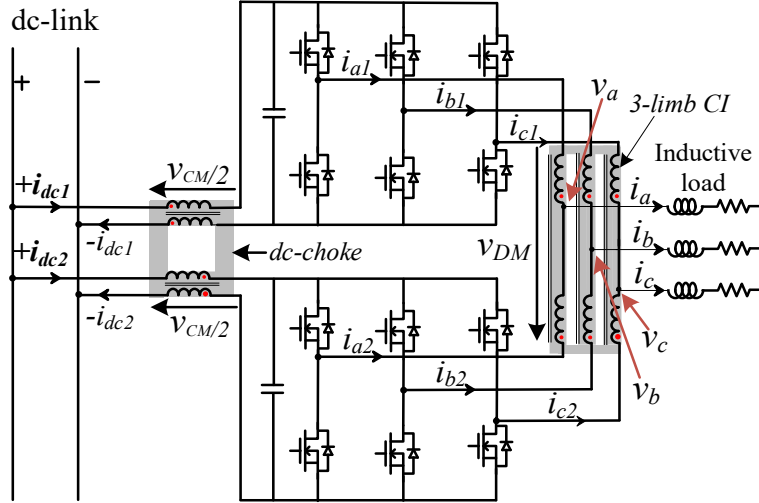
(a)
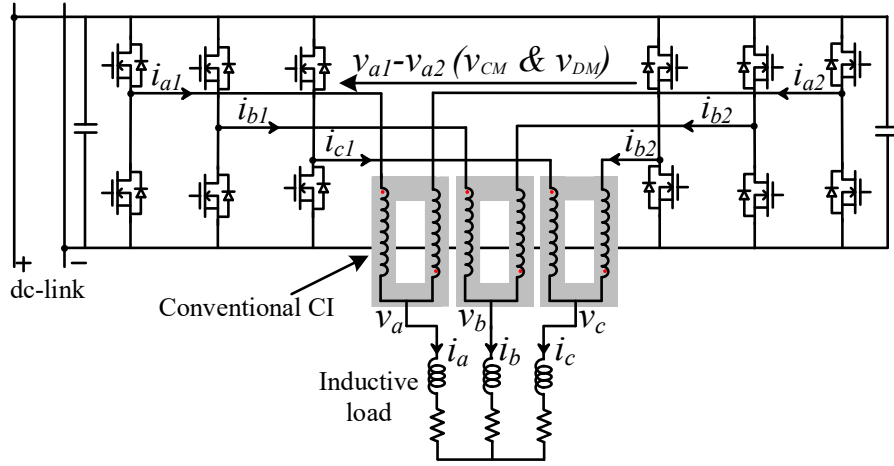
(b)

Fig. 3.1 Parallel-connected voltage source converters with (a) a dc choke & a 3-limb coupled inductor, (b) conventional coupled inductors.

$$v_{CM} = \frac{(v_{a1}-v_{a2})+(v_{b1}-v_{b2})+(v_{c1}-v_{c2})}{3} \qquad (3.1)$$

$$v_{DM} = (v_{a1} - v_{a2}) - v_{CM} \qquad (3.2)$$
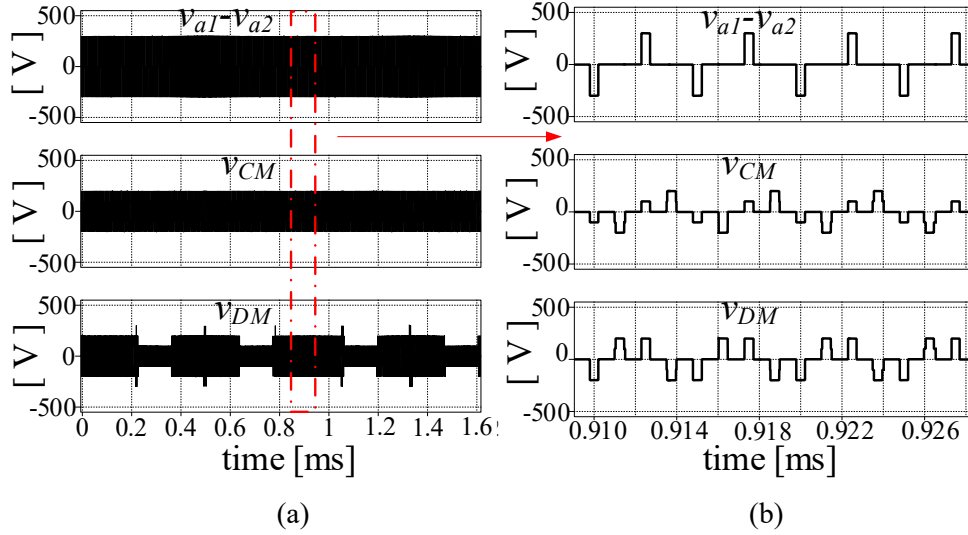
Fig. 3.2 PWM voltage between two interleaved PWM switching converters. (a) Waveforms over one fundamental cycle. (b) Expanded waveforms over a few switching cycles.

The 3-limb ac inductor filters circulating currents due to the differential mode PWM voltage and the dc inductor or dc choke filters circulating currents due to the common mode PWM voltage. The dc choke uses four windings in contrast to the six required for an equivalent common mode 3-phase ac choke. When using conventional coupled inductors with a C-shaped core in each phase the PWM voltages between interleaved PWM switching converters (e.g v_{a1}-v_{a2}) V_{CM} and V_{DM} is dropped across the inductor windings. Similarly, the dc common mode choke absorbs the common mode voltage, V_{CM}, producing a common mode flux (Φ_{CM}), and the 3-phase differential mode inductor absorbs differential mode voltage, V_{DM}, producing a differential mode flux (Φ_{DM}).

3.1. Modulation techniques for parallel VSCs

Conventional modulation schemes for parallel-connected converters, like the sinusoidal PWM scheme (SPWM), used a set of evenly phase shifted carries and the same sinusoidal reference signal in each phase to control the switching of the converters. When two voltage source converters are interleaved, a 0^0 carrier is used to control one converter and a 180^0 carrier is used to control the other converter. This modulation scheme generates 5-level PWM line voltages, but the quality of the converter PWM line voltage is poor, see

52

Fig. 3.3 (a). The quality of the PWM line voltage can be improved by swapping between two sets of evenly phase shifted carriers, modified SPWM, that uses lagging and leading carriers, see Fig. 3.3 (b). When two inverter legs in one phase have modified interleaved switching, the carrier for one inverter leg changes from 0^0 to 90^0 and the other 180^0 and 270^0 on the zero crossing of the phase reference signals [4], [101]. An alternative approach modifies the reference signals to produce high quality multi-level PWM line voltages [9], [102]. The phase angle of the carriers used to parallel-connected voltage source converters having an arbitrary number of inverter legs in each phase is presented in Table 3.1. The harmonic volt-second of the PWM line voltage of a converter using the sinusoidal PWM scheme with and without carrier swapping (SPWM, M_SPWM) are compared in Fig. 3.4.

(a)   (b)
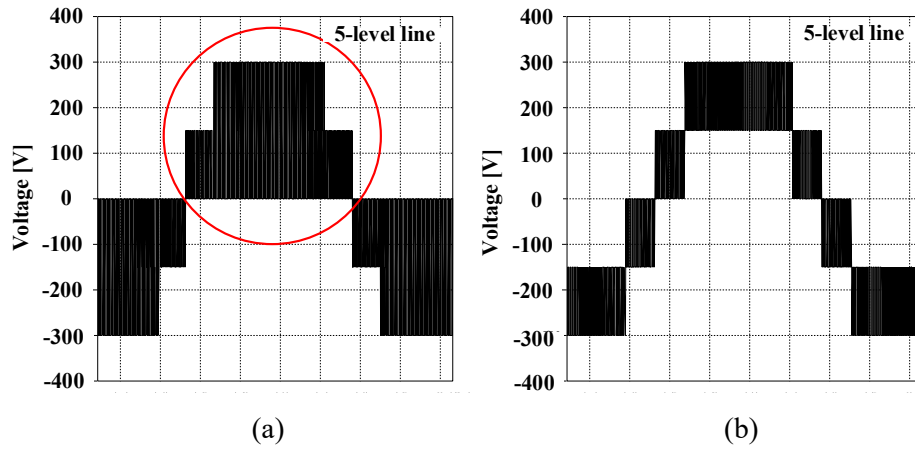
Fig. 3.3 PWM line of a voltage source converter having two parallel-connected inverter legs per phase using (a) SPWM (b) modified SPWM.

Table 3.1: Phase-shifted carriers for parallel-connected converters

Number of ILPP	Lagging carrier	Leading carrier
2	0^0, 180^0	90^0, 270^0
3	0^0, 120^0, 240^0	60^0, 180^0, 300^0
4	0^0, 90^0, 180^0, 270^0	45^0, 135^0, 225^0, 315^0
n	$360 \times [0, \frac{1}{n}, \frac{2}{n} ..., \frac{n-1}{n}]$	$360 \times [0, \frac{1}{2n}, \frac{3}{2n} ..., \frac{2n-1}{2n}]$
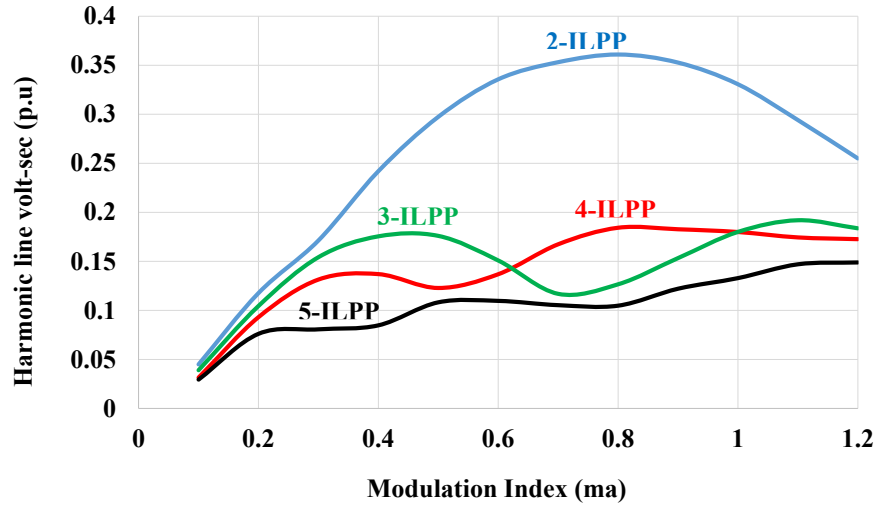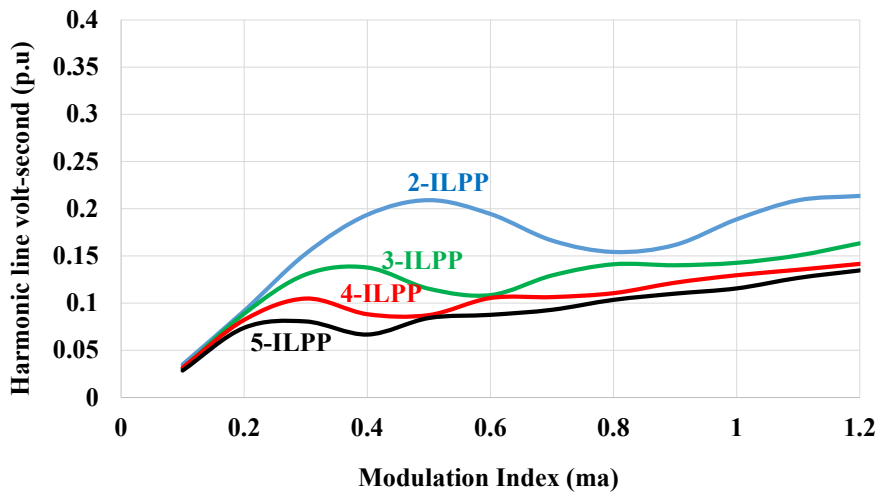
Fig. 3.4 Line voltage harmonic volt-seconds of a voltage source converter having two-five parallel-connected inverter legs per phase using (a) fixed carrier phases for each inverter leg (b) modified SPWM (carrier swapping).

The modified SPWM scheme generates higher quality PWM line voltages which can more easily be filtered using a smaller ac inductor. However, the carrier swapping causes the flux (Φ_{CI}, Φ_{CM}, Φ_{DM}) to jump whenever the phase of the carriers is changed. The flux jump in the inductors generates dc offsets, increases the peak flux, and the size/weight of the core has to be increased to avoid saturation, Fig. 3.5 and Fig. 3.6. Carrier transitions techniques were investigated to prevent these flux jumps when producing high quality outputs [7], [8], see Fig. 3.7.
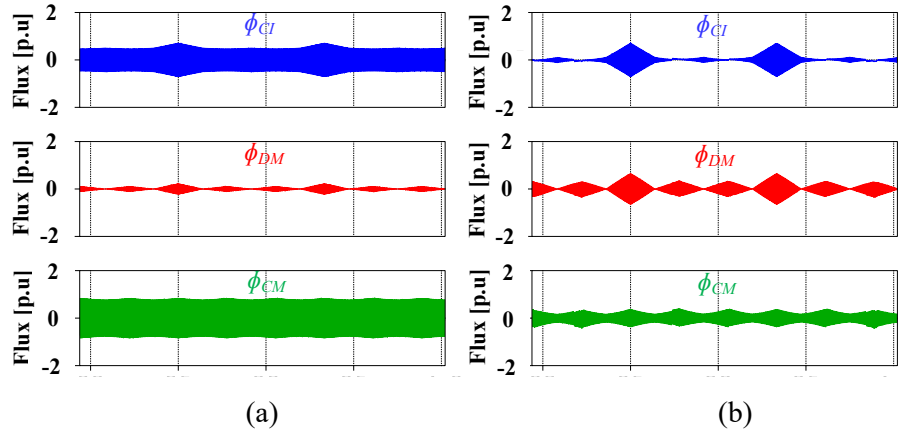
Fig. 3.5 Waveforms of the high-frequency flux in the conventional CIs, 3-limb CI and the dc choke when using the SPWM scheme (a) ma = 0.3, (b) ma = 1.15.
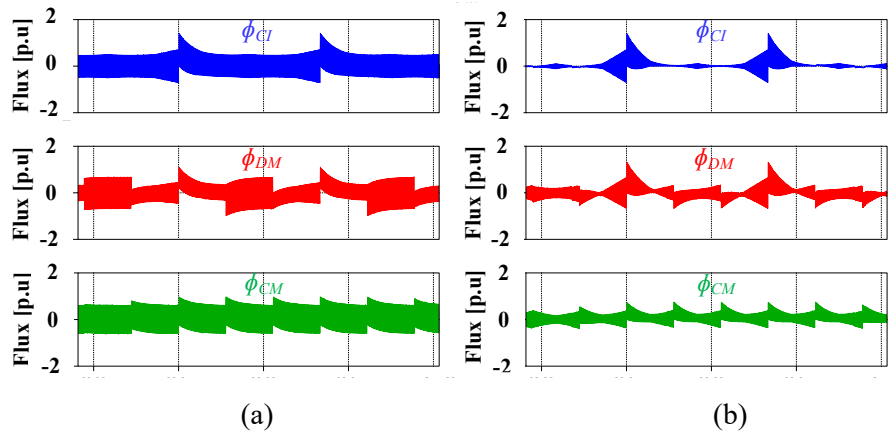
Fig. 3.6 Waveforms of the high-frequency flux in the conventional CIs, 3-limb CI and the dc choke when using the modified SPWM scheme (a) ma = 0.3, (b) ma = 1.15.
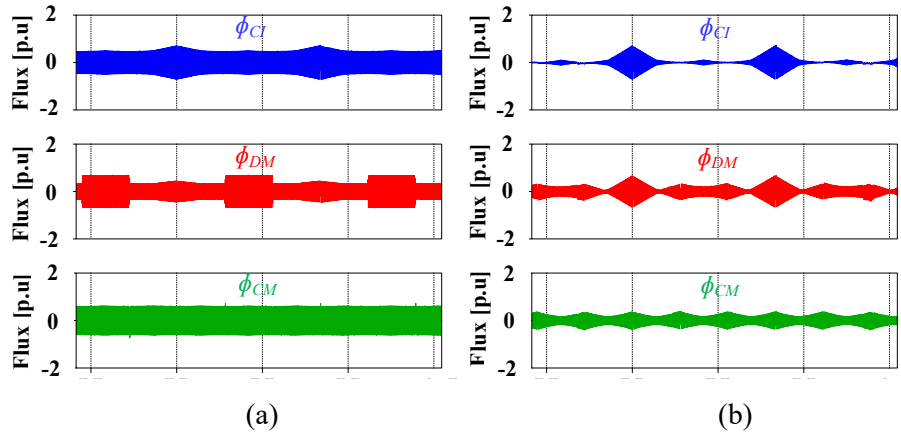
Fig. 3.7 Waveforms of the flux in the conventional CIs, 3-limb CI and the dc choke when using the modified SPWM scheme and the carrier transition technique (a) ma = 0.3, (b) ma = 1.15.

Modified SPWM (M_SPWM) using the carrier transition techniques is used throughout this chapter to produce high quality 5-level PWM line voltages when comparing the performance of three types of coupled inductors. The peak flux (Φ_{CM}, Φ_{DM}) produced by the common mode and differential mode PWM voltage components (v_{CM}, v_{DM}) are both 30% smaller than the peak flux (Φ_{CI}) produced by the two voltages combined, $V_{CM} + V_{DM}$, (e.g v_{a1}–v_{a2}), see Fig. 3.8. Appropriate design procedures reveal that an inductor size and weight can be mainly based upon the core peak flux as opposed to the power losses and maximum core temperature rise. In consequence, the 30% lower peak flux results in a combined size/weight for the dc choke and 3-limb inductor to be smaller than using three conventional C-shaped core coupled inductors. The 3-phase outputs at the center tap of the 3-limb coupled inductor windings in each phase have a very low effective per-phase output inductance. Consequently, the proposed converter structure can supply very high-frequency fundamental output voltages.
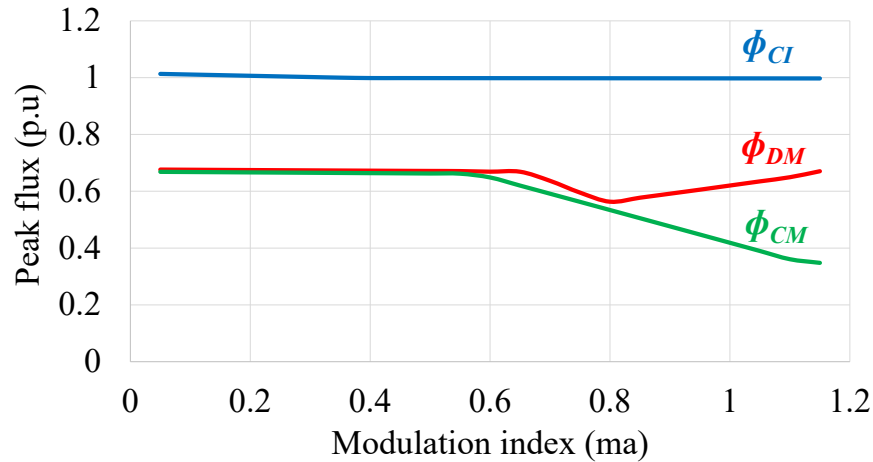
Fig. 3.8 High-frequency flux in the three coupled inductors.

3.2. Electrical model for coupled inductors

There are multiple voltages and current paths in parallel connected voltage source converters. The common mode (CM) and differential mode (DM) PWM voltages (v_{CM} and v_{DM}) refer to the voltage difference between the output of two converters without inductors.

These two voltage components are dropped across any inductance placed in the path of the circulating currents. A coupled inductor can be designed to have a separate inductor value for the common mode and differential mode components separately (L_{CM}, L_{DM}). A third significant inductance concerns the inductance in series with the phase output terminal (L_L). The models presented assume that each winding has the same number of turns N_T. For each coupled inductor type, the reference winding inductance L_w is defined as the winding inductance experienced when only that winding is excited and the other windings on the same core are open circuit.

3.2.1. Conventional coupled inductors

Two coupled windings located on separate limbs of a C-shaped core, referred to as conventional coupled inductors see Fig. 3.9 (a) are placed in series between the two converter output terminals. This inductor controls circulating currents due to the PWM voltage difference between the output terminals v_{x1}-v_{x2} (x refers to the 3 phases a, b, or c). Hence both components of the PWM voltage difference (CM and DM) are dropped across the two windings, see Fig. 3.9 (a). The effective inductances (L_{CM}, L_{DM}) for common mode and differential mode voltages (v_{CM}, v_{DM}) have the same value and are expressed as (3.3). Balanced ac currents in each winding (e.g i_{a1}, i_{a2}) form the output current in each phase of the voltage source converter, see Fig.3.9 (a). The coupled inductor forms a high inductance path for unbalanced currents, effectively forming a circulating current component, and a low inductance for the phase output current, see Fig. 3.9 (b). The effective series output inductance (L_L) is related to leakage inductance (L_e) and is expressed as (3.4). The characteristics forces the two ac currents i_{a1} and i_{a2} to be balanced and equal.

$$L_{CM} = L_{DM} \approx 4L_w \qquad (3.3)$$

$$L_L = \frac{1}{2}L_e \qquad (3.4)$$
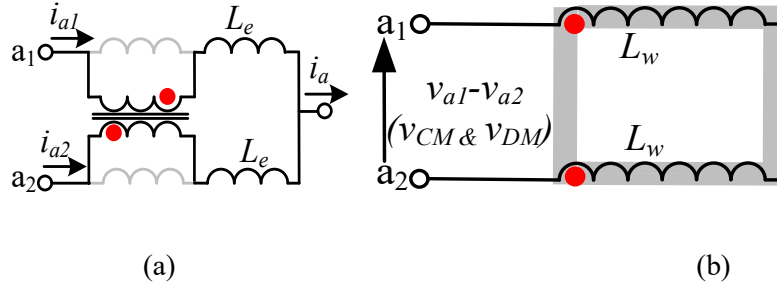
Fig. 3.9 Electrical model of conventional coupled inductors (a) CI equivalent circuit on the path of the voltage between the VSCs, (b) CI equivalent circuit to the flow of balanced ac currents.

3.2.2. 3-Limb coupled inductors

Six windings are located on a 3-limb core, two windings on each limb, Figs. 3.10 (a). The 3-phase differential mode (DM) component of the PWM voltage difference between the two converters (v_{DM}) progress through a series of switching states where: two windings on one limb are shorted by the converter; two windings on a second limb are excited, one with a positive voltage; and the other two windings on the third limb are excited with a negative voltage. Noting that L_w is a winding inductance when it alone is excited, then the effective inductance in the path of the differential mode PWM voltages (L_{DM}) can be appreciated with reference to the equivalent circuits in Fig. 3.10 (a) and (b) and is given by (3.5) derived in section 2.3.2. The common mode PWM voltage (v_{CM}) excites all three limbs identically, see Fig. 3.10 (c) and the effective inductance for this voltage (CM) voltage is related to the leakage inductance of each winding (L_e) and can be expressed as (3.6). The leakage flux produced by the common mode PWM voltage can flow through each limb but not interlimb; hence, the 3-limb core cannot effectively filter common mode circulating currents. The phase output ac current equally flows through the two-coupled windings located on the same limb. Hence, a low inductance path (L_L) exists for these balanced currents and a large inductance between the inverter leg output terminals. Therefore, the fundamental phase output current does not produce a significant flux in the core and the effective series output inductance in each phase (L_L) can be expressed as (3.7)
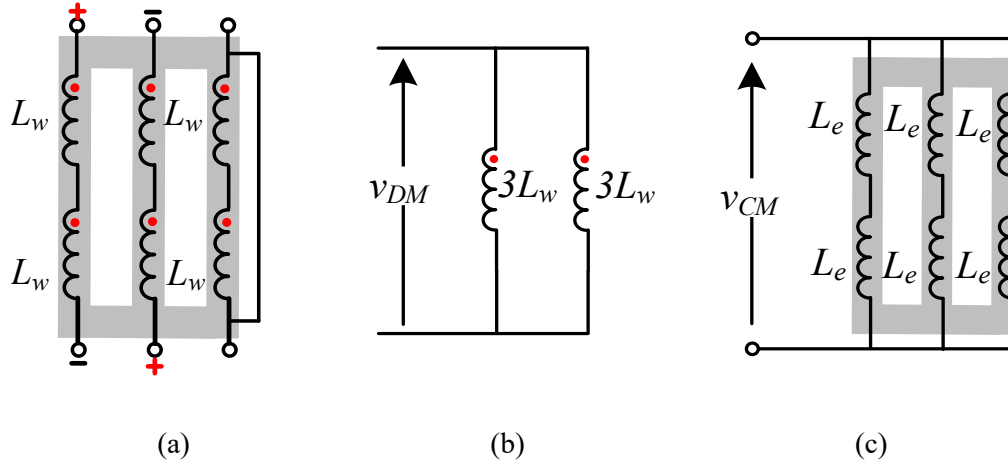
Fig. 3.10 Equivalent circuits of the 3-limb coupled inductor. (a) DM voltages across the CI windings. (b) DM circuit. (c) CM circuit.

$$L_{DM} = 3L_w \tag{3.5}$$

$$L_{CM} = \frac{2}{3}L_e \tag{3.6}$$

$$L_L = \frac{1}{2}L_e \tag{3.7}$$

3.2.3. DC choke

Four windings are placed on one C-shaped core, with two windings located on each limb, Fig. 3.11. The 4 windings are coupled in such a way that they present a large inductance between the two dc terminals of the two converters, hence a large inductance is presented in the circulating paths for the common mode PWM voltage (v_{CM}), Fig. 3.33 (a). The common mode inductance (L_{CM}) is determined by (3.8). The equivalent circuit for the differential mode PWM voltage, Fig. 3.11 (b), has a circulating current path through both windings on the same limb that does not produce flux in the core, a very low leakage flux exists between these two windings. Hence, the dc-choke cannot effectively filter differential mode circulating current. The effective inductance produced by the dc choke for the differential mode PWM voltage (L_{DM}) can be expressed as (3.9). Since the two voltage source converters have capacitance across their dc input terminals, they provide a decoupling effect where the effective output inductance per phase is related to the leakage

inductance of the 3-limb core only. Lastly, one feature worthy of note is the current drawn from the dc supply through the windings of the dc choke, see Fig. 3.11 (c). The dc input current has a circuit path that includes the winding resistances and the leakage inductance related to two windings located on the same limb. The close coupling of these windings presents a low inductance for balanced currents during transients and a high inductance for unbalanced currents. Similar to the phase output currents, hence, rapid changes in the dc supply input currents are possible during transients, The effective series inductance of the dc-choke (L_L) is determined as (3.10).
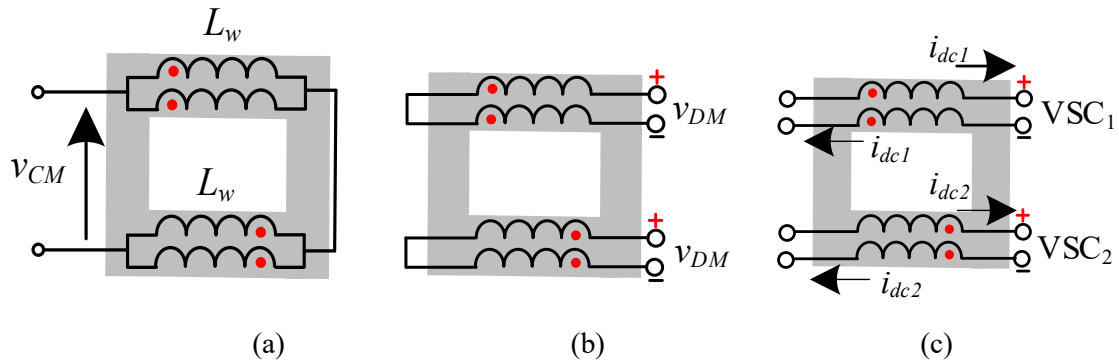
Fig. 3.11 Electrical model of the dc choke (a) CM circuit, (b) DM circuit, (c) Balanced dc currents.

$$L_{CM} \approx 4L_w \tag{3.8}$$

$$L_{DM} = \frac{1}{2}L_e \tag{3.9}$$

$$L_L = \frac{1}{2}L_e \tag{3.10}$$

3.3. Simulations

Semiconductors and inductors losses, hence the power conversion efficiencies of the dual voltage source converter system were obtained. The simulation compares the system performance between using the conventional coupled inductors using C-shaped cores versus the dc choke with the 3-limb inductor (or dual coupled inductor in short). The

experimental coupled inductors used were designed based on the peak flux in the core and their parameters are compared Tables 3.2 and 3.3.

Table 3.2: Parameters of the designed coupled inductors.

		1 Conventional CI	3-Limb	DC choke
Material		Iron based metglas amorphous alloy		
B_{max}		0.72 T	0.7 T	0.74 T
Core Size	A_{CS}	1.35 cm^2	0.8cm^2	1.35cm^2
	A_W	3.3 cm^2	2.66 cm^2	3.3 cm^2
Wire		AWG 15, 10.44 mΩ/m		
N^0 of turns		26 turns	23 turns	17 turns
L_W		0.76 mH	0.71mH	0.65 mH
L_L		3.8uH	0.4 uH	0.32uH
L_{CM}		3.01mH	0.25 uH	2.54mH
L_{DM}		3.01mH	2.12 mH	0.31uH
Core volume		12.91 cm^3	12.67 cm^3	12.91 cm^3
Core mass		92.67 g	90.95g	92.67 g
Wire mass		53.81 g	102.0 g	95.21 g
Wire volume		6.0 cm^3	11.39 cm^3	10.63 cm^3
Core & Cu volume		18.91 cm^3	24.05 cm^3	23.53 cm^3
Core & Cu mass		146.48 g	192.96 g	187.88 g
CI Eff	ma=0.1	57.3	85.3	82.5
	ma=1.15	99.7	9.83	99.84

Table 3.3: Comparing the size and performance of the designed coupled inductors.

		3 Conventional CIs	3-Limb & dc choke	Difference
Core volume		38.72 cm^3	25.57 cm^3	**-34%**
Core mass		278.01 g	183.6 g	**-34%**
Wire mass		161.44 g	197.21 g	**+22 %**
Core & Cu volume		56.74 cm^3	47.58 cm^3	**-16.4%**
Core & Cu mass		439.45 g	380.84 g	**-13.4%**
Eff of the VSC	ma=0.1	42%	61%	**+45.2%**
	ma=1.15	99.7 %	99.8%	**+0.1%**
THD_f	ma=0.1	5.85%	5.95%	**+1.7%**
	ma=1.15	4.5%	4.53%	**+0.6%**

Silicon carbide (SiC) switching devices (SCT3120AL, 650 V/21A/120 mΩ) were used to simulate the dual voltage source converter. Switch datasheet information was programmed into PLECS simulation software to estimate the semiconductor losses due to factors such as conduction, switching, and diode reverse recovery. Linear models were used to simulate the coupled inductors and resistance of the inductors operating with a temperature rise of 60 °C. Various power losses were compared between using the

proposed dual coupled inductor versus the conventional coupled inductors. The simulated inductor peak flux density per switching cycle was used with the inductor design parameters in Tables 3.2 and 3.3. Inductor loss equations were then used to estimate the switching cycle inductor losses, and then averaged over a fundamental cycle to obtain the average inductor power losses.

The dual voltage source converter using both inductor types produced high-quality 5-level PWM line voltages (v_{line}) with a fundamental frequency of 600 Hz, see Fig. 3.12. The flat voltage levels in the waveforms illustrates the high coupling between the two windings located on the same limb for the 3-limb coupled inductor hence has a very low fundamental output voltage droop when compared with conventional coupled inductors using C-shaped cores, Fig. 3.13. This is as a result of the tight coupling between windings located on the same limb for the 3-limb coupled inductor as compared with the weaker coupling between windings on separate limbs for the conventional CI.
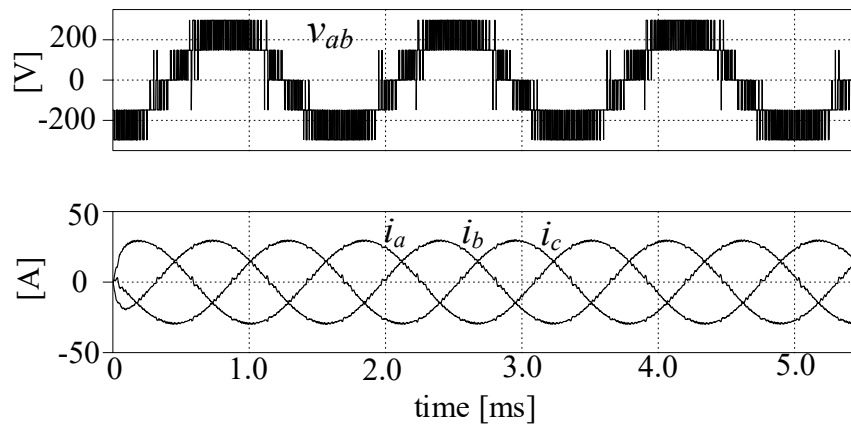
Fig. 3.12 Simulated waveforms of the parallel-connected VSCs using the 3-limb CI and the dc choke, $f_1 = 600$ Hz.
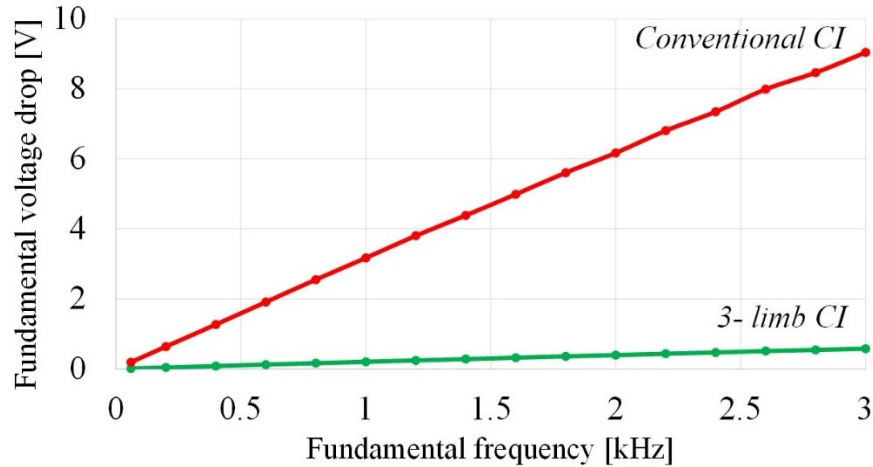
Fig. 3.13 Output fundamental voltage drop with fundamental frequency.

For the loss results presented in Figs. 3.14–3.18, the load current was changed proportionally with the output voltage hence the modulation index (ma). The loss differences between the dual CI and the conventional CIs, see Figs. 3.14 – 3.16 were obtained by taking the average of the loss differences over the range of amplitude modulation index (ma) used. The inductor core losses show that the dual CI have an average loss 40% smaller than the conventional CIs, including 40% less when the losses are at their minimum, ma= 1.15 in grid connected converters.

The inductor copper losses, Fig. 3.15 for the dual CI are considered to have an average 24% higher loss over the range of amplitude modulation index used, approximately 41% where the losses are at their highest. However, note that the output voltage for the conventional CI dropped significantly as the amplitude modulation index was increased, resulting in a lower output current, hence lower Cu losses. When averaged over the range of amplitude modulation index considered, the dual CI have a 16% lower total loss. This is due to the core losses being significantly higher than the Cu losses. When the dual voltage source converter is operated with the same output power for both inductor cases, similar semiconductor losses were experienced, see Fig. 3.16, with the dual CI having slightly higher losses at high amplitude modulation index and slightly lower losses at low amplitude modulation index. The small differences can be related to slight variations in the system currents as a result of using the two inductor types. The dual CI can be said to be competitive with the conventional CI when it comes to the semiconductor losses. The

63

dual CI has a slightly higher overall efficiency when they operated at a low amplitude modulation index (ma < 0.5) (see Fig. 3.17). When comparing the power conversion efficiency of the coupled inductors alone, the dual CI have a higher conversion efficiency than the conventional coupled inductors (CIs) at low values of amplitude modulation index, see Fig. 3.18. This can be linked to the dc choke and 3-limb CI having a lower peak flux, hence lower core losses, than the conventional CI. When operated at constant load current over a range of modulation indexes, the load current total harmonic distortion (THD_f) is very similar, Fig. 3.19. The current THD_f is mainly determined by the nature of the PWM scheme, and not by the choice of inductors used.
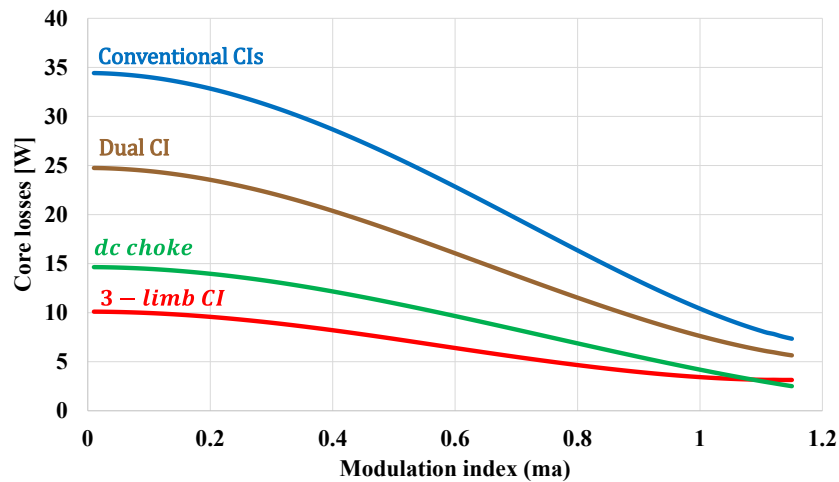
Fig. 3.14 losses in the conventional CIs, 3-limb CI, and the dc-choke.
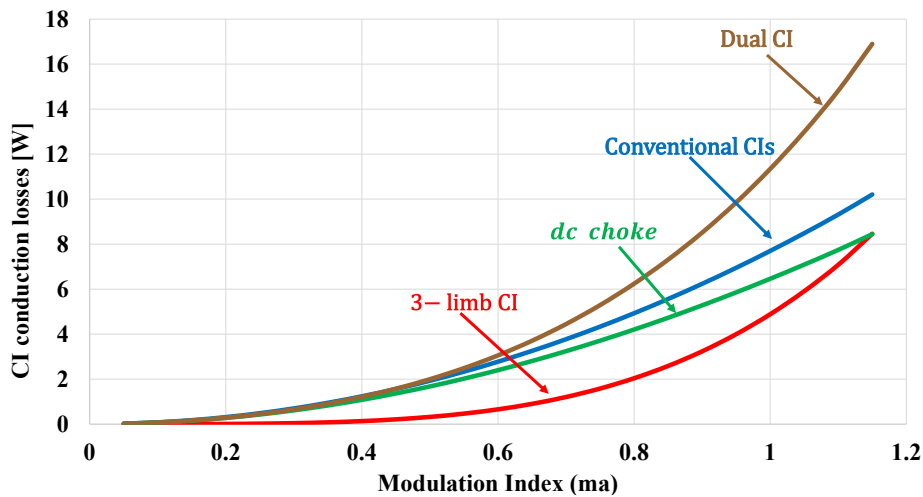
Fig. 3.15 Conduction losses in the conventional CIs, 3-limb CIs and dc-choke.

64
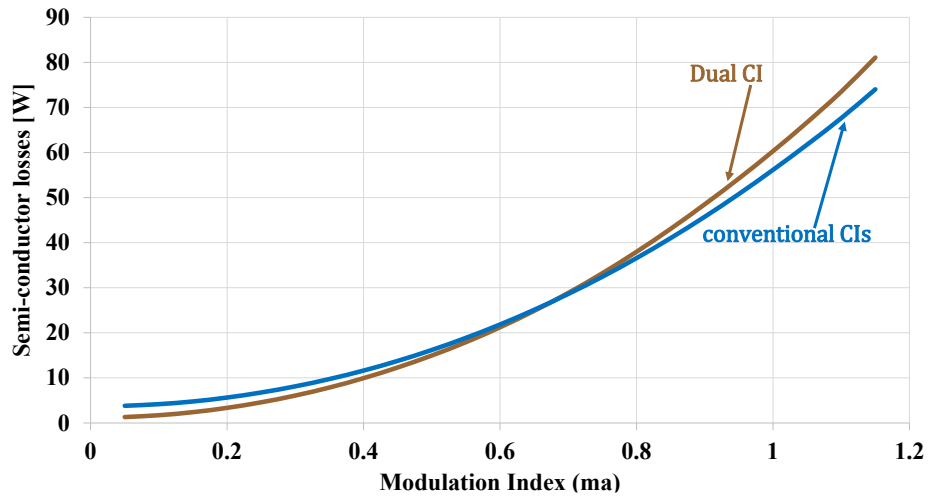
Fig. 3.16 Semi-conductor losses in the VSCs
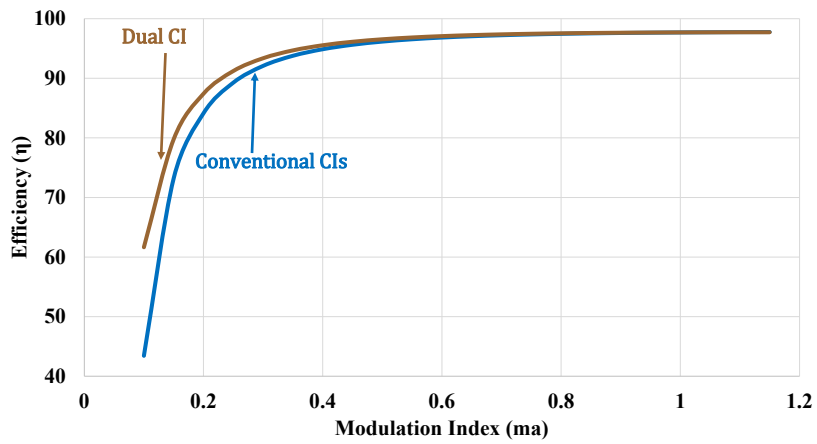
Fig. 3.17 Efficiency of the two VSCs (only semiconductor losses considered)
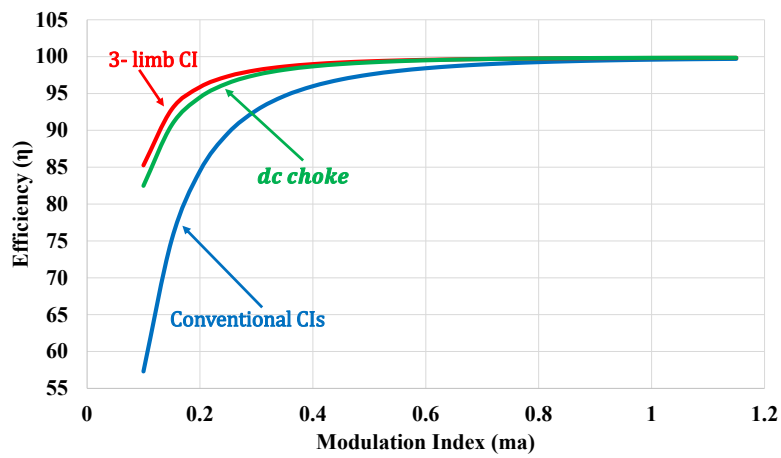
Fig. 3.18 Efficiency of the CIs in VSCs operating with the M_SPWM and the transition techniques.
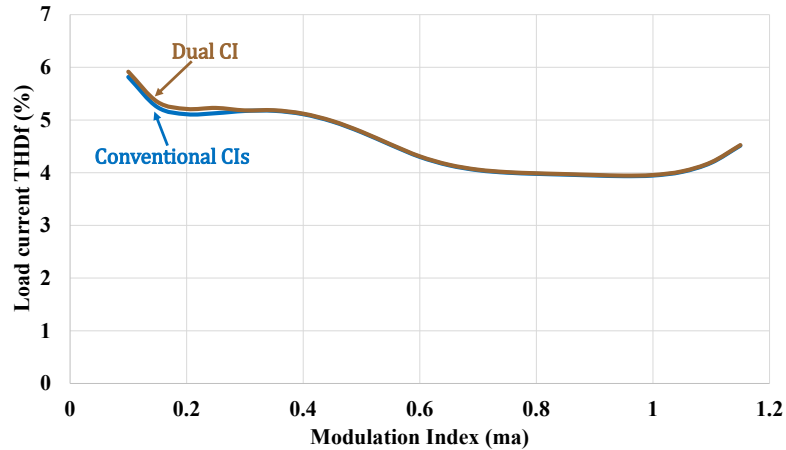
Fig. 3.19 Current THD of the two VSCs operating with the M_SPWM and the carrier transition techniques, $f_1 = 60$ Hz and constant current operation.

3.4. Experimental verification.

Test were conducted using a three-phase RL-load (R=3.5Ω, 70 uH), IGBT half-bridge modules (SKiM306GD12E4), and the PLECS RT-box was used as a digital controller. The setup and the various inductors used are presented in Fig. 3.20 and Fig. 3.21 respectively. The PWM voltage waveforms across the windings of the 3-limb CI and dc choke are similar to the simulated waveforms, compare Fig. 3.2 (b) with Fig. 3.22.
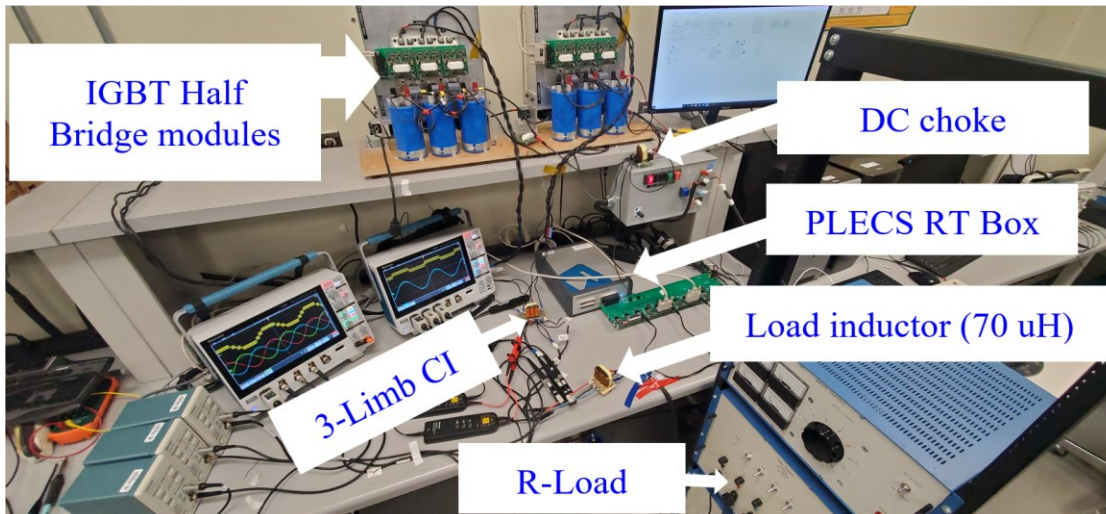
Fig. 3.20 Experimental setup.

66
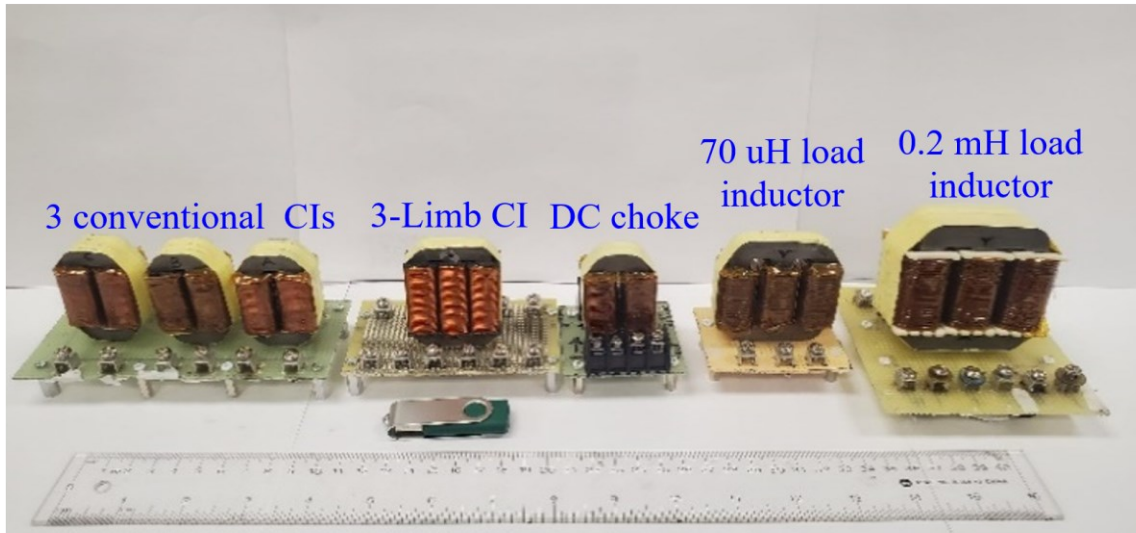
Fig. 3.21 Coupled inductors and load inductors built to run experimental tests.

These results confirm that the common mode component of the voltage between the two converters is dropped across the dc choke and the differential mode component is dropped across the 3-limb CI. This is as a result of the dc choke having a high inductance for common mode voltage and a low inductance for the differential mode voltage. Conversely, the 3-limb inductor has a high inductance for the differential mode voltage and a low inductance for the common mode voltage.

(a)

67
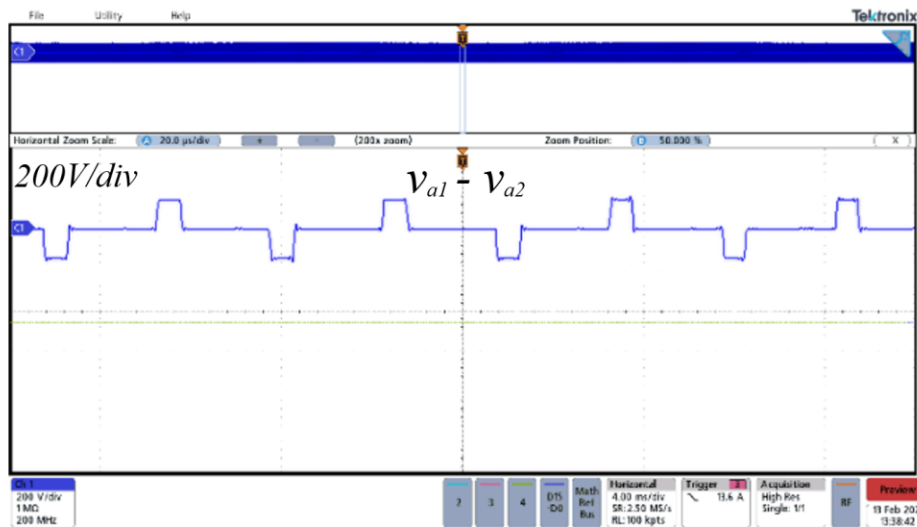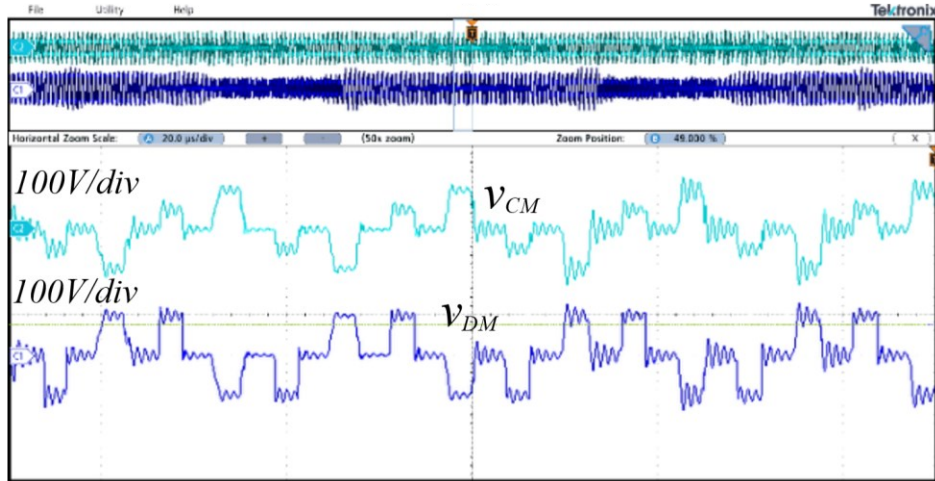
(b)

Fig. 3.22 Voltage across the CIs windings (a) Conventional CIs (b) 3-limb CI and dc choke.

Both coupled inductor types generate high-quality 5-level PWM line voltages with a PWM voltage step of $V_{dc}/2$. The frequency of the PWM line voltage is four times greater than the carrier frequency ($4f_c$). Such PWM voltages can be more easily filtered using a smaller ac filter inductor. The PWM phase voltage (v_{pha}), the 3-limb CI winding currents (i_{a1}, i_{a2}) and the load currents (i_a, i_b, i_c) are presented in Fig. 3.23 when using the dual CI.

(a)

68
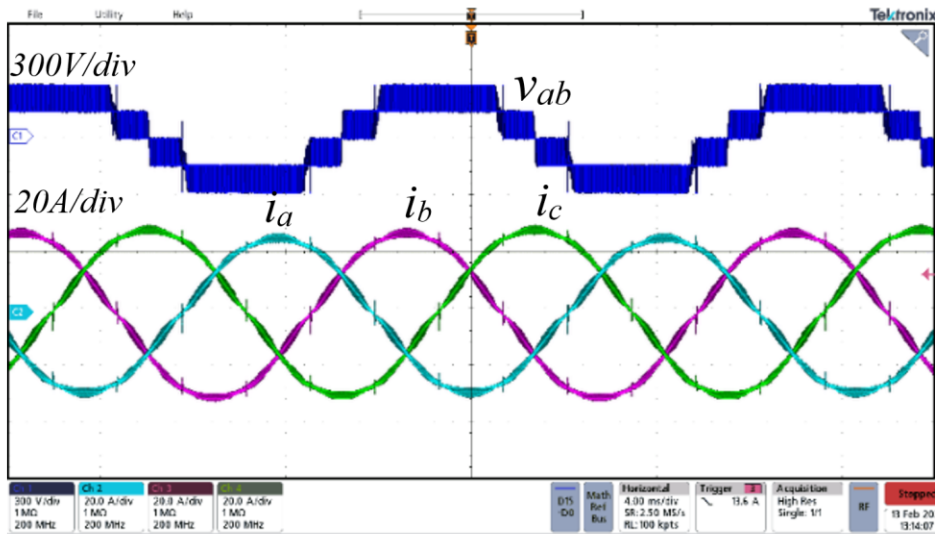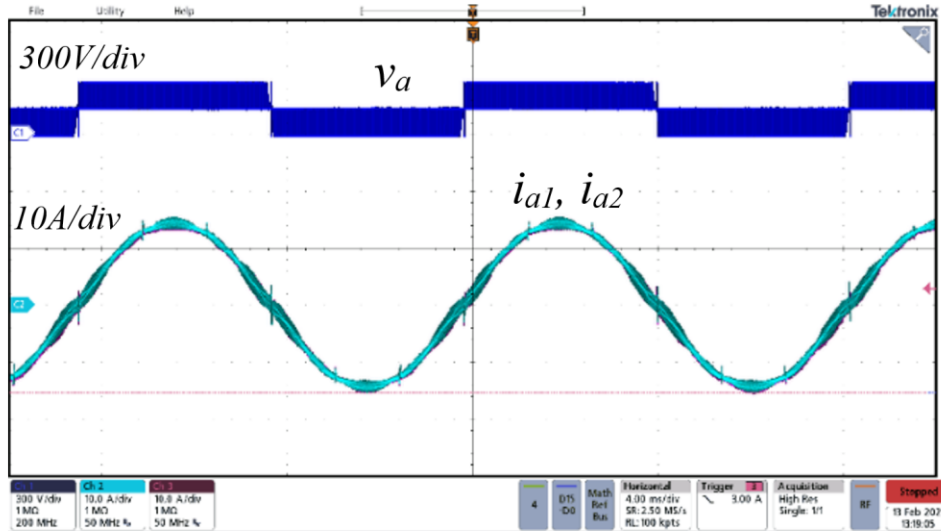
(b)

Fig. 3.23 Experimental waveforms of the dual CIs operating using the M_SPWM with carrier transition techniques (a) PWM line voltage and the load currents (b) PWM phase and CI winding currents (V_{dc}= 300 V_{dc}, f_c=20 kHz, L=70uH, f_1=60Hz)

The output line voltage, 3-phase output currents and circulating currents are shown at 60 Hz and 1.1 kHz in Fig. 3.24 for the conventional CI, and Fig. 3.25 for the dual CI. For the conventional CI case, the line voltage has a significant curve on the voltage levels. This is caused by a significant fundamental voltage drop due to the higher output inductance linked to the higher leakage inductance between windings: the conventional CI has the two-coupled windings located on separate limbs.

69
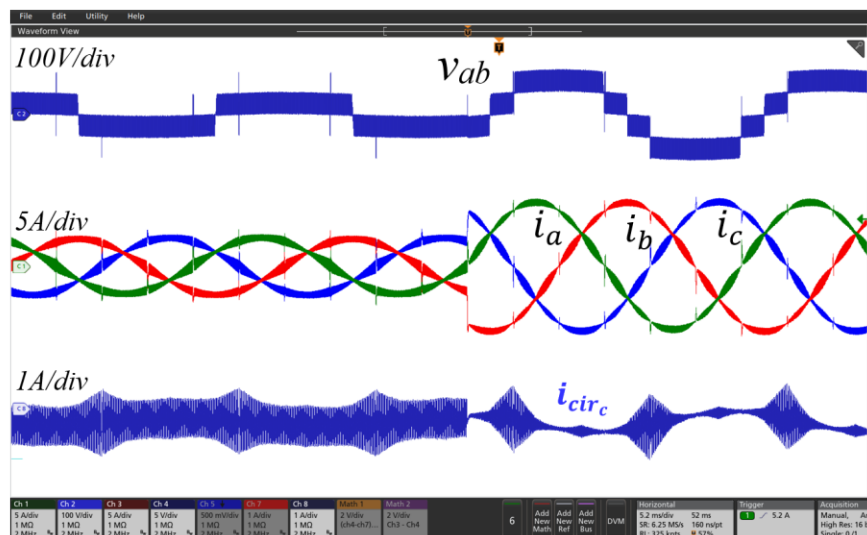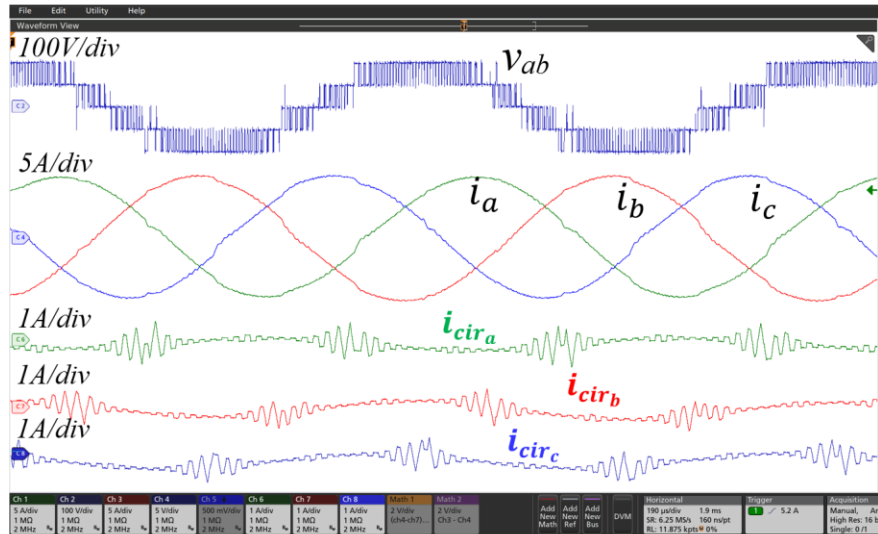
(b)

Fig. 3.24 Experimental waveforms of the dual voltage source converter using the conventional CIs (a) f_1 = 60 Hz. L = 70 uH, (b) f_1= 1.1 kHz, L= 0.2 mH.
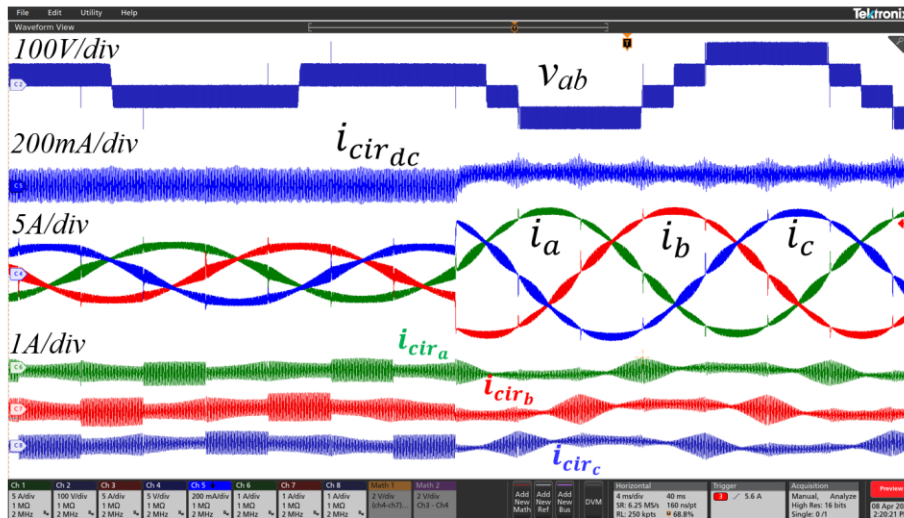
(a)
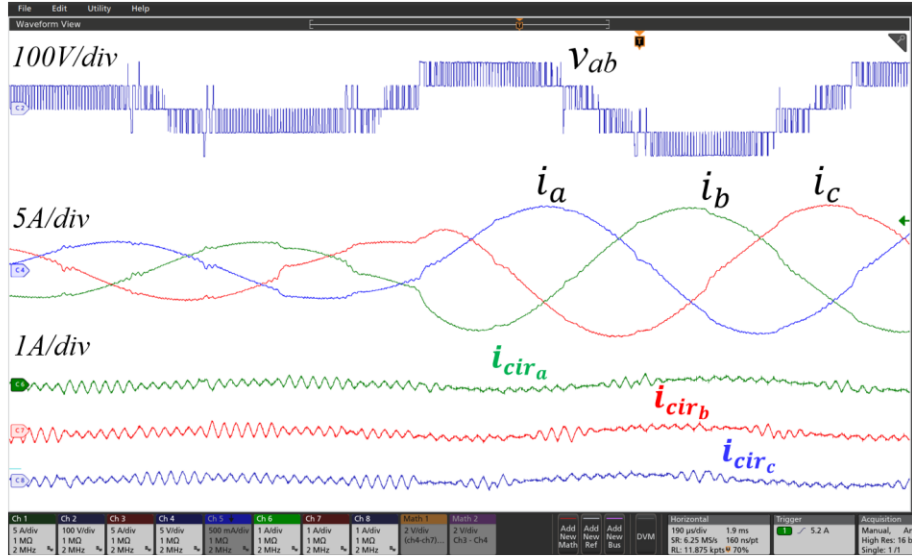
(b)

Fig. 3.25 Experimental waveforms for the dual coupled inductors: (a) f_1 = 60 Hz, L= 70 uH, (b) f_1 = 1.1 kHz, L= 0.2 mH.

For the dual CI case, the output line voltages have flat voltage levels. The tightly coupled windings in the 3-limb core significantly lowers the fundamental voltage drop across its windings and the resultant output line voltage can be said to have a high quality with vastly reduced curving when compared with the conventional CI. This characteristic makes it feasible to generate high-frequency fundamental PWM output voltages in the kHz range.

3.5. Conclusion.

A dc-choke and a 3-limb coupled inductors, or dual CIs, where presented as a means to connect two parallel voltage source converters and to control circulating currents due to the PWM voltage difference that is normally experienced between the 3-phase output voltages of the two converters. This voltage difference can be seperated into two components: a differential mode PWM voltage and a common mode PWM voltage. The flux due to the two components is observed to be 30% lower than the flux due to the combined voltage. The dc choke is used to provide a high inductance for the common mode PWM voltage but a low inductance for the differential mode PWM voltage. Conversely,

71

the 3-limb coupled inductor provides a high inductance for the differential mode PWM voltage and a low inductance for the common mode PWM voltage.

Examination of the two inductor types reveals: (a) the 3-limb coupled has a very low inductance for 3-phase output currents, resulting in a low output voltage droop and that is useful in systems generating high fundamental output frequencies; (b) the dc choke has a very low inductance for currents drawn from the input dc supply and so can have a very fast transient load response similar to that can be experienced at the ac outputs.

A design study shows that the dual coupled inductors can be on average is 16% less lossy and 13% smaller when compared with using three conventional CIs. The dual CIs are shown to provide a high inductance for controlling circulating currents whilst having a low output and input inductance. The inductor designs examined show that the dual CI is useful to reduce the size, weight, and material cost of the magnetics in parallel connected voltage source converters. The performance of dual coupled inductors was compared with that of conventional CIs using simulations and experimental results for an 8 kW (300 V_{dc}, 208Vac/22A) laboratory prototype operating over a wide range of fundamental frequencies (60Hz~1.1kHz). Target applications include uninterrupted power supplies, flywheel energy storage systems, electric vehicles and mobile systems where lightweight magnetics is required.

Chapter 4

Neutral point clamped voltage source converters.

Two neutral point clamped voltage source converters (VSC) are presented. Both types use two level PWM modules connected to coupled inductors at the output and a

neutral point clamped (NPC) as the input. The resultant converter can be used in high voltage, high current applications such as fast/ultra fast ac electric vehicle chargers, battery energy storage systems, flywheel energy storage devices, and electric drives. The first topology variation has a reduced switch count, with unidirectional power flow in a grid rectifier. A larger number of output voltage levels are produced with smaller voltage steps by using two level converter modules when compared with other topologies having the same number of switching devices. The second topology validation is a bidirectional converter using a 3-limb output coupled inductor connected to two level dual inverter legs in each phase and a four switch NPC input stage. This represents the use of a minimal coupled inductor size with multi-level outputs which have a very small harmonic content and can easily be filtered using a small ac inductor, thereby reducing the overall size/ weight of high-power voltage source converter.

With the growing trend toward higher dc-link voltage in electric vehicles, multi-level topologies capable of reducing the voltage stress on switching devices are investigated as a feasible and efficient option for replacing the conventional two level six switch converter. There is a need for electric vehicle chargers with power greater than 400 kW and output dc voltage of at least 800 V. However, high dc-link voltages lead to higher switching losses which reduce the overall efficiency of power converters. In addition, higher dc-link voltages increase the peak flux in interface coupled inductors, thereby increasing the size/ weight of magnetic core required to avoid saturation.

4.1. Neutral point clamped converter topology

The multi-level coupled inductor (CI) converters presented in this chapter use (a) one outer module, four series connected semi-conductor devices across the dc-link to form the NPC stage that clamps and reduces the voltage stress of all the switching devices to $V_{dc}/2$ (b) inner inverter legs or modules whose outputs are connected to coupled inductors to produce multi-level output voltages, with voltage steps much lower than the supply voltage, see Fig. 4.1. The common mode voltage between the 3-phase grid and the output dc grid is drastically reduced as a result. The outer modules in the NPC stage operate at the fundamental frequency while the inner modules use two level inverter legs that receive

interleaved PWM signals and have a high switching frequency. N-inner modules or high-frequency modules can be used together with the output coupled inductors generate 4n+1 level PWM line voltages with a PWM frequency 2n times greater than the switching frequency of the inner modules. These multi-level PWM outputs have a very small harmonic content and can more easily be filtered by the low winding inductance of high-speed machines or small ac filter inductors; thereby reducing the size/ weight of the converter magnetics.

(a)

(b)
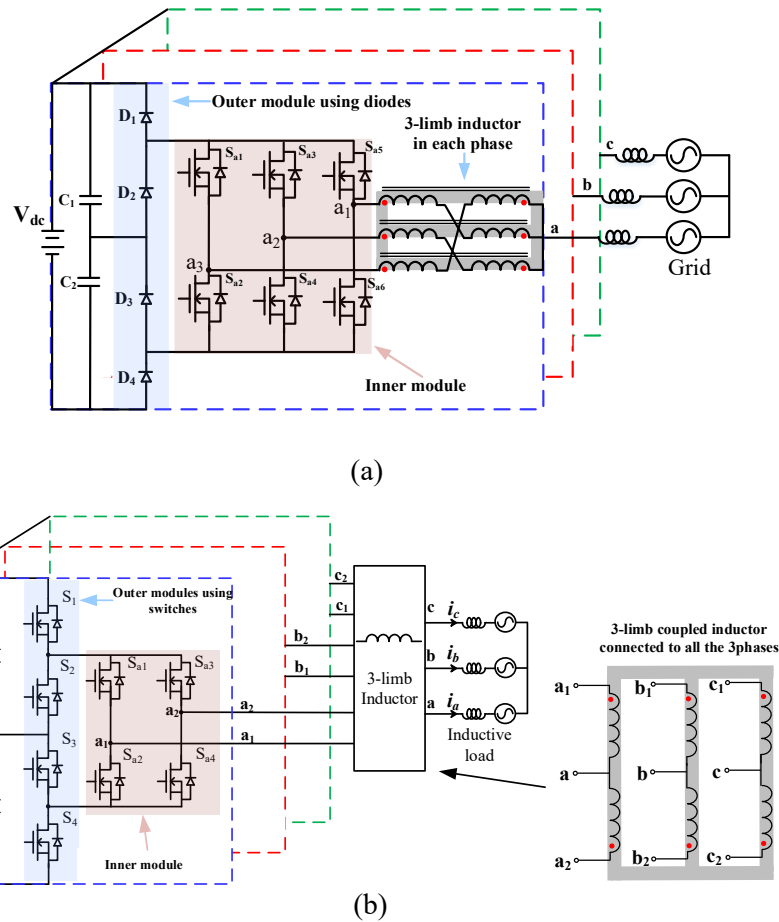
Fig. 4.1 Neutral point clamped CI converters (a) unidirectional, (b) bidirectional.

The outer module can connect the input dc terminals of the inner module across the upper dc capacitor, C1, see Fig. 4.2 (a), (b). When using diodes in the outer module, this occurs in a grid connected system when the phase current is flowing into the converter, Fig. 4.2 (c), (d). The high-frequency inner modules are connected to coupled inductors which produce multi-level output voltages. Fig. 4.1 (a) is shown using 3 inverter leg inner

74

module with a 3-limb coupled inductor connected to the phase output terminals. These inductors have cross coupled windings to improve the quality of the multi-level output voltages, see Fig. 4.1 (a). Since the windings on the 3-limb inductor are Y-connected, they can cope with both common mode (CM) and differential mode (DM) voltage between the inverter legs without saturating. The bidirectional converter, Fig. 4.1 (b), uses a 3-limb inductor with windings that connect the 2 outputs of all 3 phases. This situation cannot have common mode voltages across its windings, so a PWM scheme that produces no common mode voltage between the inverters is used to produce multi-level PWM output voltages [103]-[108]. It is worth nothing that three separate coupled inductors on C-shaped cores can also be used here, which can cope with both common mode and differential mode voltages across their windings, but the 3-limb inductor was chosen here to minimize the inductor size and weight as well as lowering the inductor losses.

(a)   (b)   (c)   (d)
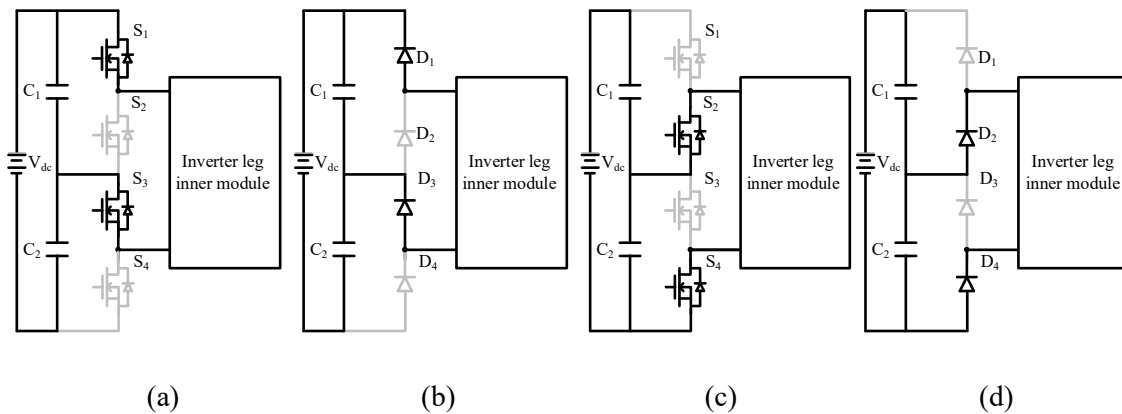
Fig. 4.2 Active outer switching devices when (a) & (b) the load currents are positive (c) & (d) the load currents are negative.

4.2. Pulse width modulation and control

Parallel-connected voltage source converters are often operated using interleaved PWM switching with multiple phases shifted carriers. The PWM scheme for the two neutral point clamped topologies is described in this section.

4.2.1. Unidirectional NPC using a 3-inverter leg inner module

Since the inner module is connected across either the top dc capacitor or the lower capacitor depending upon the sign of the input current, which matches the sign of the grid voltage when operating at unity power factor, the sinusoidal modulating signals to control the inner module must be modified, see Fig. 4.3. The same modulating reference signal is used in each phase of the converter, for example ref_a expressed as (4.1) is used for all the switching devices in phase "a", and the three carriers allocated to each inverter legs control their PWM switching. This modulation scheme generates 7-level phase and 13-level PWM line voltages at the output of the 3-limb coupled inductors.
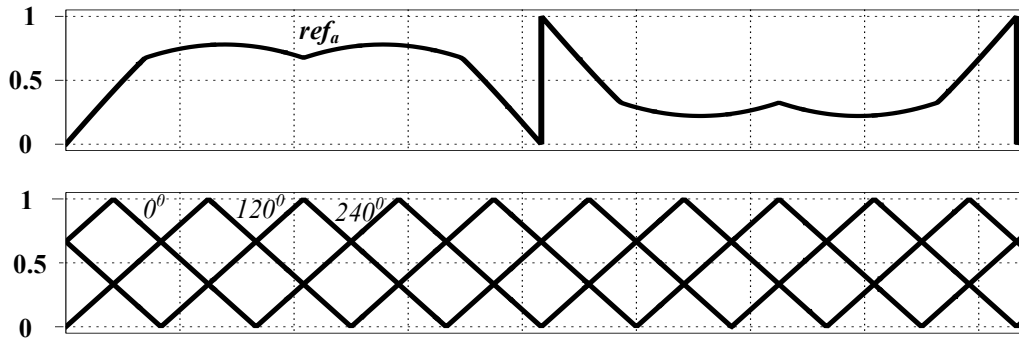
Fig. 4.3 Reference and carriers of the neutral point clamped coupled inductor rectifier.

$$ref_a = \begin{pmatrix} |m_a| \sin\Theta, & |m_a| \sin\Theta \geq 0 \\ |m_a| \sin\Theta + 1, & |m_a| \sin\Theta < 0 \end{pmatrix} \qquad (4.1)$$

A standard 3-phase grid current controller was used as the focus is to prove the functionality of the proposed converter. The control algorithm consists of three blocks to transfer power from the grid to the converter dc-link, Fig. 4.4. The first block is a current controller, which regulates the magnitude of the converter phase currents. This block compares the measured converter phase currents in the αβ reference frame ($i_{αβ}$) with that of the calculated reference current ($i_{αβ}'$) and the error is processed using a proportional

integral resonant controller (PIR) to determine the signal $\xrightarrow{m_1}$. The grid voltage ($v_{abc}/v_{\alpha\beta}$) is measured for feed-forward control. The second block is a capacitor voltage controller. In this block, the error obtained by comparing a zero-reference voltage with the difference between the capacitor voltages on the dc-link is processed using a PI controller to produce a signal $\xrightarrow{m_2}$. The outputs of the current controller and the capacitor voltage-balancing controllers are added in the third block to produce sinusoidal signals ($\xrightarrow{m}$). The reference signals ($\xrightarrow{m_{ref}}$: ref_a, ref_b, ref_c) used to control the PWM switching of the rectifier's inner switching devices can be expressed as (4.2) and illustrated in Fig. 4.3.
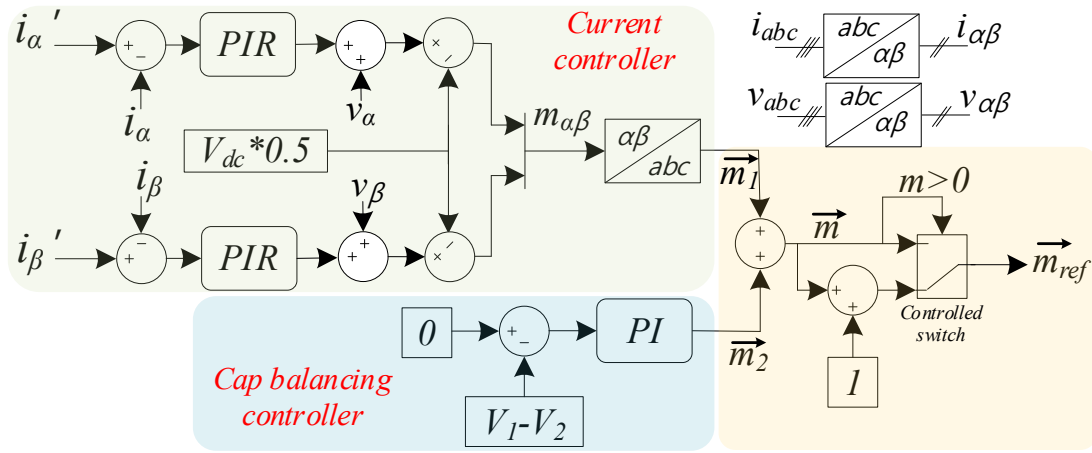
Fig. 4.4 Block diagram of the rectifier control algorithm.

$$\xrightarrow{m_{ref}} = \begin{pmatrix} \xrightarrow{m}, & \xrightarrow{m} \geq 0 \\ \xrightarrow{m} + 1, & \xrightarrow{m} < 0 \end{pmatrix} \qquad (4.2)$$

4.2.2. Bidirectional NPC using a 2-inverter leg inner module

The converter presented, Fig. 4.1(b) interleaves the PWM switching of inner modules in each phase. Since a 3-limb inductor option was chosen for this converter, a PWM scheme is required that produces no common mode between the 3-phase -inverter

leg modules in each phase, between (a₁, b₁, c₁ & a₂, b₂, c₂). A discontinuous PWM scheme was chosen to lower switching losses and also to eliminate common mode voltages across the windings of the 3-limb inductor [103]-[108]. However, traditional DPWM schemes are designed for 2-level systems and cannot be used directly on neutral point converter. Modulating reference signals are required that vary in the range 0 and 1rather than ± 1, see Fig. 4.5 (a) The reference signals (*ref*ₐ, *ref*ᵦ, *ref*𝒸) of a conventional DPWM for neutral point converter, expressed as (4.3), Fig. 4.5 (b), can be modified to generate two different type of reference signals: an average (*v*σ) and a differential reference (*v*Δ) voltage signal, Fig. 4.6.

(a)

(b)
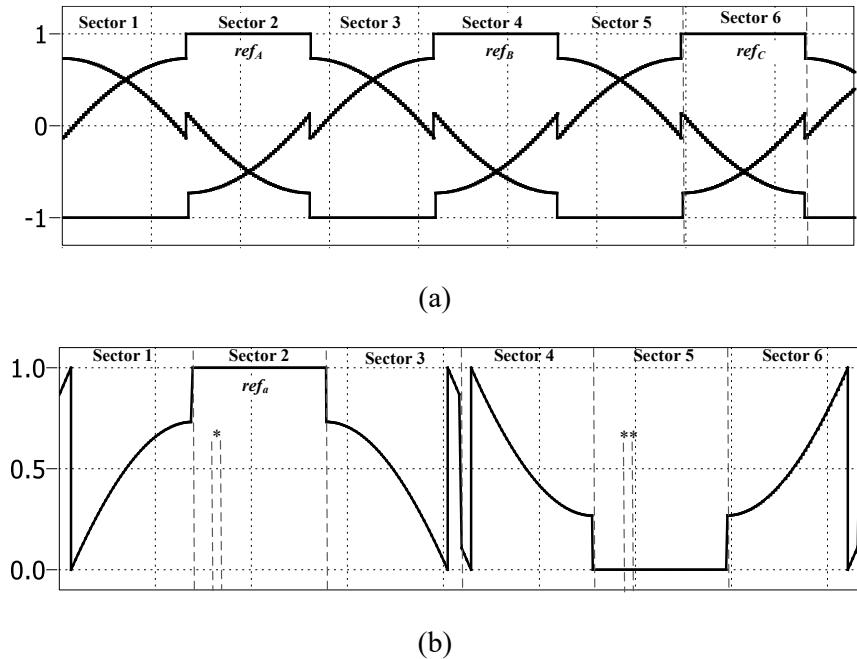
Fig. 4.5 DPWM reference signals for (a) 2-level converters, (b) neutral point clamped converters.

$$ref_a = \begin{pmatrix} ref_A, & ref_A \geq 0 \\ ref_A + 1, & ref_A < 0 \end{pmatrix} \tag{4.3}$$

The average and difference voltage reference signals can be expressed as (4.4) and (4.5) respectively when *ref*ₐ is clamped to 1, sector 2, with appropriate changes being made to define their values in the other sectors, see Fig. 4.6. Considering the segments "*" and "**" in sectors "2" and "5" identified in Fig. 4.5 with *ref*ᵦ and *ref*𝒸 being the active phases, then the reference voltage signals (*v*σ, *v*Δ) are compared with two 180^0 phase shifted carrier signals (X, Y) to generate the eight digital signals (S_{AX}, S_{AY}, S_{DX}, S_{DY}, $\overline{S_{AX}}$, $\overline{S_{AY}}$, $\overline{S_{DX}}$, and

$\overline{S_{DY}}$), Fig. 4.7. The digital signals S_{AX} and S_{AY} are obtained by comparing the average reference (v_σ) signal with the two 180^0 phase shifted carriers. Likewise, the digital signals S_{DX} and S_{DY} are obtained by comparing the difference reference signal (v_Δ) with the two 180^0 phase shifted carriers, see Fig. 4.7. The signals $\overline{S_{AX}}$, $\overline{S_{AY}}$, $\overline{S_{DX}}$, and $\overline{S_{DY}}$ are complementary to S_{AX}, S_{AY}, S_{DX}, and S_{DY}.

$$v_\sigma = \frac{(v_{ref\_B} + v_{ref\_C})}{2} \tag{4.4}$$

$$v_\Delta = \begin{cases} 1 - \left| \dfrac{(v_{ref\_B} - v_{ref\_C})}{2} \right| ; v_{ref\_A} = 1 \\[3mm] \left| \dfrac{(v_{ref\_B} - v_{ref\_C})}{2} \right| ; v_{ref\_A} = 0 \end{cases} \tag{4.5}$$
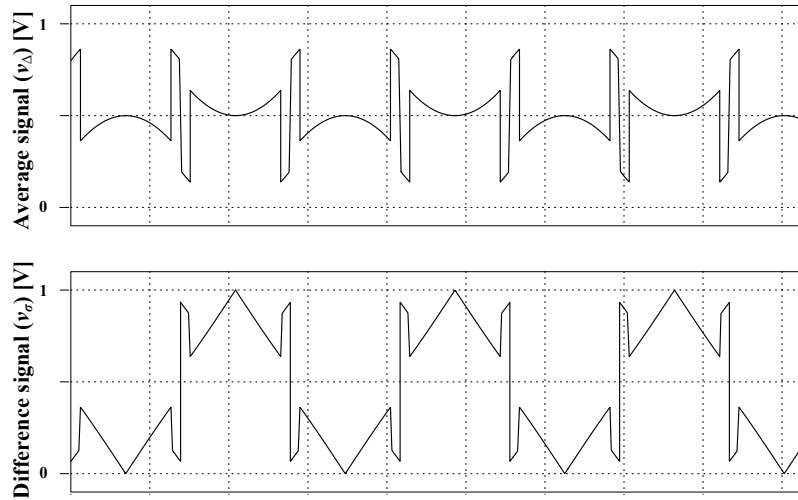
Fig. 4.6 Average and difference signals.
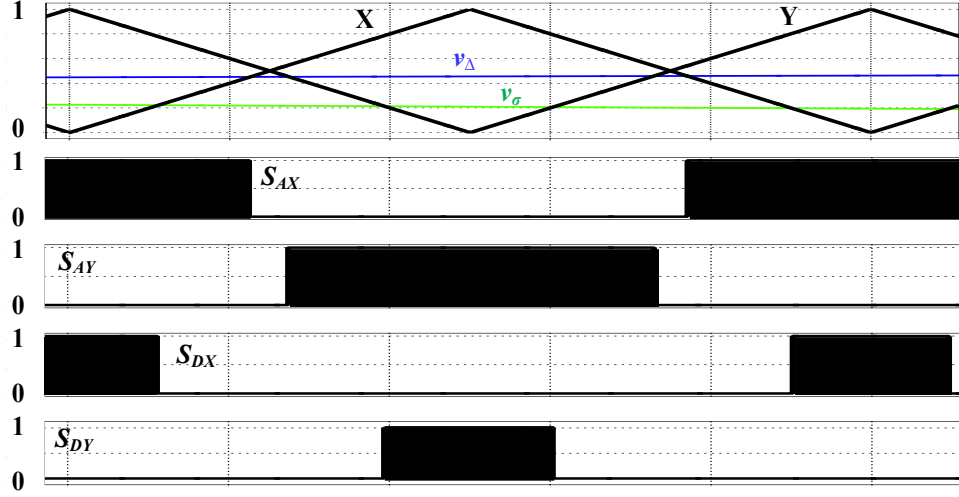
Fig. 4.7 Digital signals obtained by modulating the average and difference reference signals.

These digital signals are passed through a logic stage to generate the actual gate signals for the converter. When the reference signal ref_a is clamped to 1 and ref_b is greater than ref_c, the logic presented in Fig. 4.8 (a) is used to determine the gate signals of the converter switching devices. When the reference signal ref_a is clamped to 1 and ref_b is less than ref_c, the logic in Fig. 4.8(b) is used. The logic in Fig. 4.9 (a) is used to determine the gate signals of the converter switching devices whenever the reference signal ref_a is clamped to 0 and ref_b is greater than ref_c. Whereas the logic presented in Fig. 4.9 (b) is used when ref_a is clamped to 0 and ref_b is less than ref_c. This modulation scheme eliminates the common mode switched mode voltage (v_{CM}) across the 3-limb inductor [103]-[108] and allows the use of a compact and small 3-limb core. In addition, the modified DPWM does not affect the phase voltage of the converter expressed as (4.6). The 3-limb inductor winding voltages (v_{b1}- v_{b2}, v_{c1}-v_{c2}) and the common mode voltage (v_{CM}) between the inner inverters are presented, see Fig. 4.10, when the reference ref_a is clamped to 1. Note that winding voltage v_{a1}- v_{a2} is zero and is a magnetic short circuit.

$$v_{pha} = \frac{1}{n} \sum_{x=1}^{n} v_{ax} \qquad (4.6)$$
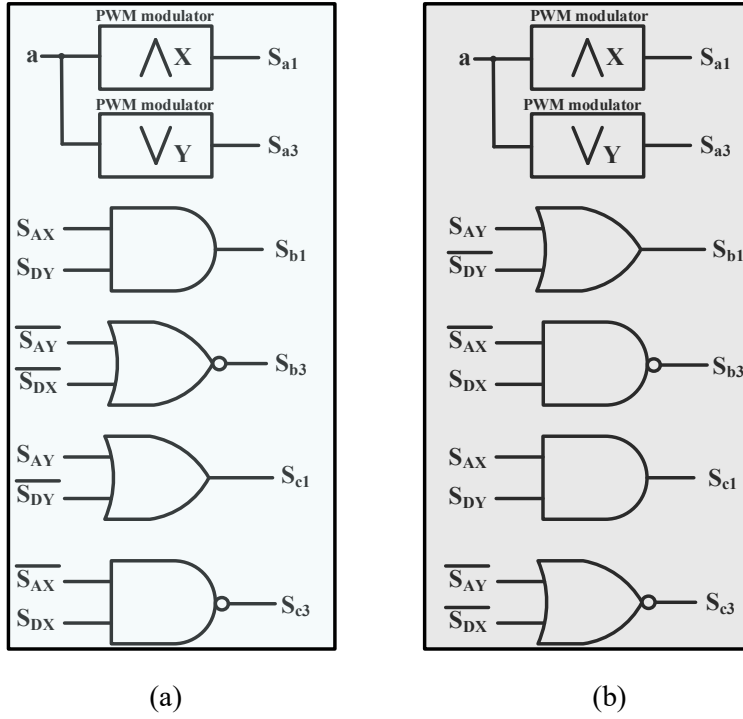
Fig. 4.8 Gate signals of the inner inverter legs when ref_a =1 (a) ref_b > ref_c, (b) ref_b < ref_c.
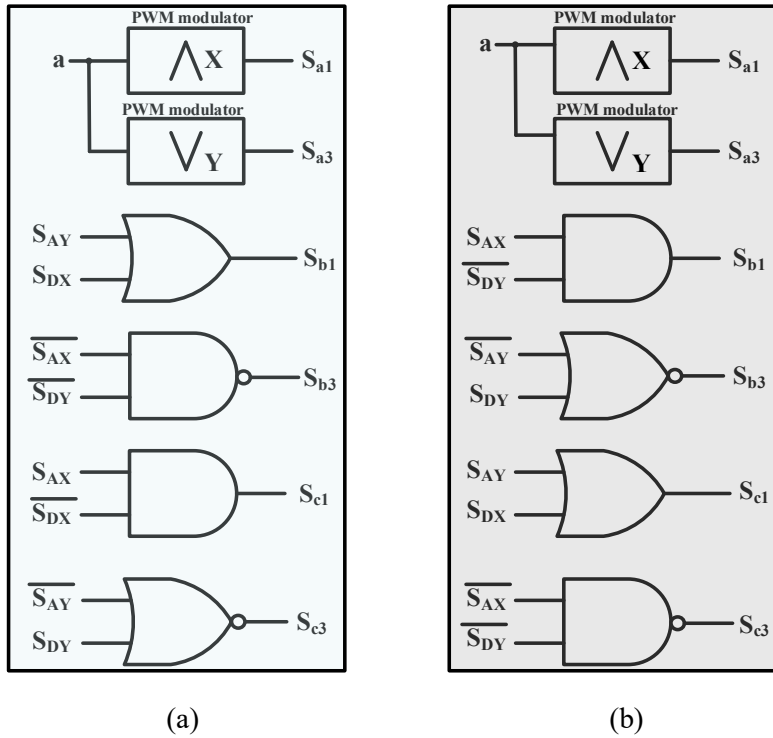
Fig. 4.9 Gate signals of the inner inverter legs when ref_a =0 (a) ref_b > ref_c, (b) ref_b < ref_c.
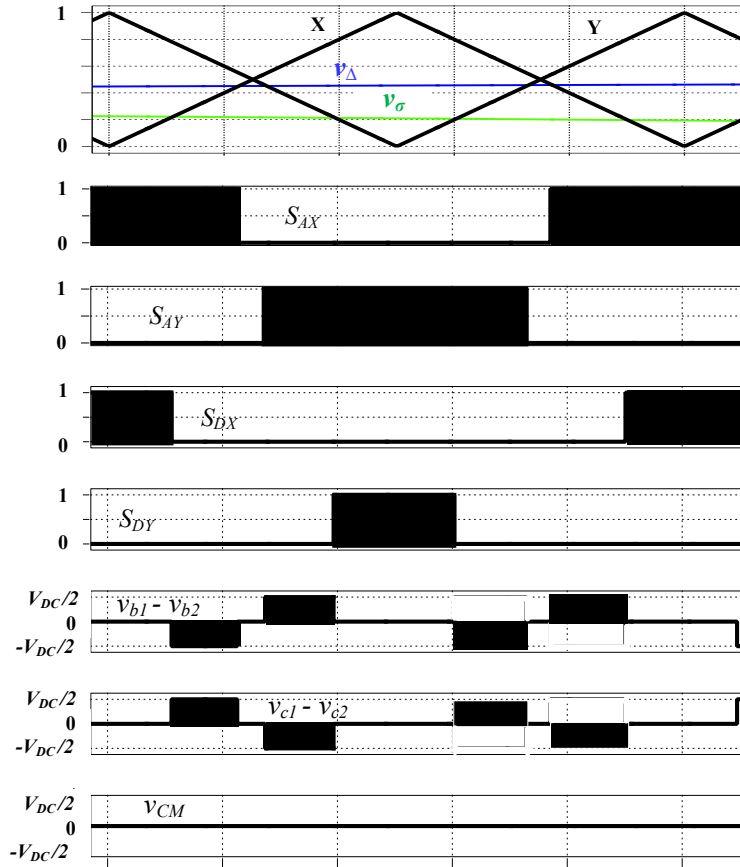
Fig. 4.10 Carrier period illustrating the 3-limb inductor winding voltages of the active phases and the common mode voltage between the parallel-connected inverter legs.

4.3. Simulation.

The parameters presented in Table 4.1 was used to approximate results of a 3.8kW neutral point clamped laboratory prototype using the PLECS simulation software. Simulation confirms that all the switching devices of the neutral point clamped topologies experience a maximum voltage stress of $V_{dc}/2$, see Fig. 4.11.

Table 4.1: Converter specifications

Parameters	values
Dc link voltage (V_{dc})	300 V
Line voltage/ phase current (V_{line}/i_a)	208 V/10.5A
Ac filter inductor (L_f)	70 uH
Carrier frequency (f_c)	20kHz

The unidirectional NPC converter produces 7-level phase (v_{pha}) and 13-level PWM line voltages (v_{line}) at the outputs of the 3-limb inductors, see Fig. 4.12.
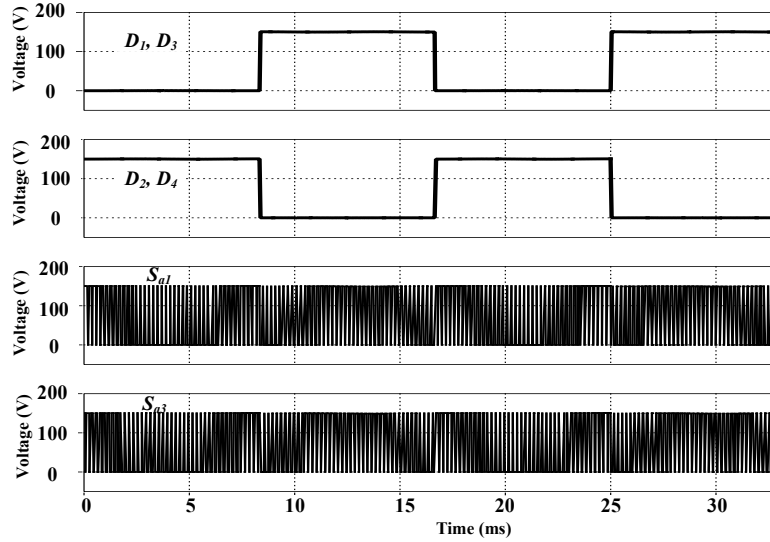
Fig. 4.11 Simulated waveforms of the voltage across the switching devices of the unidirectional neutral point clamped converter.
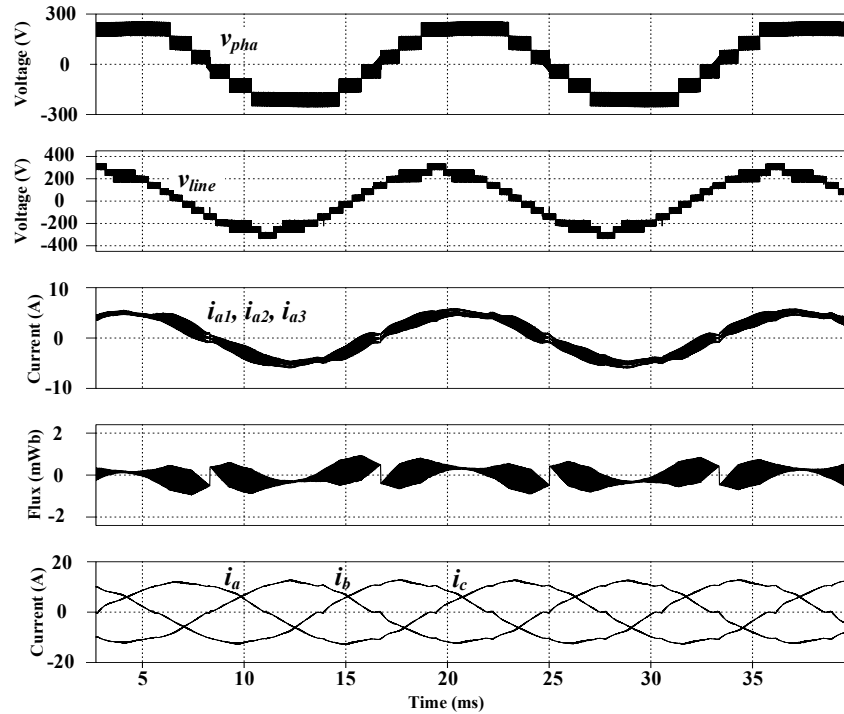
Fig. 4.12 Simulated waveforms of the unidirectional neutral point clamped converter using 3-limb coupled inductors having cross coupled windings, V_{dc}=300 V, f_c= 20kHz, L_f= 70 uH

The bidirectional NPC converter having one 3-limb coupled inductor output was simulated using the modified DPWM scheme that produces no common mode voltages between the inner modules. This converter generated 5-level PWM phase (v_{pha}) and 9-level PWM line voltages (v_{line}). The sum of the 3-limb inductor winding currents in each phase (e.g i_{a1}, i_{a2}) equaled the load currents (i_a, i_b, i_c), see Fig. 4.13.

Both sets of results confirm the absence of large high-frequency common mode circulating currents between the converter inner modules. The 3-limb CI, designed based on peak flux, can be smaller and lighter than three conventional coupled inductors using C-shaped cores designed to cope with the same peak flux as the 3-limb CI. This justifies the use of the modified DPWM, and a 3-limb CI. The bidirectional NPC converter produces fewer levels when compared with the unidirectional converter because it has 2 inverter legs vs 3 inverter legs. The DPWM scheme produces flux jumps in the 3-limb coupled inductor, making it difficult to precisely design them, Fig. 4.14.
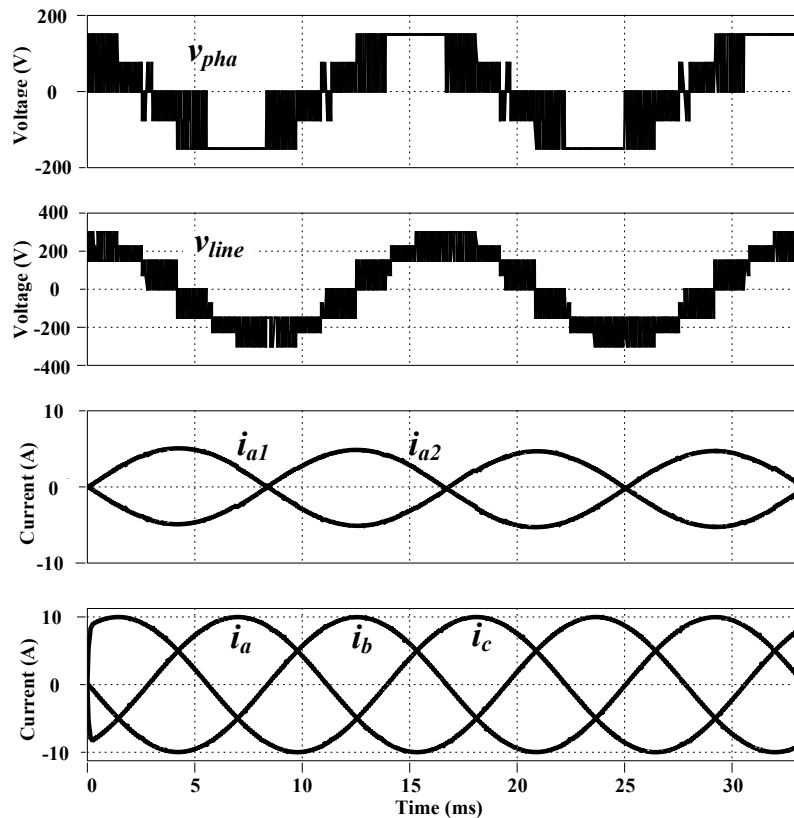
Fig. 4.13 Simulated waveforms of the neutral point clamped VSC using a 3-limb interface CI.
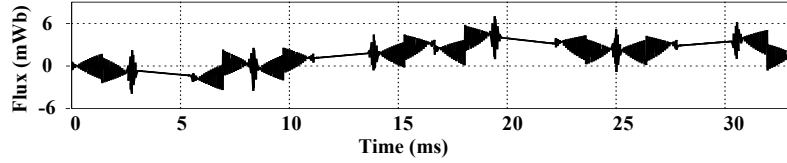
Fig. 4.14 Simulated waveforms of the neutral point clamped VSC using a 3-limb interface CI.

4.6. Experimental Verification.

4.6.1. Unidirectional NPC

3-limb inductors having cross coupled windings, Table 2.3, and the converter specifications in Table 4.2 were used to implement the unidirectional NPC converter. A DSP digital controller was used to control the PWM switching of the converter's inner modules. The experimental setup is presented in Fig. 4.15. The system generated 7-level phase and 13-level PWM line voltages which have a small harmonic content, see Fig. 4.16. The clamping diodes reduce the voltage stress across the 3-limb inductor to $V_{dc}/2$. In consequence, the size and weight of the interphase 3-limb coupled inductor designed based on peak flux can be significantly smaller when compared with that of 3-limb inductor using two level 3-phase inverter legs only.

Table 4.2: Unidirectional converter specifications

Parameters	values
Dc link voltage (V_{dc})	250 V
Line voltage/ phase current (V_{line}/i_a)	145 V/20A
Ac filter inductor (L_f)	50 uH
Carrier frequency (f_c)	20kHz
Dc-load resistor	20 Ω
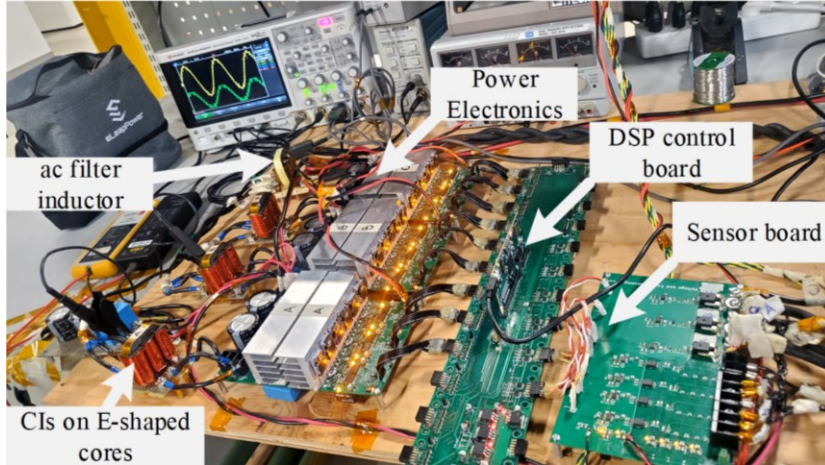
Fig. 4.15 Experimental setup of the neutral point clamped rectifier.
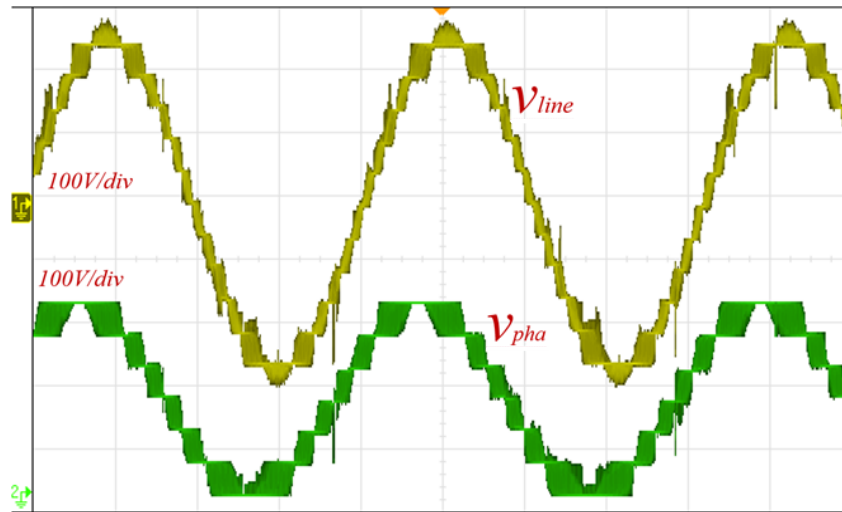
Fig. 4.16 Waveforms of the neutral point clamped rectifier, V_{dc}=250 V, f_c=20kHz, L_f= 70 uH.

4.6.2. Bidirectional NPC

A 3-limb coupled inductor (CI), whose parameters are presented in Table 4.3, was designed to test the bidirectional NPC converter using the modified DPWM. The PLECS RT-Box was used as a digital controller and an R-L Load (11 Ω, 0.4 mH) was used to demonstrate the converter's performance over a wide range of fundamental frequencies (f_1: 60Hz ~ 1.1kHz). The laboratory setup is presented in Fig. 4.17. The converter generated 5-level PWM phase (v_{pha}) and 9-level PWM line voltages (v_{line}). Most importantly, the sum of the 3-limb CI winding currents (e.g i_{a1}, i_{a2}) equaled the load currents (i_a, i_b, i_c), see Fig. 4.18.

Table 4.3: Parameters of the designed 3-limb CIs

Parameters	values
CI Winding inductance (Lw)	2.02 mH
Leakage inductance (Le)	1.3 uH
Magnetizing inductance (Lm)	8.01 mH
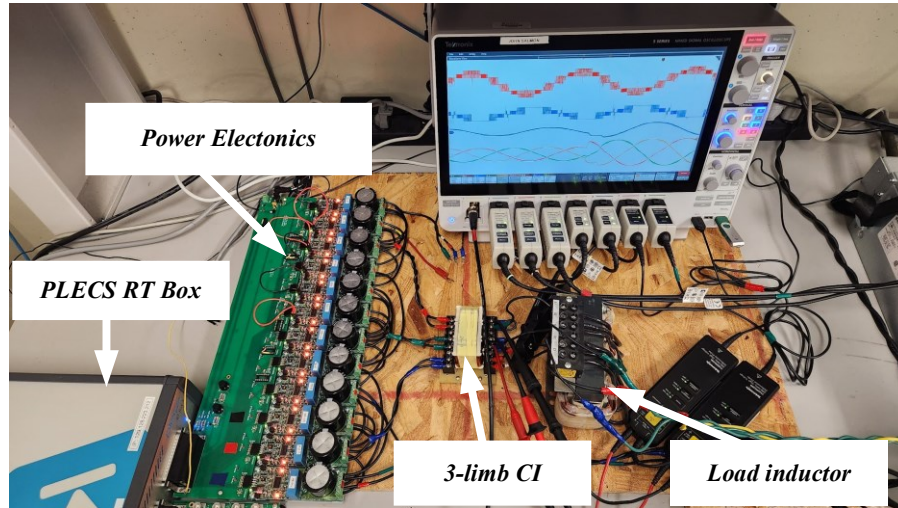
Fig. 4.17 Experimental setup of the neutral point clamped VSC with a 3-limb interface inductor.

These results confirm the absence of large common mode circulating currents between the inner modules. The 3-limb CI used had tight coupled windings which significantly lowered the inductor series inductance and made it feasible to generate high frequency fundamental multi-level PWM outputs in the kilohertz range with a very small fundamental voltage drop across the coupled inductors. Consequently, the converter outputs had flat voltage levels, see Fig. 4.19. The converter load currents are evenly shared between the inner inverter legs even during transient states, Fig. 4.18 – Fig. 4.20. Dynamic results were obtained by changing the load and the modulation index (ma).
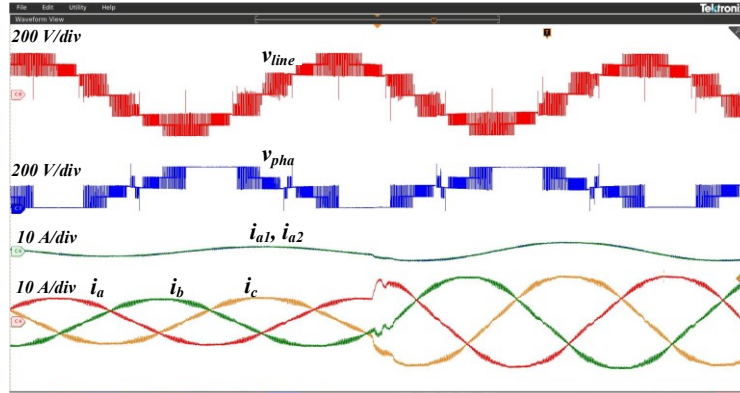
(a)
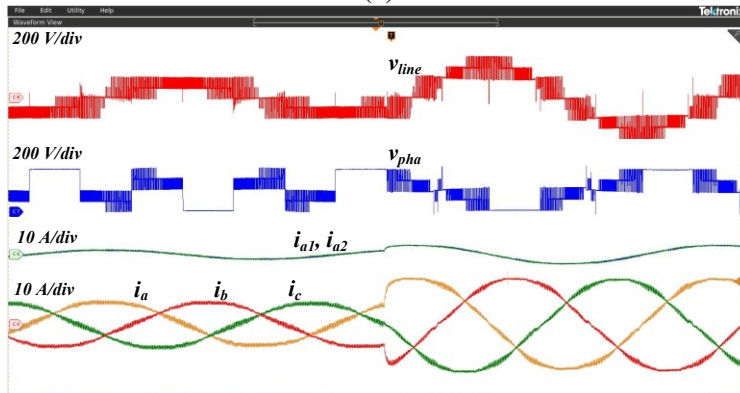
(b)

Fig. 4.18 Experimental waveforms of the bidirectional neutral point clamped converter using an interface 3-limb inductor during a transient state (a) load change, (b) change in ma, f_1= 60Hz, V_{dc}= 300 V, f_s= 20Hz, L_f= 4 mH.
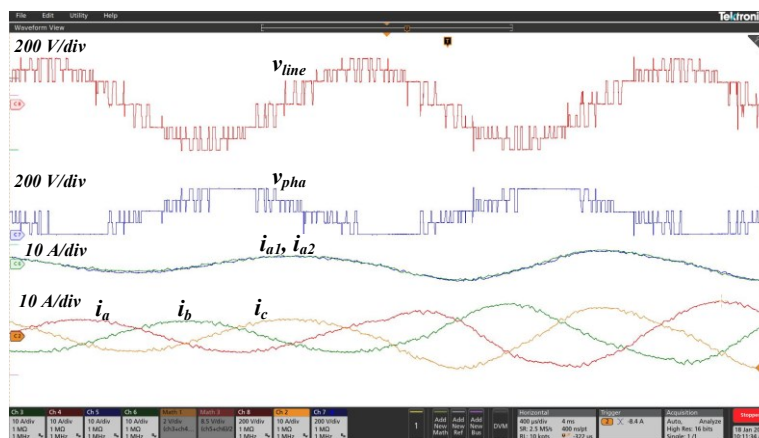
Fig. 4.19 Experimental waveforms of the bidirectional neutral point clamped converter using an interface 3-limb coupled inductor during a transient state (load change) f_1= 1.1kHz, V_{dc}= 300 V, f_s= 20Hz, L_f= 4 mH.

88
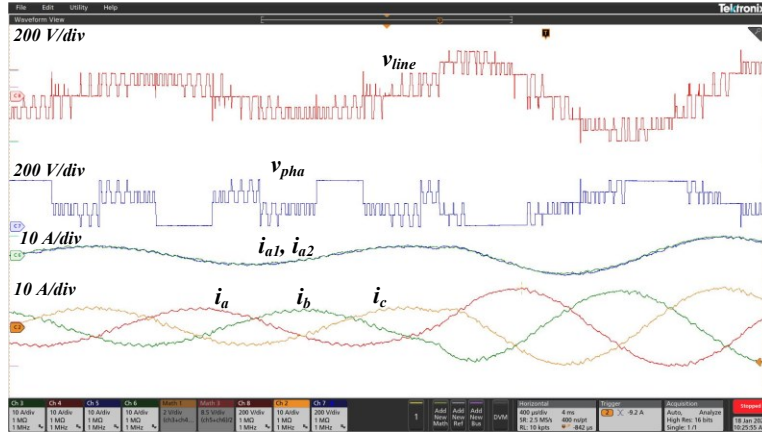
Fig. 4.20 Experimental waveforms of the bidirectional neutral point clamped converter using an interface 3-limb inductor during a transient state (change in ma), f_l= 1.1 kHz, V_{dc}= 300 V, f_s= 20Hz, L_f= 4 mH.

4.7. Conclusion.

Two neutral point clamped coupled inductor topologies using PWM controlled inner modules with 2-level inverter legs were investigated for high voltage high current converters. The proposed converter structures have outer modules acting as an NPC clamp to reduce the voltage stress across all the switching devices. The outer modules equally reduce the voltage drop across the coupled inductors which lowers their peak flux and their size/weight.

The unidirectional NPC converter has a reduced switch count and produces multi-level voltage outputs with more voltage levels (13-levels) when compared with other converter, having the same number of switching devices. The multi-level outputs have a very small harmonic content and can more easily be filtered using small ac inductors.

The bidirectional NPC converter uses a modified DPWM scheme that produces no common mode voltage between the inner modules located in each phase of the 3-phase system. This makes it feasible to use a compact/light-weight 3-limb coupled inductor to connect the outer two terminals from each phase and to produce 9-level PWM line voltages. These voltages can more easily be filtered by the low winding inductance of high-speed

machines or a small ac inductor, thereby reducing the size and weight of the power converter. The feasibility of the neutral point clamped converters has been verified using simulations and experimental results of a 3.8kW laboratory prototype. Target applications include fast/ultra-fast ac electric vehicle charging, battery energy storage systems, flywheel energy storage devices, grid connected rectifiers, and electric drives.

Chapter 5

Discontinuous PWM control for neutral point clamped coupled inductor converters.

A modulation technique which prevents flux jumps produced by conventional discontinuous PWM schemes (DPWM) in coupled inductors connected to a neutral point clamped (NPC) converter using inner 2-level inverter modules in each phase is presented. The technique is useful to reduce the converter magnetics, thereby improving the converter power density.

NPC converters with inner 2-inverter modules connected to coupled inductors, see Fig. 5.1, can be interleaved using DPWM to lower the converter switching losses by 30%. This is because certain portions of the DPWM reference signals are clamped to the maximum/minimum of the carrier for a given period, e.g 60^0 period twice, see Fig. 5.2. The transition from continuous to discontinuous PWM switching and vice versa causes the flux in the coupled inductors to experience a jump which increases the peak flux and the size/weight of the core required to prevent saturation, see Fig. 5.3. A transition technique is required to mitigate this drawback.
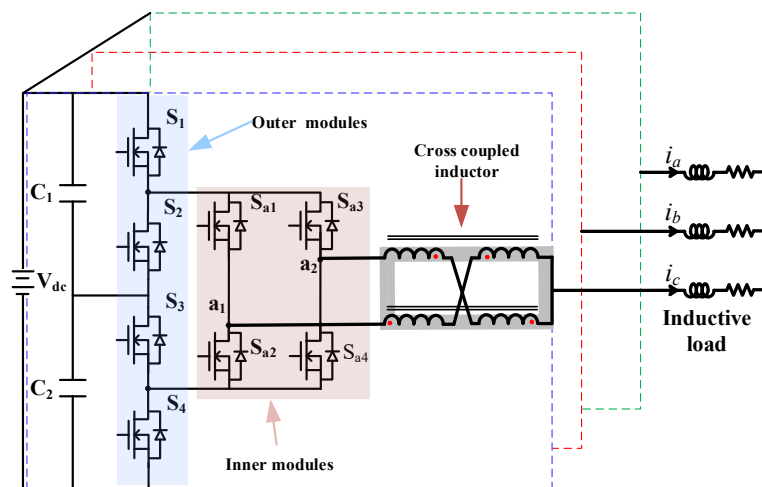
Fig. 5.1 Neutral point clamped converter with inner moules connected to cross coupled inductors.
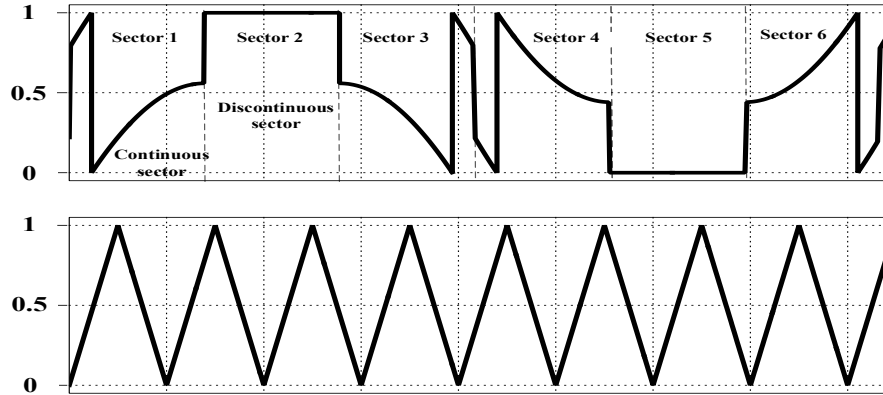
Fig. 5.2 Discontinuous reference signal.
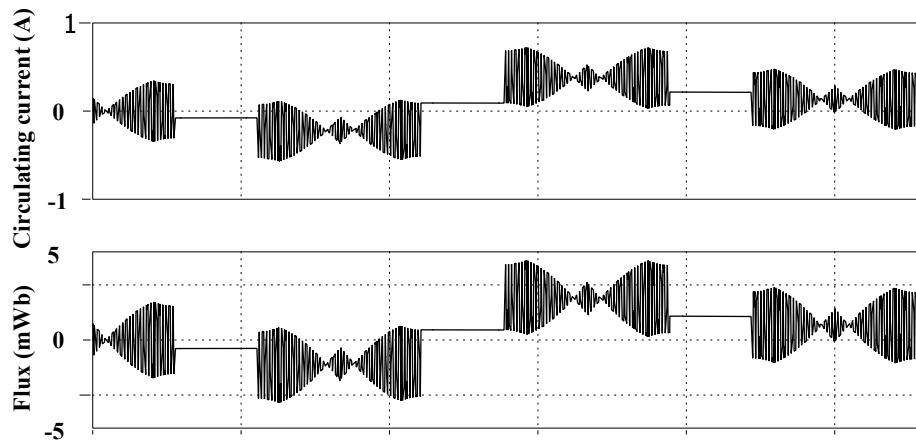
Fig. 5.3 Circulating current and flux jumps in interface coupled inductors.

5.1. Discontinuous PWM control.

Conventional interleaved DPWM uses the same reference signal for all the parallel-connected inverter legs in the same phase and evenly phase shifted carriers (0^0, 180^0) to control the PWM switching of the inner modules. DPWM involves moving between the continuous and discontinuous regions. Depending on when the reference is clamped, the circulating current and flux in interface coupled inductors may experience a dc offset and can propagate sector by sector. It is important to note that the flux remains constant throughout the discontinuous regions and becomes the starting point from where the flux beings to ramp up/down at the begging/end of the continuous sectors, see Fig. 5.3 & Fig.

5.4. Also, the flux crosses zero at the maximum or minimum of the carrier, which is the location in the PWM cycle where the magnitude of the flux in the coupled inductor is smallest. To prevent the circulating current (i_{cir}) and the flux in coupled inductors from experiencing a jump, the transition into and out of the discontinuous regions is done exclusively at the maximum or minimum of the carrier used to control each inverter legs. This technique guarantees that the flux remains at zero throughout the discontinuous PWM regions and at the start/end of the continuous PWM regions. Most importantly, the flux remains center at zero without a jump throughout the fundamental period. The DPWM reference signal of phase "a" ($ref_{a_{NT}}$, ref_{a_T}), the PWM voltage between the interface coupled inductors ($v_{a1} - v_{a2}$: $V_{W_{NT}}$, V_{W_T}) and the flux induced (ϕ_{NT}, ϕ_T) by the DPWM with and without the sector transition control are compared in Fig. 5.4.
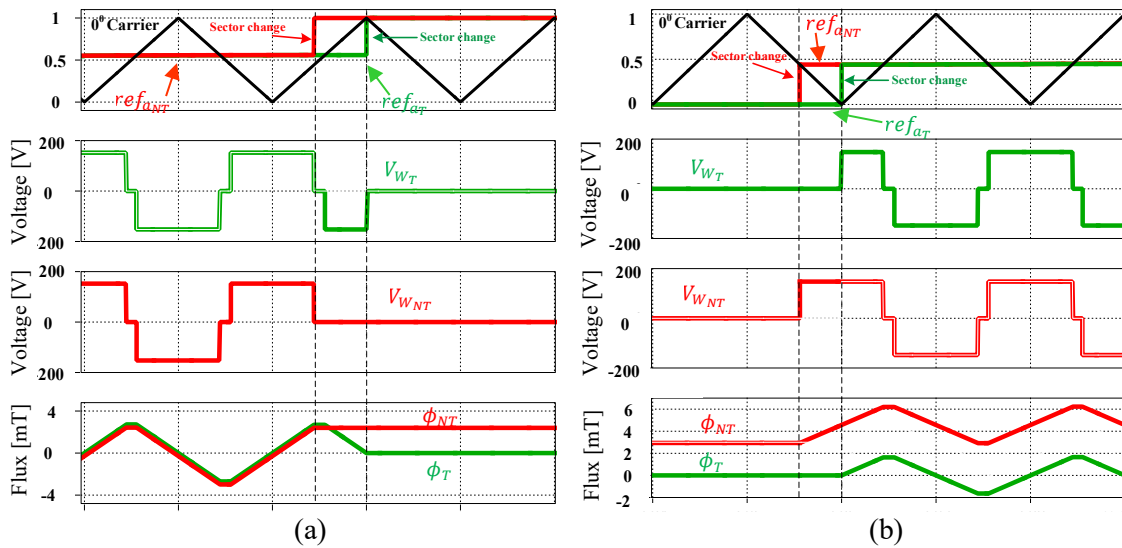
Fig. 5.4 Offset in flux due to sector changes (a) transition into the discontinues sector, (b) transition out of the discontinues sector.

5.2. Simulation.

The sector change transition technique was simulated using an NPC converter having 2-inverter legs in each phase whose outputs are connected to cross-coupled inductors, see Fig. 5.1. A dc-link of 300V, a switching frequency of 20kHz, and an RL-load were used to approximate results of a 3.8kW laboratory prototype. The converter

produced 5-level phase (v_{pha}) and 9-level PWM line voltages with PWM voltage step much smaller than the dc-link voltage. The phase voltage illustrates the use of a 60^0 clamped DPWM scheme, see Fig. 5.5. Most importantly, the circulating currents (i_{cir}) and the high-frequency flux in the coupled inductors did not experience a jump and was centered at zero. These results indicate that the coupled inductors can be designed more precisely with a reduced size/weight. Also, the load currents (i_a, i_b, i_c) are evenly shared between the parallel-connected inverter legs (i_{a1}, i_{a2}) which reduces current stress and switching losses.
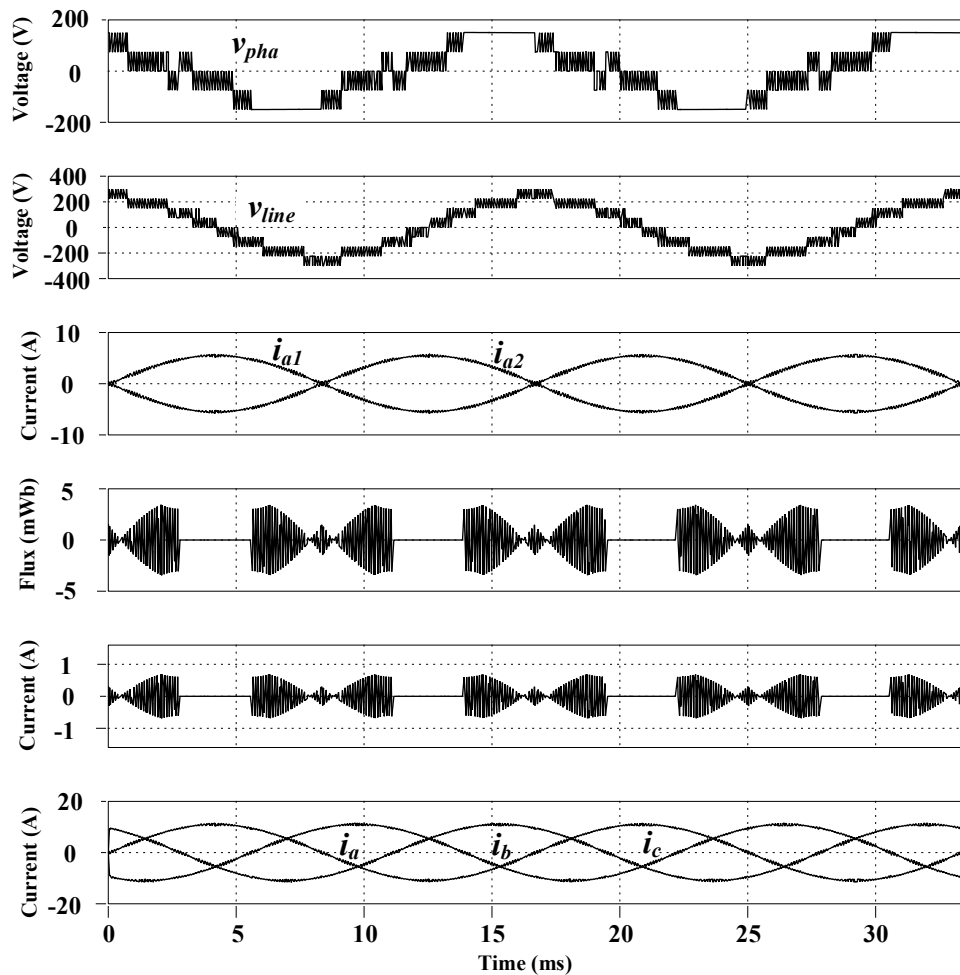
Fig. 5.5 Simulated waveforms of the neutral point clamped converter using the sector transition technique.

5.3. Experimental verification.

A 3.8 kW NPC laboratory prototype using inner 2-level inverter modules in each phase was used to verify the feasibility of the DPWM control transition technique. Cross coupled inductors, whose parameters are presented in Table 2.2 were used to average the outputs of the parallel-connected inverter legs. A dc-link of 300V, a switching frequency of 20kHz, and an RL-load was used to carry the test over a wide range of fundamental frequency (60Hz ~ 1.1kHz). The PLECS RT box was used as a digital controller, see Fig. 5.6. The system generated 5-level phase (v_{pha}), 9-level PWM line voltages (v_{line}) and the load currents (i_a, i_b, i_c) were evenly shared between the parallel inverters. Since the flux in the core cannot be measured experimentally, the circulating current (i_{cir}), which has the same waveform as the flux in the core, was measured. The measured circulating current was centered at zero and did not experience a jump, indicating that the flux in the core did not experience a jump as well, see Fig. 5.7. This validates the sector transition technique.

The transient results were obtained using a step change in modulation index and step change in load. The cross coupled inductors have tightly coupled windings with low series output inductance which favor the production of high-frequency fundamental outputs in the kilohertz range with a very small fundamental voltage drop across the inductor windings. Consequently, the converter output voltages have flat levels, see Fig. 5.8.
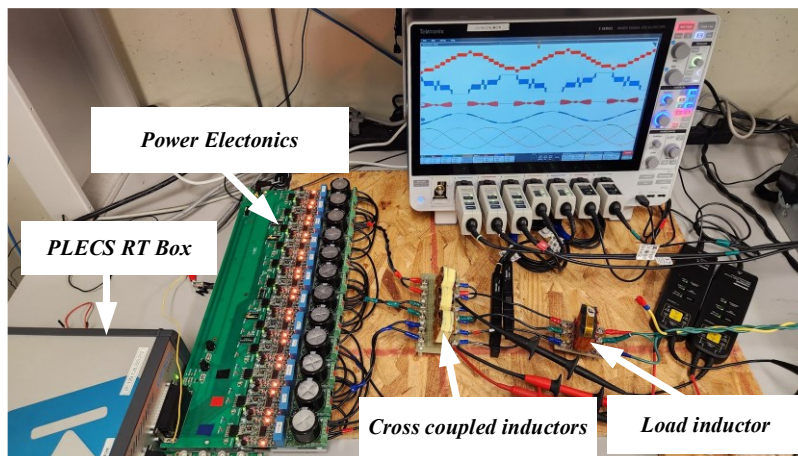
Fig. 5.6 Experimental setup of the neutral point clamped VSC with cross coupled inductor.
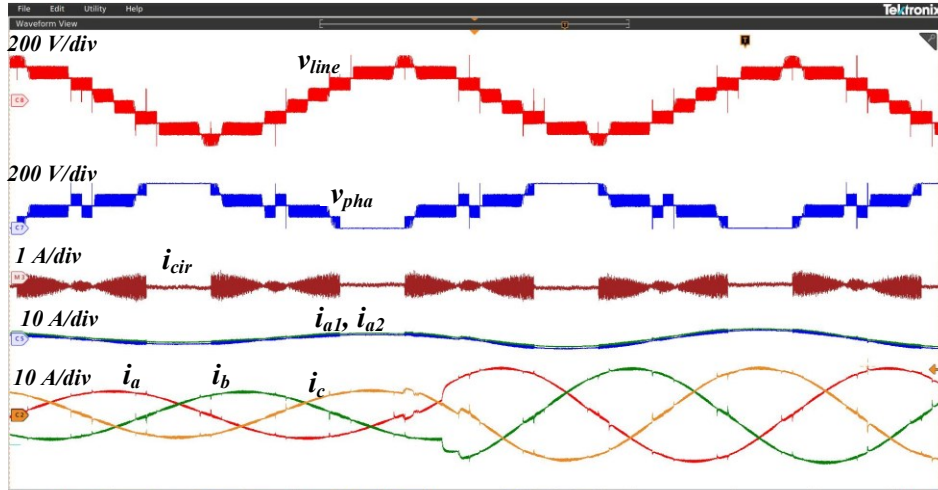
(a)
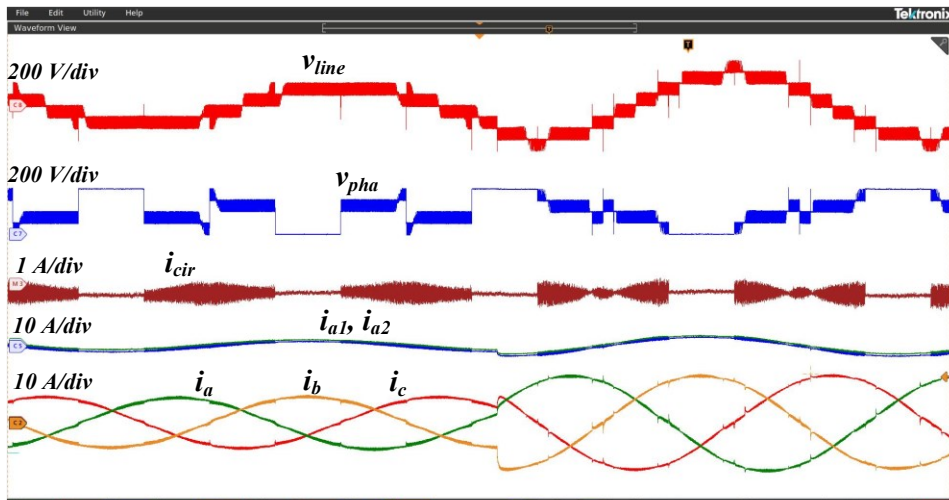
(b)

Fig. 5.7 Experimental waveforms of the neutral point converter with cross coupled inductors in a transient state (a) load change, (b) amplitude modulation index change, f_1= 60Hz, V_{dc}= 300 V, f_s= 20Hz, L_f= 70 uH.
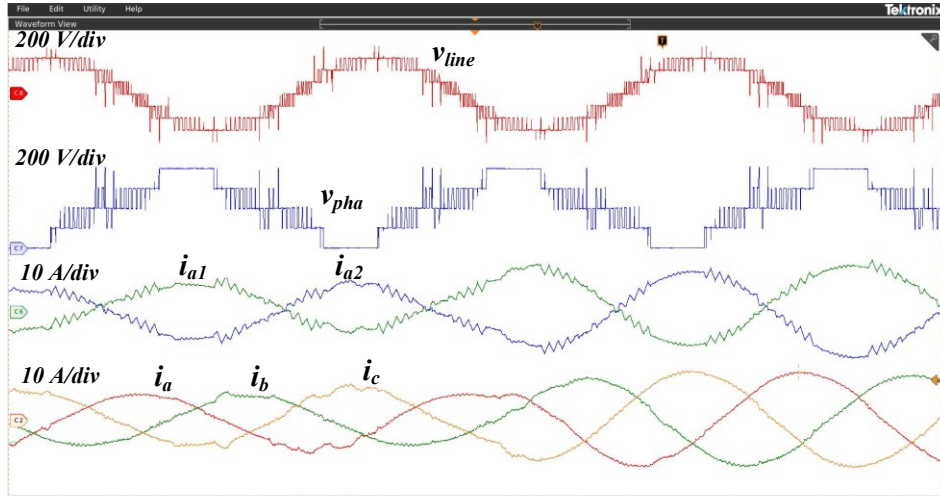
(a)
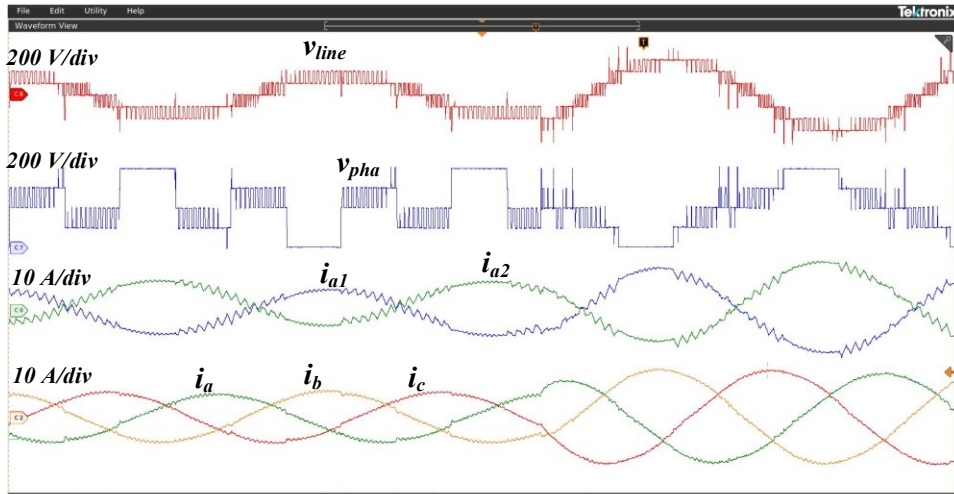
(b)

Fig. 5.8 Experimental waveforms of the neutral point converter with cross coupled inductors in a transient state (a) load change, (b) amplitude modulation index change, f_l= 1.1 kHz, V_{dc}= 300 V, f_s= 20Hz, L_f= 70 uH.

The DPWM control technique significantly reduces the peak flux in the interface coupled inductors and the flux pattern can be predicted precisely, see Fig. 5.9 (a). In consequence, the size/weight of the coupled inductors and hence the overall size/weight of the converter magnetics designed based on peak flux can significantly be reduced as well, leading to high power density. The control technique has an insignificant effect on the quality of the output

waveforms: Line voltage harmonic volt-seconds and the current total harmonic distortions (THD$_f$), see Fig. 5.9 (b) and (c).

(a)

(b)

(c)
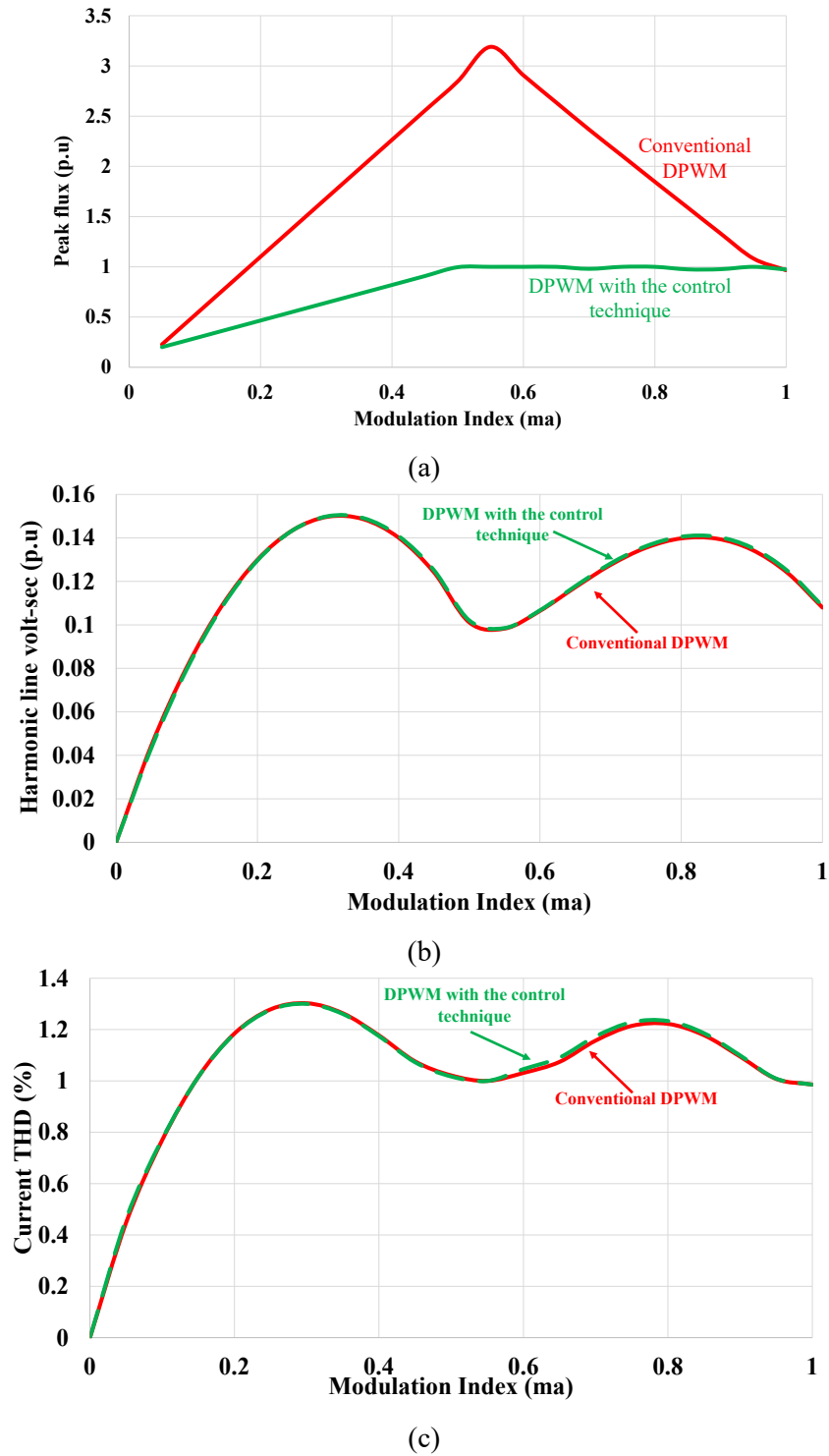
Fig. 5.9 Performance curves of the NPC with two interleaved PWM switching inverter legs in each phase (a) per unite peak flux (b) line voltage harmonic volt-second, and (c) current THD$_f$.

5.5. Conclusion.

A DPWM control technique which prevents the circulating currents and the flux in inductors from experiencing a jump whenever the discontinuous PWM, DPWM, scheme is implemented was presented. The reference signal of the DPWM has continuous and discontinuous sectors. Uncontrol sector transitions introduce dc offsets in the circulating currents and cause flux jumps in interface coupled inductors. A solution to this problem is to transition into and out of the discontinuous regions exclusively at the maximum or minimum of the carrier used to control the 2-inverter legs in each phase of the converter. This control technique guarantees that the flux remains at zero throughout the discontinuous PWM regions and at start/end of the continuous PWM regions; thereby reducing the peak flux and the size/weight of the magnetics required.

The feasibility of the DPWM control technique has been demonstrated using simulations and experimental results of a 3.8kW NPC laboratory prototype connected to cross coupled inductors. Both simulation and experimental results confirm that the circulating current and the flux patterns in the coupled inductors remained centered at zero without experiencing a jump. The DPWM control technique is suitable to reduce the size/weight of the magnetics in high power converters, thereby improving their power density. Target applications include fast/ultra-fast EV charging, battery energy storage systems, flywheel energy storage, high-frequency electric drives, and grid connected converters.

Chapter 6

Conclusion and recommendation for future work.

The summary of the conclusions of each chapter and a recommend research area is presented. Coupled inductor VSC topologies using parallel-connected two-level inverter legs, and advanced modulation schemes can be used to generate high quality multi-level PWM output voltages while reducing the size/weight of magnetics required to average their outputs. The numerous attractive features of these multi-level coupled inductor converter topologies such as modularity, fault tolerant operation, lightweight magnetics, and high-quality waveforms, make them suitable for many applications in power electronics. The goal of the research presented is to develop high power converters with a reduced footprint. This is achieved by developing coupled inductor converter topologies and advanced switching techniques that reduces the size/weight of the magnetics while improving their output qualities. As a result, five different multi-level coupled inductor topologies and two modulating techniques were investigated for high frequency electric drives, battery energy storage, and grid connected converters.

6.1. Conclusion.

Two-level inverter legs connected to coupled inductors (CIs) having cross-coupled windings was a topic examined for low voltage high power converters, see chapter 2. The cross coupled inductor winding arrangement significantly lowered the series output inductances which made it feasible to produce high frequency multi-level PWM outputs in the kilohertz range with a very small fundamental voltage drop across the inductor. The low fundamental voltage drop reduced the fundamental flux and peak flux in the inductor magnetic core, thereby reducing the size/weight of the magnetic required. The cross coupled inductors present a very large inductance between the inverter legs, related to the inductor magnetizing inductance, and is useful to control the peak circulating current ripple. In addition, cross coupled inductors guarantee the even distribution of the load currents between the parallel inverter legs without the need for a current controller. The

100

performance of the proposed multi-level converters was verified using PLECS simulation and experimental results of a high frequency electric drive.

A dc-choke and a 3-limb coupled inductor, dual CI, where presented as a means to connect two parallel voltage source converters and to control circulating currents due to the voltage difference that is normally experienced between the 3-phase output voltages of the two converters. The inductor types presented place one CI between the 3-phase output terminals of the two converters, a 3-limb CI, and a second inductor located between the two converter dc input terminals, a dc CI or dc choke, see chapter 3. The 3-limb CI connecting the outputs of the two interleaved voltage source converters has a high inductance for differential mode PWM voltages but has a very low inductance for common mode voltages between the converters. The dc choke place on the dc link has a high inductance for common mode voltage between the two converters. In consequence, the two inductors: dc-choke and a 3-limb CI, can be used to separately filter the common mode and differential mode components of the voltage between the two converters connected to the same dc-link. The dc-choke and the 3-limb CI have a very low series output inductance which favor rapid changes in the supply and output currents during transients. The low series output inductance of the two coupled inductors equally favors the production of high quality high-frequency fundamental multi-level PWM output voltages in the kilohertz range with a very small fundamental voltage drop across the inductor windings. Most importantly, the coupled inductors can be 16% more efficient and 13% smaller when compared with that of three conventional coupled inductors which can cope with both common mode and differential mode switched mode voltage across their windings without saturating. The system described is useful to reduce common mode to ground noise in uninterrupted power supplies and motor drives, reduce cable interactions, and increase the power density of interleaved PWM switching converters by reducing the size/ weight of the converter's magnetics.

Two neutral point clamped (NPC) coupled inductor converters using inner inverter modules were investigated for high voltage high current converters. The converters have outer modules that clamp and reduce the voltage stress across all the switching device and coupled inductors, thereby reducing the peak flux and the size of core required to prevent

saturation. The first converter, unidirectional converter, has a reduced switch count and produces multi-level outputs with more voltage levels when compared with other converters, having the same number of switching devices. The multi-level outputs have a very small harmonic content and can more easily be filtered using small ac inductors. The second converter, bidirectional converter, uses a modified discontinuous PWM scheme that produces no common mode voltage between the inner inverter modules and makes it feasible to use a compact/light-weight 3-limb CI to produce 9-level PWM line voltages. These voltages can easily be filtered by the low winding inductance of high-speed machines or a small ac inductor in a grid connected system, thereby reducing the size and weight of the converter. The feasibility of the NPC converters has been verified using simulations and experimental results of a 3.8kW laboratory prototype. Target applications include fast/ultra-fast EV ac charging, battery energy storage systems, grid connected rectifiers, and electric drives.

A control technique that prevents the circulating currents and the flux in CIs, connected to an NPC with inner inverter modules, from experiencing a jump whenever the discontinuous PWM is used was presented. The reference signal of the DPWM has continuous and discontinuous sectors. Uncontrol sector transitions can introduce dc offsets in the circulating currents and flux jumps in the CIs. To prevent the flux in the inductors from experiencing a jump, the transition into and out of the discontinuous regions are done exclusively at the maximum or minimum of the carrier used to control the inner inverter modules in each phase of the converter. This technique guarantees that the flux remains at zero throughout the discontinuous PWM regions and at start/end the continuous PWM regions which reduces the peak flux and the size/weight of the magnetics required. The feasibility of the transition technique has been demonstrated using simulations and experimental results of a 3.8kW NPC laboratory prototype. Target applications include fast/ultra-fast EV ac charging, battery energy storage systems, flywheel energy storage, high-frequency electric drives, and grid connected converters.

The performance of proposed coupled inductor topologies has been demonstrated using converters connected to a stiff dc-link and/ ac grid. A rapid and robust control is

required to protect the circuit from failing during faults: short circuit, the collapse of the dc-link…

6.2. Recommendation for future work.

The modified discontinuous PWM, DPWM, scheme that produces no common mode (CM) voltage between parallel inverter legs causes the circulating currents and the flux in the coupled inductors to experience a jump just like the conventional DPWM, see Fig. 4.14. This modified DPWM favor the use of a compact/smaller 3-limb CI instead of three separate conventional coupled inductors, one for each phase of the VSC. The size/weight of the 3-limb CI used with this PWM scheme can further be reduced by eliminating the flux jumps produced by sector transitions in the modified DPWM scheme. The investigation of techniques to suppress flux jumps when implementing the modified DPWM are recommended for future research to further reduce the size/weight of inductors in high power converters.

Also, the design of coupled inductors requires numerous iterations, see Fig. 2.28. A simpler design procedure that facilitates the scaling up/down of magnetic cores depending on the converter specifications (Dc-link voltage, switching frequency, and phase currents) with fewer iteration is recommended.

Biography

[1]   M. Takongmo and J. Salmon, "Design of Three Limb Coupled Inductor using Cross-Coupled Windings to Produce Multi-Level Output Voltages and Reduced Magnetics," 2021 IEEE Applied Power Electronics Conference and Exposition (APEC), 2021, pp. 226-232, doi: 10.1109/APEC42165.2021.9487260.

[2]   M. Takongmo, C. Zhang and J. Salmon, "Multi-level Voltage Source Converters using Coupled Inductors and Parallel Connected Inverter Legs," 2022 IEEE Applied Power Electronics Conference and Exposition (APEC), 2022, pp. 524-530, doi: 10.1109/APEC43599.2022.9773376.

[3]   M. Takongmo, C. Zhang and J. Salmon, "Coupled Inductors for High-Frequency Drives With Parallel-Connected Inverter Legs," in *IEEE Transactions on Power Electronics*, vol. 37, no. 6, pp. 7055-7066, June 2022.

[4]   M. Takongmo, C. Zhang and J. Salmon, "Parallel Inverters using a DC Common Mode PWM Filter with an AC Differential Mode PWM Filter," 2021 IEEE Applied Power Electronics Conference and Exposition (APEC), 2021, pp. 1189-1196, doi: 10.1109/APEC42165.2021.9487453.

[5]   M. Takongmo, C. Zhang, S. Wdaan, W. A. M. Telmesani, D. Yapa and J. Salmon, "Parallel-Connected Voltage Source Converters With a DC Common Mode and an AC Differential Mode PWM Filter," in *IEEE Transactions on Power Electronics*, vol. 38, no. 3, pp. 3664-3675, March 2023

[6]   C. Zhang, M. Takongmo and J. Salmon, "High-Quality PWM Scheme for High-Speed Electric Drives," in *IEEE Transactions on Power Electronics*, vol. 37, no. 2, pp. 1228-1233, Feb. 2022, doi: 10.1109/TPEL.2021.3108667.

[7]   C. Zhang, M. Takongmo and J. Salmon, "Enhanced Interleaved PWM Scheme with Flux Compensation for Three-Parallel Connected Inverters," 2021 IEEE

Energy Conversion Congress and Exposition (ECCE), 2021, pp. 1946-1952, doi: 10.1109/ECCE47101.2021.9595211.

[8] C. Zhang, M. Takongmo, S. Wdaan, W. A. M. Telmesani, D. Yapa and J. Salmon, "Carrier Transition Techniques for Parallel Connected VSCs Using Cross-Coupled Inductors," in *IEEE Transactions on Power Electronics*, vol. 37, no. 8, pp. 9652-9662, Aug. 2022, doi: 10.1109/TPEL.2022.3161484.

[9] S. Singh, M. Takongmo and J. Salmon, "Multi-Level Power Converters using Coupled Inductors and Parallel Connected 2-Level Inverters," 2020 IEEE Applied Power Electronics Conference and Exposition (APEC), New Orleans, LA, USA, 2020, pp. 1168-1175.

[10] J. Zuniga, M. Takongmo, C. Perera, V. Perera and J. Salmon, "Bidirectional DC-AC Converter Using a High- Frequency Transformer with Multi-Frequency Decoupled Power Control," 2021 IEEE Energy Conversion Congress and Exposition (ECCE), 2021, pp. 1910-191.

[11] C. Zhang, M. Takongmo, V. Perera and J. Salmon, "Flux Minimization in Interphase Coupled Inductors of Parallel-Connected Voltage Source Converters," 2022 IEEE Applied Power Electronics Conference and Exposition (APEC), 2022, pp. 843-847, doi: 10.1109/APEC43599.2022.9773424.

[12] A. Poorfakhraei, M. Narimani and A. Emadi, "A Review of Multilevel Inverter Topologies in Electric Vehicles: Current Status and Future Trends," in *IEEE Open Journal of Power Electronics*, vol. 2, pp. 155-170, 2021, doi: 10.1109/OJPEL.2021.3063550.

[13] M. Abarzadeh, W. A. Khan, N. Weise, K. Al-Haddad and A. M. EL-Refaie, "A New Configuration of Paralleled Modular ANPC Multilevel Converter Controlled by an Improved Modulation Method for 1 MHz, 1 MW EV Charger," in *IEEE Transactions on Industry Applications*, vol. 57, no. 3, pp. 3164-3178, May-June 2021, doi: 10.1109/TIA.2020.3019778.

[14]   M. Narimani, B. Wu, Z. Cheng and N. R. Zargari, "A New Nested Neutral Point-Clamped (NNPC) Converter for Medium-Voltage (MV) Power Conversion," in *IEEE Transactions on Power Electronics*, vol. 29, no. 12, pp. 6375-6382, Dec. 2014, doi: 10.1109/TPEL.2014.2306191.

[15]   X. He, J. Peng, P. Han, Z. Liu, S. Gao and P. Wang, "A Novel Advanced Traction Power Supply System Based on Modular Multilevel Converter," in *IEEE Access*, vol. 7, pp. 165018-165028, 2019, doi: 10.1109/ACCESS.2019.2949099.

[16]   A. Poorfakhraei, M. Narimani and A. Emadi, "A Review of Modulation and Control Techniques for Multilevel Inverters in Traction Applications," in *IEEE Access*, vol. 9, pp. 24187-24204, 2021, doi: 10.1109/ACCESS.2021.3056612.

[17]   D. Ronanki and S. S. Williamson, "A Simplified Space Vector Pulse Width Modulation Implementation in Modular Multilevel Converters for Electric Ship Propulsion Systems," in IEEE Transactions on Transportation Electrification, vol. 5, no. 1, pp. 335-342, March 2019, doi: 10.1109/TTE.2018.2884610.

[18]   M. Z. Youssef, K. Woronowicz, K. Aditya, N. A. Azeez and S. S. Williamson, "Design and Development of an Efficient Multilevel DC/AC Traction Inverter for Railway Transportation Electrification," in *IEEE Transactions on Power Electronics*, vol. 31, no. 4, pp. 3036-3042, April 2016, doi: 10.1109/TPEL.2015.2448353.

[19]   D. Gerling, R. Hildebrand, H. Hofmann, K. Jungnickel, B. Lange and M. Pye, "Test-bench for ultra high-speed electrical drives," 2005 European Conference on Power Electronics and Applications, Dresden, Germany, 2005, pp. 5 pp.-P.5.

[20]   R. Abebe, M. Di Nardo, D. Gerada, G. L. Calzo, L. Papini and C. Gerada, "High speed drives review: Machines, converters and applications," IECON 2016 - 42nd Annual Conference of the IEEE Industrial Electronics Society, Florence, Italy, 2016, pp. 1675-1679.

[21]   D. Hong, B. Woo, J. Lee and D. Koo, "Ultra High Speed Motor Supported by Air Foil Bearings for Air Blower Cooling Fuel Cells," in IEEE Transactions on Magnetics, vol. 48, no. 2, pp. 871-874, Feb. 2012.

[22]   R. K. Jardan, P. Stumpf, Z. Varga and I. Nagy, "Novel Solutions for High-Speed Self-Excited Induction Generators," in IEEE Transactions on Industrial Electronics, vol. 63, no. 4, pp. 2124-2132, April 2016.

[23]   L. Zhao et al., "A Highly Efficient 200 000 RPM Permanent Magnet Motor System," in IEEE Transactions on Magnetics, vol. 43, no. 6, pp. 2528-2530, June 2007.

[24]   ABB. [Online]. Available: www.abb.com

[25]   SIEMENS. [Online]. Available: www.siemens.com

[26]   TMEIC-GE. [Online]. Available: www.tmeic-ge.com

[27]   Rongxin Power Electronic Co. (RXPE). [Online]. Available: www.rxpe.co.uk

[28]   LS Industrial Systems. [Online]. Available: http://eng.lsis.biz/

[29]   Yaskawa. [Online]. Available: www.yaskawa.eu.com

[30]   R. Marquardt, "Stromrichterschaltungen mit verteilten energiespeichern," German Patent DE10103031A1, Jan. 24, 2001.

[31]   A. Lesnicar, J. Hildinger, and R. Marquardt, "Modulares strom-richterkonzept für netzkupplungsanwendungen bei hohen spannungen," ETG, Herzogenaurach, Germany, 2002.

[32]   A. Lesnicar and R. Marquardt, "A new modular voltage source inverter topology," in Proc. 10th EPE, 2003, pp. 1–10.

[33]   M. Glinka, "Prototype of multiphase modular-multilevel-converter with 2 MW power rating and 17-level-output-voltage," in Proc. IEEE 35th Power Electron. Spec. Conf., 2004, vol. 4, pp. 2572–2576.

[34]   Beijing Leader & Harvest Electric Technologies. [Online]. Available: www.ld-harvest.com

[35]   Schneider-Electric. [Online]. Available: www.schneider-electric.com

[36]   Alstom. [Online]. Available: www.alstom.com

[37]   N. Pallo, T. Foulkes, T. Modeer, S. Coday and R. Pilawa-Podgurski, "Power-dense multilevel inverter module using interleaved GaN-based phases for electric aircraft propulsion," *2018 IEEE Applied Power Electronics Conference and Exposition (APEC)*, San Antonio, TX, USA, 2018, pp. 1656-1661, doi: 10.1109/APEC.2018.8341239

[38]   V. G. Agelidis and H. C. Goh, \Low-distortion variable-level PWM technique," *IEE Proc. Electr. Power Appl.*, vol. 145, no. 2, pp. 73-78, Mar. 1998.

[39]   Z. Qiu and G. Chen, \Study and design of grid connected inverter for 2 MW wind turbine," in *Conf. Rec. IEEE IAS Annu. Meeting*, New Orleans, LA, 23-27 Sep.2007, pp. 165-170.

[40]   I. W. Jaskulski, H. Pinheiro, and L. Mariotto, \Multi-leg voltage source converter for grid connected wind turbines," in *Proc. ICCEP*, Capri, Italy, May 21-23 2007, pp. 229-235.

[41]   C. Wen, J. Li, X. Zhu, and H. Xu, \Research on circulation of parallel three-phase converters in MW wind power system," in *Proc. Workshop PEITS*, Guangzhou, China, Aug. 2-3 2008, pp. 349-354.

[42]   L. Jian-lin, H. Shu-ju, L. Mei, Z. Ying, K. De-guo, and X. Hong-hua, \Research on the application of parallel back-to-back PWM converter on direct-drive wind power system," in *Proc. IEEE Int. Conf. Elect. Utility DRPT*, Nanjuing, China, Apr. 6-9 2008, pp. 2504-2508.

[43]   W. Hu, Y. Wang, W. Yao, J. Wu, H. Zhang, and Z. Wang, \An efficient experimental method for high power direct drive wind energy conversion

systems," in *Proc. IEEE Power Electron. Spec. Conf. (PESC)*, Rhodes, Greece, Jun. 15-19 2008, pp. 3955-3959.

[44]   H. Cai, R. Zhao, and H. Yang, \Study on ideal operation status of parallel inverters," *IEEE Trans. Power Electron.*, vol. 23, no. 6, pp. 2964-2969, Nov. 2008.

[45]   V. Agarwal and D. Krishna, \Statistical approach to robust design of control schemes for series or parallel connected power devices," *EPE J.*, vol. 19, no. 3, pp. 15-21, Sep. 2009.

[46]   B. Cougo, G. Gateau, T. Meynard, M. Bobrowska-Rafal, and M. Cousineau, \PD modulation scheme for three-phase parallel multilevel inverters," *IEEE Trans. Ind. Electron.*, vol. 59, no. 2, pp. 690-700, Feb. 2012.

[47]   R. Stala, \A natural DC-link voltage balancing of diode-clamped inverters in parallel systems," *IEEE Trans. Ind. Electron.*, vol. 60, no. 11, pp. 5008-5018, Nov. 2013.

[48]   V. Agarwal and D. Krishna, "Statistical approach to robust design of control schemes for series or parallel connected power devices," EPE J., vol. 19, no. 3, pp. 15–21, Sep. 2009.

[49]   J. J. Nelson, G. Venkataramanan, and B. C. Beihoff, "Investigation of parallel operation of IGBTs," in Conf. Rec. IEEE IAS Annu. Meeting, vol. 4, Pittsburgh, PA, USA, Oct. 13–18 2002, pp. 2585–2591.

[50]   S. Musumeci, R. Pagano, A. Raciti, F. Frisina, and M. Melito, "Parallel strings of IGBTs in short circuit transients: analysis of the parameter influence and experimental behavior," in Proc. IEEE Ind. Electron. Society Conf. (IECON), vol. 1, Nov. 5–8 2002, pp. 555–560.

[51]   X. Zhuang, L. Rui, Z. Hui, X. Dianguo, and C. H. Zhang, \Control of parallel multiple converters for direct-drive permanent-magnet wind power generation

systems," IEEE Trans. Power Electron., vol. 27, no. 3, pp. 1259-1270, Mar. 2012.

[52]　R. Maheshwari, G. Gohil, L. Bede, and S. Munk-Nielsen, "Analysis and modelling of circulating current in two parallel-connected inverters," IET Power Electron., vol. 8, no. 7, pp. 1273–1283, Jul. 2015.

[53]　 Z. Zou, F. Hahn, G. Buticchi, S. Günter and M. Liserre, "Interleaved Operation of Two Neutral-Point-Clamped Inverters with Reduced Circulating Current," in IEEE Transactions on Power Electronics, vol. 33, no. 12, pp. 10122-10134, Dec. 2018.

[54]　H. Akagi, A. Nabae, and S. Atoh, "Control strategy of active power filter using multiple voltage-source PWM converters," IEEE Trans. Ind. Appl., vol. IA-22, no. 3, pp. 460–465, May 1986.

[55]　T. Qi and J. Sun, "Circulating currents and CM EMI reduction for interleaved three-phase VSC," in Proc. 27th Annu. IEEE Appl. Power Electron. Conf. Expo., Orlando, FL, USA, Mar. 2012, pp. 2448–2454.

[56]　B. Cougo, T. Meynard, and G. Gateau, "Parallel three-phase inverters: Optimal PWM method for flux reduction in intercell transformers," IEEE Trans. Power Electron., vol. 26, no. 8, pp. 2184–2191, Aug. 2011.

[57]　D. Zhang, F. Wang, R. Burgos, and D. Boroyevich, "Total flux minimization control for integrated inter-phase inductors in paralleled interleaved three-phase two-level voltage-source converters with discontinuous space-vector modulation," IEEE Trans. Power Electron., vol. 27, no. 4, pp. 1679–1688, Apr. 2012.

[58]　I. G. Park and S. I. Kim, "Modeling and analysis of multi-interphase transformers for connecting power converters in parallel," in Proc. IEEE Power Electron. Spec. Conf., St. Louis, MO, USA, Jun. 1997, vol. 2, pp. 1164–1170.

[59] R. Hausmann and I. Barbi, "Three-phase DC–AC converter using four-state switching cell," IEEE Trans. Power Electron., vol. 26, no. 7, pp. 1857–1867, Jul. 2011.

[60] G. J. Capella, J. Pou, S. Ceballos, J. Zaragoza, and V. G. Agelidis, "Current-balancing technique for interleaved voltage source inverters with magnetically coupled legs connected in parallel," IEEE Trans. Ind. Electron., vol. 62, no. 3, pp. 1335–1344, Mar. 2015.

[61] K. Park, F. D. Kieferndorf, U. Drofenik, S. Pettersson, and F. Canales, "Optimization of LCL filter with integrated intercell transformer for two-interleaved high-power grid-tied converters," IEEE Trans. Power Electron., vol. 35, no. 3, pp. 2317–2333, Mar. 2020.

[62] F. Ueda, K. Matsui, M. Asao, and K. Tsuboi, "Parallel-connections of pulsewidth modulated inverters using current sharing reactors," IEEE Trans. Power Electron., vol. 10, no. 6, pp. 673–679, Nov. 1995.

[63] F. Forest et al., "Optimization of the supply voltage system in interleaved converters using intercell transformers," IEEE Trans. Power Electron., vol. 22, no. 3, pp. 934–942, May 2007.

[64] F. Forest, E. Laboure, T. Meynard, and V. Smet, "Design and comparison of inductors and intercell transformers for filtering of PWM inverter output," IEEE Trans. Power Electron., vol. 24, no. 3, pp. 812–821, Mar. 2009.

[65] J. Salmon, J. Ewanchuk, and A. Knight, "PWM inverters using split-wound coupled inductors," IEEE Trans. Ind. Appl., vol. 45, no. 6, pp. 2001–2009, Nov./Dec. 2009.

[66] G. Gohil, L. Bede, R. Teodorescu, T. Kerekes, and F. Blaabjerg, "Integrated inductor for interleaved operation of two parallel three-phase voltage source converters," in Proc. 17th Eur. Conf. Power Electron. Appl., Geneva, Switzerland, 2015, pp. 1–10.

[67] G. Gohil, L. Bede, R. Teodorescu, T. Kerekes, and F. Blaabjerg, "An integrated inductor for parallel interleaved three-phase voltage source converters," IEEE Trans. Power Electron., vol. 31, no. 5, pp. 3400–3414, May 2016.

[68] G. Gohil, L. Bede, R. Teodorescu, T. Kerekes, and F. Blaabjerg, "An integrated inductor for parallel interleaved VSCs and PWM schemes for flux minimization," IEEE Trans. Ind. Electron., vol. 62, no. 12, pp. 7534–7546, Dec. 2015

[69] G. Mondal, J. Robinson, and S. Haensel, "Design and verification of compact inductor for interleaved AC/DC converter," in Proc. 21st Eur. Conf. Power Electron. Appl., 2019, pp. P.1–P.9.

[70] S. Ohn, X. Zhang, R. Burgos, and D. Boroyevich, "Differential-mode and common-mode coupled inductors for parallel three-phase AC–DC converters," IEEE Trans. Power Electron., vol. 34, no. 3, pp. 2666–2679, Mar. 2019.

[71] S. Ohn, X. Zhang, R. Burgos and D. Boroyevich, "Two core implementation of coupled inductor for parallel three-phase power converters," *2017 IEEE Applied Power Electronics Conference and Exposition (APEC)*, Tampa, FL, USA, 2017, pp. 898-905, doi: 10.1109/APEC.2017.7930803.

[72] S. Ohn, H. Jung, D. Boroyevich, and S. Sul, "A novel filter structure to suppress circulating currents based on the sequence of sideband harmonics for high-power interleaved motor-drive systems," IEEE Trans. Power Electron., vol. 35, no. 1, pp. 853–866, Jan. 2020.

[73] S. Ohn et al., "Modeling of N-parallel full-SiC AC–DC converters by four per-phase circuits," IEEE Trans. Power Electron., vol. 36, no. 6, pp. 6142–6146, Jun. 2021.

[74] R. Phukan, S. Ohn, D. Dong, R. Burgos, G. Mondal, and S. Nielebock, "Design and optimization of a highly integrated modular filter building block for three-level grid tied converters," in Proc. IEEE Energy Convers. Congr. Expo., Oct. 2020, pp. 4949–4956.

[75]   R. Phukan, S. Ohn, D. Dong, R. Burgos, G. Mondal, and S. Nielebock, "Evaluation of modular AC filter building blocks for full SiC based grid-tied three phase converters," in Proc. IEEE Energy Convers. Congr. Expo., Oct. 2020, pp. 1835–1841.

[76]   Y. Sahali and M. K. Fellah, "Selective harmonic eliminated pulse-width modulation technique (SHE PWM) applied to three-level inverter/converter," in IEEE Int. Symp. Ind. Electron. (ISIE), vol. 2, Jun. 9–11 2003, pp. 1112–1117.

[77]   S. R. Pulikanti and V. G. Agelidis, "Five-level active NPC converter topology:

SHE-PWM control and operation principles," in Proc. Australasian Univ. Power Eng. Conf. (AUPEC), 9–12 Dec. 2007, pp. 1–5.

[78]   G. Konstantinou, V. G. Agelidis, and J. Pou, "Theoretical considerations for single-phase interleaved converters operated with SHE-PWM," IEEE Trans. Power Electron., vol. 29, no. 10, pp. 5124–5128, Oct. 2014.

[79]   M. Narimani and G. Moschopoulos, "Improved method for paralleling reduced switch VSI modules: harmonic content and circulating current," IEEE Trans. Power Electron., vol. 29, no. 7, pp. 3308–3317, Jul. 2014.

[80]   B. McGrath, D. Holmes, and T. Lipo, "Optimized space vector switching sequences for multilevel inverters," IEEE Trans. Power Electron., vol. 18, no. 6, pp. 1293–1301, Nov. 2003.

[81]   W. Teh and Y. Lai, "Comparison of PWM techniques for 3-Phase inverters connected in parallel," in Proc. IEEE 4th Int. Future Energy Electron. Conf., 2019, pp. 1–8, doi: 10.1109/IFEEC47410.2019.9015136.

[82]   I. W. Jaskulski, I. J. Gabe, J. P. da Costa, M. Stefanello, and H. Pinheiro, "Spacevector modulation extended to voltage source converters with multiple legs in parallel," in Proc. EPE Conf. Appl., Aalborg, Denmark, Sep. 2–5 2007, pp. 1–10.

[83] T.-P. Chen, "Dual-modulator compensation technique for parallel inverters using space-vector modulation," IEEE Trans. Ind. Electron., vol. 56, no. 8, pp. 3004–3012, Aug. 2009.

[84] P. Rodriguez, J. Pou, R. Pindado, J. Montanya, R. Burgos, and D. Boroyevich, "An alternative approach on three-dimensional space-vector modulation of three-phase inverters," in Proc. IEEE Power Electron. Spec. Conf. (PESC), Recife, Brazil, Jun. 15–18 2005, pp. 822–828.

[85] G. Konstantinou, G. J. Capella, J. Pou, and S. Ceballos, "Single-carrier phase-disposition PWM techniques for multiple interleaved voltage source converter legs," IEEE Trans. Ind. Electron., vol. 65, no. 6, pp. 4466–4474, Jun. 2018, doi: 10.1109/TIE.2017.2767541.

[86] C. A. Teixeira, B. P. McGrath, and D. G. Holmes, "A state machine decoder for phase disposition pulsewidth modulation of three-phase coupled inductor semi-bridge converters," IEEE Trans. Ind. Appl., vol. 52, no. 3, pp. 2378–2386, May/Jun. 2016.

[87] G. Gohil, L. Bede, R. Teodorescu, T. Kerekes, and F. Blaabjerg, "Flux balancing scheme for PD modulated parallel interleaved inverters," IEEE Trans. Power Electron., vol. 32, no. 5, pp. 3442–3457, May 2017.

[88] B. Li, R. Yang, D. Xu, G. Wang, W. Wang, and D. Xu, "Analysis of the phase-shifted carrier modulation for modular multilevel converters," IEEE Trans. Power Electron., vol. 30, no. 1, pp. 297–310, Jan. 2015, doi: 10.1109/TPEL.2014.2299802.

[89] E. Laboure, A. Cuniere, T. A. Meynard, F. Forest, and E. Sarraute, "A theoretical approach to intercell transformers, application to interleaved converters," IEEE Trans. Power Electron., vol. 23, no. 1, pp. 464–474, Jan. 2008.

[90] B. P. McGrath and D. G. Holmes, "A comparison of multicarrier PWM strategies for cascaded and neutral point clamped multilevel inverters," in Proc.

IEEE Power Electron. Spec. Conf. (PESC), vol. 2, Galway, Ireland, Jun. 18–23 2000, pp. 674–679.

[91]   B. P. McGrath and D. G. Holmes, "Multicarrier PWM strategies for multilevel inverters," in *IEEE Transactions on Industrial Electronics*, vol. 49, no. 4, pp. 858-867, Aug. 2002, doi: 10.1109/TIE.2002.801073.

[92]   V. G. Agelidis and M. Calais, "Application specific harmonic performance evaluation of multicarrier PWM techniques," in Proc. IEEE Power Electron. Spec. Conf. (PESC), vol. 1, Fukuoka, Japan, May 17–22 1998, pp. 172–178.

[93]   J. Pou, J. Zaragoza, G. J. Capella, I. Gabiola, S. Ceballos, and E. Robles, "Current balancing strategy for interleaved voltage source inverters," EPE J., vol. 21, no. 1, pp. 29–34, Jun. 2011.

[94]   S. K. T. Miller, T. Beechner, and S. Jian, "A comprehensive study of harmonic cancellation effects in interleaved three-phase VSCs," in Proc. IEEE Power Electron. Spec. Conf. (PESC), Orlando, FL, USA, Jun. 17–21 2007, pp. 29–35.

[95]   D. G. Holmes and B. P. McGrath, "Opportunities for harmonic cancellation with carrier-based PWM for a two-level and multilevel cascaded inverters," IEEE Trans. Ind. Appl., vol. 37, no. 2, pp. 574–582, Mar./Apr. 2001.

[96]   B. P. McGrath, D. G. Holmes, M. Manjrekar, and T. A. Lipo, "An improved modulation strategy for a hybrid multilevel inverter," in Conf. Rec. IEEE IAS Annu. Meeting, vol. 4, Rome, Italy, Oct. 8–12 2000, pp. 2086–2093.

[97]   S. Singh and J. Salmon, "Multilevel voltage source parallel inverters using coupled inductors," in Proc. 20th Workshop Control Model. Power Electron., 2019, pp. 1–8, doi: 10.1109/COMPEL.2019.8769636.

[98]   J. Lee and K. Lee, "Carrier-Based Discontinuous PWM Method for Vienna Rectifiers," in IEEE Transactions on Power Electronics, vol. 30, no. 6, pp. 2896-2900, June 2015, doi: 10.1109/TPEL.2014.2365014.

[99] W. Zhu, C. Chen, S. Duan, T. Wang and P. Liu, "A Carrier-Based Discontinuous PWM Method With Varying Clamped Area for Vienna Rectifier," in IEEE Transactions on Industrial Electronics, vol. 66, no. 9, pp. 7177-7188, Sept. 2019, doi: 10.1109/TIE.2018.2873524.

[100] J. Zhou, J. O. Ojo, F. Tang, J. Haruna and P. C. Loh, "A Carrier-Based Discontinuous PWM for Single and Parallel Three-Level T-Type Converters with Neutral-Point Potential Balancing," in *IEEE Transactions on Industry Applications*, vol. 57, no. 5, pp. 5117-5127, Sept.-Oct. 2021, doi: 10.1109/TIA.2021.3093500.

[101] G. J. Capella, J. Pou, S. Ceballos, G. Konstantinou, J. Zaragoza, and V. G. Agelidis, "Enhanced phase-shifted PWM carrier disposition for interleaved voltage-source inverters," IEEE Trans. Power Electron., vol. 30, no. 3, pp. 1121–1125, Mar. 2015.

[102] S. Singh and J. Salmon, "Multilevel voltage source parallel inverters using coupled inductors," in Proc. 20th Workshop Control Model. Power Electron., 2019, pp. 1–8, doi: 10.1109/COMPEL.2019.8769636.

[103] J. Salmon and J. Ewanchuk, "A discontinuous PWM scheme for lowering the switching frequency and losses in a 3-phase 6-switch 3/5- level PWM VSI using a 3-limb inductor," in Proc. 27th Annu. IEEE Appl. Power Electron. Conf. Expo., 2012, pp. 120–127.

[104] J. Ewanchuk, S. Member, and J. Salmon, "Three-limb coupled inductor operation for voltage sourced inverters," IEEE Trans. Ind. Electron., vol. 60, no. 5, pp. 1979–1988, May 2013.

[105] A. M. Knight, J. Ewanchuk, and J. C. Salmon, "Coupled three-phase inductors for interleaved inverter switching," IEEE Trans. Magnetics, vol. 44, no. 11, pp. 4119–4122, Nov. 2008.

[106] B. Vafakhah, J. Ewanchuk, and J. Salmon, "Multicarrier interleaved PWM strategies for a five-level NPC inverter using a three-phase coupled inductor," IEEE Trans. Ind. Appl., vol. 47, no. 6, pp. 2549–2558, Nov. 2011.

[107] J. Salmon, J. Ewanchuk and R. Ul Haque, "Eliminating common mode winding voltages for a 3-limb coupled inductor used in 3/5-level PWM voltage source inverters," *2012 IEEE Energy Conversion Congress and Exposition (ECCE)*, Raleigh, NC, 2012, pp. 4525-4532, doi: 10.1109/ECCE.2012.6342205.

[108] N. Perera, R. U. Haque and J. Salmon, "DSP based Pre-Processed PWM scheme for 3-Limb core coupled inductor inverters," *2015 IEEE Energy Conversion Congress and Exposition (ECCE)*, Montreal, QC, Canada, 2015, pp. 2091-2098, doi: 10.1109/ECCE.2015.7309955.

[109] J. C. Le Claire and G. Lembrouck, "A simple feedback for parallel operation of current controlled inverters involved in UPS," in Proc. EPE Conf. Appl., Aalborg, Denmark, Sep. 2–5 2007, pp. 1–10.

[110] H. M. Hsieh, T. F. Wu, Y. E. Wu, H. S. Nien, and Y. K. Chen, "A compensation strategy for parallel inverters to achieve precise weighting current distribution," in Conf. Rec. IEEE IAS Annu. Meeting, vol. 2, Hong Kong, Oct. 2–6 2005, pp. 954–960.

[111] M. Xie, Y. Li, K. Cai, P. Wang, and X. Sheng, "A novel controller for parallel operation of inverters based on decomposing of output current," in Conf. Rec. IEEE IAS Annu. Meeting, vol. 3, Hong Kong, Oct. 2–6 2005, pp. 1671–1676.

[112] M. Yu, Y. Kang, Y. Zhang, M. Yin, S. Duan, H. Shan, and G. Chen, "A novel decoupled current-sharing scheme based on circulating-impedance in parallel multi-inverter system," in Proc. IEEE IECON, Taipei, Taiwan, Nov. 5–8 2007, pp. 1668–1672.

[113] B. Shi and G. Venkataramanan, "Parallel operation of voltage source inverters with minimal intermodule reactors," in Conf. Rec. IEEE IAS Annu. Meeting, vol. 1, Seattle, USA, Oct. 3–7 2004, pp. 156–162.

[114]   Z. Ye, D. Boroyevich, J.-Y. Choi, and F. C. Lee, "Control of circulating current in two parallel three-phase boost rectifiers," IEEE Trans. Power Electron., vol. 17, no. 5, pp. 609–615, Sep. 2002

[115]   C. T. Pan and Y. H. Liao, "Modeling and coordinate control of circulating currents in parallel three-phase boost rectifiers," IEEE Trans. Ind. Electron., vol. 54, no. 2, pp. 825–838, Apr. 2007.

[116]   konen, J. Luukko, A. Sankala, T. Laakkonen, and R. Pollanen, "Modeling and analysis of the dead-time effects in parallel PWM two-level three-phase voltage-source inverters," IEEE Trans. Power Electron., vol. 24, no. 11, pp. 2446–2455, Nov. 2009.

[117]   Xu, R. Li, H. Zhu, D. Xu, and C. Zhang, "Control of parallel multiple converters for direct-drive permanent-magnet wind power generation systems," IEEE Trans. Power Electron., vol. 27, no. 3, pp. 1259–1270, Mar. 2012.

[118]   R. Li and D. Xu, "Parallel operation of full power converters in permanent magnet direct-drive wind power generation system," IEEE Trans. Ind. Electron., vol. 60, no. 4, pp. 1619–1629, Apr. 2013.

[119]   Hurng-Liahng Jou, Jinn-Chang Wu, Kuen-Der Wu, Wen-Jung Chiang and Yi-Hsun Chen, "Analysis of zig-zag transformer applying in the three-phase four-wire distribution power system," in IEEE Transactions on Power Delivery, vol. 20, no. 2, pp. 1168-1173, April 2005,

[120]   Kassim Rasheed Hameed, September 2015. "Zig-Zag Grounding Transformer Modeling For Zero-Sequence Impedance Calculation Using Finite Element Method" , Diyala Journal of Engineering Sciences, Vol. 08, No. 06, pp. 36- 7 8.

[121]   P. S. Prakash, R. Kalpana, B. Singh and G. Bhuvaneswari, "Power Quality Improvement in Utility Interactive Based AC–DC Converter Using Harmonic Current Injection Technique," in IEEE Transactions on Industry Applications, vol. 54, no. 5, pp. 5355-5366, Sept.-Oct. 2018.

[122] K. P. Basu and S. K. Mukerji, "Experimental investigation into operation under single-phasing condition of a three-phase induction motor connected across a zigzag transformer," in IEEE Transactions on Education, vol. 47, no. 3, pp. 365-368, Aug. 2004.

[123] K. P. Basu, "Mitigation of Power Supply Disturbance in Single-phase Loads," 2006 IEEE International Power and Energy Conference, 2006, pp. 254-256

[124] K. P. Basu, N. M. Nor and S. A. Hafidz, "Mitigation of power supply disturbance in electronic loads," 2011 International Conference on Energy, Automation and Signal, 2011, pp. 1-5.

[125] C. Young, S. Wu and P. Liao, "A new multilevel inverter based on single DC input source and zig-zag connected transformers," 2011 6th IEEE Conference on Industrial Electronics and Applications, 2011, pp. 692- 697.

[126] S. Kim, "New multiple DC-DC converter topology with a high frequency zig-zag transformer," Nineteenth Annual IEEE Applied Power Electronics Conference and Exposition, 2004. APEC '04., 2004, pp. 654- 660 Vol.1.